ARL-TR-7447 ● SEP 2015

US Army Research Laboratory

Improving Weather Research and Forecasting Model Initial Conditions via Surface Pressure Analysis

by Brian P Reen

Approved for public release; distribution unlimited.

NOTICES

Disclaimers

The findings in this report are not to be construed as an official Department of the Army position unless so designated by other authorized documents.

Citation of manufacturer's or trade names does not constitute an official endorsement or approval of the use thereof.

Destroy this report when it is no longer needed. Do not return it to the originator.

ARL-TR-7447 ● SEP 2015

US Army Research Laboratory

Improving Weather Research and Forecasting Model Initial Conditions via Surface Pressure Analysis

by Brian P Reen
Computational and Information Sciences Directorate, ARL

Approved for public release; distribution unlimited.

REPORT DOCUMENTATION PAGE

Form Approved
OMB No. 0704-0188

Public reporting burden for this collection of information is estimated to average 1 hour per response, including the time for reviewing instructions, searching existing data sources, gathering and maintaining the data needed, and completing and reviewing the collection information. Send comments regarding this burden estimate or any other aspect of this collection of information, including suggestions for reducing the burden, to Department of Defense, Washington Headquarters Services, Directorate for Information Operations and Reports (0704-0188), 1215 Jefferson Davis Highway, Suite 1204, Arlington, VA 22202-4302. Respondents should be aware that notwithstanding any other provision of law, no person shall be subject to any penalty for failing to comply with a collection of information if it does not display a currently valid OMB control number.
PLEASE DO NOT RETURN YOUR FORM TO THE ABOVE ADDRESS.

1. REPORT DATE *(DD-MM-YYYY)*	2. REPORT TYPE	3. DATES COVERED (From - To)
Sep 2015	Final	

4. TITLE AND SUBTITLE
Improving Weather Research and Forecasting Model Initial Conditions via Surface Pressure Analysis

5a. CONTRACT NUMBER

5b. GRANT NUMBER

5c. PROGRAM ELEMENT NUMBER

6. AUTHOR(S)
Brian P Reen

5d. PROJECT NUMBER

5e. TASK NUMBER

5f. WORK UNIT NUMBER

7. PERFORMING ORGANIZATION NAME(S) AND ADDRESS(ES)
US Army Research Laboratory
ATTN: RDRL-CIE-M
2800 Powder Mill Road
Adelphi, MD 20783-1138

8. PERFORMING ORGANIZATION REPORT NUMBER
ARL-TR-7447

9. SPONSORING/MONITORING AGENCY NAME(S) AND ADDRESS(ES)

10. SPONSOR/MONITOR'S ACRONYM(S)

11. SPONSOR/MONITOR'S REPORT NUMBER(S)

12. DISTRIBUTION/AVAILABILITY STATEMENT
Approved for public release; distribution unlimited.

13. SUPPLEMENTARY NOTES

14. ABSTRACT

A preprocessor (Obsgrid) that creates input data for the Advanced Research version of the Weather Research and Forecasting model (WRF-ARW) is modified to perform a surface pressure objective analysis to allow surface analyses of other fields to be more fully utilized in the WRF-ARW initial conditions. Nested 27-, 9-, 3-, and 1-km horizontal grid spacing domains centered over San Francisco, California, on 9 February 2012 reveal an area in the initial condition surface fields of the 1-km domain in which horizontal gradients are very small, with sharp gradients at its edges. The lack of an objective analysis of surface pressure unnecessarily limits the application of other surface analyses into the WRF initial conditions and contributes to the creation of these structures. Therefore, a surface pressure objective analysis was added to Obsgrid for 9 February and also 4 additional case days. The surface pressure objective analysis allows surface analyses of other fields to be more fully utilized in the WRF initial conditions and leads to improvements in model air temperature and especially dewpoint. However, these improvements are not seen in observation nudging experiments since the observation nudging corrects for the errors introduced by the original lack of surface pressure objective analyses.

15. SUBJECT TERMS
WRF, Obsgrid, surface pressure, objective analysis, mesoscale modeling

16. SECURITY CLASSIFICATION OF:			17. LIMITATION OF ABSTRACT	18. NUMBER OF PAGES	19a. NAME OF RESPONSIBLE PERSON
					Brian P Reen
a. REPORT	b. ABSTRACT	c. THIS PAGE			19b. TELEPHONE NUMBER (Include area code)
Unclassified	Unclassified	Unclassified	UU	84	301-394-3072

Standard Form 298 (Rev. 8/98)
Prescribed by ANSI Std. Z39.18

Contents

List of Figures **v**

List of Tables **viii**

Acknowledgments **ix**

1. Introduction **1**

2. Model Description and Configuration **2**

2.1 Initial Condition Sources 5

2.2 Obsgrid 6

2.3 WRF-ARW 7

3. Case Description **9**

4. Methodology **9**

4.1 Ungrib Vertical Interpolation Bug Fix 9

4.2 Surface Pressure Estimation 10

4.3 Surface Pressure Quality Control 11

4.4 Surface Pressure Objective Analysis 12

5. Experimental Design **12**

5.1 Developmental Testing 12

5.2 Evaluation of Methodology 13

6. Results **14**

6.1 Developmental Testing 14

6.1.1 Motivation 14

6.1.2 Pre-Verification Evaluation 20

6.1.3 Verification 31

6.2 Evaluation of Methodology 39

6.2.1 Initial Conditions 39

6.2.2 Verification of Model Integration 48

7. Summary, Discussion, and Conclusions 63

8. References 68

List of Symbols, Abbreviations, and Acronyms 70

Distribution List 71

List of Figures

Fig. 1 WRF domain configuration consisting of nested 27-, 9-, 3-, and 1-km horizontal grid spacing domains 2

Fig. 2 The 2 innermost WRF domains: 3- and 1-km horizontal grid spacing domains centered over San Francisco, California.....3

Fig. 3 The land/water layout of the innermost WRF domain (1-km) 4

Fig. 4 Terrain height of the innermost WRF domain (1 km) 5

Fig. 5 WRF water vapor mixing ratio at the lowest prognostic model level (≈12 m above ground level [AGL]) at the initial time (12 UTC) for Exp. Control.....15

Fig. 6 WRF v-wind component at the lowest prognostic model level (≈12 m AGL) at the initial time (12 UTC) for Exp. Control.....16

Fig. 7 WRF potential temperature at the lowest prognostic model level (≈12 m AGL) at the initial time (12 UTC 9 February 2012) for Exp. Control. Three locations discussed in the text are labeled "A", "B", and "C".....17

Fig. 8 Diagram of the near-surface levels in the Obsgrid output at 12 UTC 9 February 2012 showing which of these levels is used to construct the WRF surface value for Exp. Control. A red X indicates levels removed from consideration due to being within 5 hPa of the Obsgrid output surface; a blue X indicates levels removed from consideration due to having a pressure greater than that of the sixth WRF model layer.....19

Fig. 9 Temperature profile (K) for the first 21 levels in the Metgrid output for a) Exp. Control and b) Exp. Ungrib.....21

Fig. 10 Histogram of the change in estimated surface pressure of observations at 12 UTC 9 February 2012 as a result of fixing the bug in the Ungrib vertical interpolation (Exp. Ungrib vs. Exp. Control). Note that all observations whose surface pressure did not change are in the rightmost column. 22

Fig. 11 Histogram of the change in estimated surface pressure of observations at 12 UTC 9 February 2012 as a result of enhancing the surface pressure estimation technique for observations below the lowest first-guess level. Note that observations whose surface pressure did not change are omitted from this figure. 23

Fig. 12 Surface pressure at 12 UTC 9 February 2012 for 1-km domain output by Obsgrid for a) Exp. PQ, and b) Exp. PQO, compared to c) the WRF initial condition surface pressure for both experiments.....24

Fig. 13 WRF potential temperature at the lowest prognostic model level (≈12 m AGL) at the initial time (12 UTC 9 February 2012) for a) Exp. PQ and b) Exp. PQO. The five locations discussed in the text are labeled "A", "B", "C", "D", and "E". 25

Fig. 14 Diagram of the near-surface levels in the Obsgrid output at 12 UTC 9 February 2012 and which of these levels is used to construct the WRF surface value for Exp. PQ and Exp. PQO. A red X indicates levels removed from consideration due to being within 5 hPa of the Obsgrid output surface; a blue X indicates levels removed from consideration due to having a pressure greater than that of the sixth WRF model layer....27

Fig. 15 WRF v-wind component at the lowest prognostic model level (≈12 m AGL) at the initial time (12 UTC 9 February 2012) for a) Exp. PQ and b) Exp. PQO....29

Fig. 16 WRF water vapor mixing ratio at the lowest prognostic model level (≈12 m AGL) at the initial time (12 UTC 9 February 2012) for a) Exp. PQ and b) Exp. PQO....30

Fig. 17 Histogram of change in absolute error of initial condition surface temperature resulting from the use of a surface pressure objective analysis (Exp. PQ vs. Exp. PQO) for the a) 27-km, b) 9-km, c) 3-km, and d) 1-km domains. Note that the lowest diagnostic level temperature (≈12 m) was evaluated against 2-m observations....32

Fig. 18 Time series of MAE of WRF 1-km domain a) 2-m temperature and b) 2-m dewpoint both evaluated against the model 2-m diagnostic values....33

Fig. 19 Time series of MAE of WRF 27-km domain a) 2-m temperature and b) 2-m dewpoint both evaluated against the model 2-m diagnostic values....36

Fig. 20 Time series of MAE of WRF 27-km domain a) 10-m wind speed and b) 10-m wind direction both evaluated against the model 10-m diagnostic values....37

Fig. 21 Time series of MAE of WRF 2-m temperature evaluated against the model 2-m diagnostic values for the WRF a) 27-km and b) 1-km domains....38

Fig. 22 Histogram of the change in absolute error of initial condition (12 UTC) surface temperature resulting from the use of a surface pressure objective analysis (Exp. Control+ vs. Exp. PQO931) for 4 case days. Note that the lowest diagnostic level temperature (≈12 m AGL) was evaluated against 2-m AGL observations. The symbols are plotted in the center of each 1-K-wide bin on the x-axis. The number of observations in each bin is plotted logarithmically....40

Fig. 23 WRF potential temperature at the lowest prognostic model level (≈12 m AGL) at the initial time (12 UTC) on 7 February 2012 for a) Exp. Control+ and b) Exp. PQO931. The location of points D and E discussed in the text are also shown. 42

Fig. 24 WRF potential temperature at the lowest prognostic model level (≈12 m AGL) at the initial time (12 UTC) on 16 February 2012 for a) Exp. Control+ and b) Exp. PQO931 43

Fig. 25 WRF potential temperature at the lowest prognostic model level (≈12 m AGL) at the initial time (12 UTC) on 1 March 2012 for a) Exp. Control+ and b) Exp. PQO931 44

Fig. 26 WRF potential temperature at the lowest prognostic model level (≈12 m AGL) at the initial time (12 UTC) on 5 March 2012 for a) Exp. Control+ and b) Exp. PQO931 45

Fig. 27 Diagram of the near-surface levels in the Obsgrid output at 12 UTC on 7 February for Exp. Control+ and Exp. PQO931 and on 9 February for Exp. PQ and Exp. PQO. The locations of points D and E are shown in Fig. 23 for 7 February and in Fig. 13 for 9 February. A blue X indicates levels removed from consideration due to having a pressure greater than that of the sixth WRF model layer. 46

Fig. 28 Time series of the difference in MAE between Exp. Control+ and Exp. PQO931 for surface a) temperature and b) dewpoint. Note that a positive value indicates that Exp. PQO931 has a lower MAE than Exp. Control+ and thus is an improvement over Exp. Control+. 49

Fig. 29 Time series of the difference in MAE between Exp. Control and Exp. PQO931 for surface a) wind speed and b) wind direction. Note that a positive value indicates that Exp. PQO931 has a lower MAE than Exp. Control+ and thus is an improvement over Exp. Control+. 51

Fig. 30 Time series of the difference in MAE between Exp. Nud and Exp. NudPQO931 for surface a) temperature and b) dewpoint. Note that a positive value indicates that Exp. NudPQO931 has a lower MAE than Exp. Nud and thus is an improvement over Exp. Nud.....52

Fig. 31 Time series of the difference in MAE between Exp. Nud and Exp. NudPQO931 for surface a) wind speed and b) wind direction. Note that a positive value indicates that Exp. NudPQO931 has a lower MAE than Exp. Nud and thus is an improvement over Exp. Nud.....53

Fig. 32 Time series of the difference in MAE between Exp. PQO931 and Exp. NudPQO931 for surface a) temperature and b) dewpoint. Note that a positive value indicates that Exp. NudPQO931 has a lower MAE than Exp. PQO931 and thus is an improvement over Exp. PQO931. 55

Fig. 33 Time series of the difference in MAE between Exp. PQO931 and Exp. NudPQO931 for surface a) wind speed and b) wind direction. Note that a positive value indicates that Exp. NudPQO931 has a lower MAE than Exp. PQO931 and thus is an improvement over Exp. PQO931.....56

Fig. 34 Time series of the difference in surface temperature MAE between Exp. Control+ and Exp. PQO931 for each of the 4 domains for a) 7 February, b) 16 February, c) 1 March, and d) 5 March. Note that a positive value indicates that Exp. PQO931 has a lower MAE than Exp. Control+ and thus is an improvement over Exp. Control+. 58

Fig. 35 Time series of the difference in surface dewpoint MAE between Exp. Control+ and Exp. PQO931 for each of the 4 domains for a) 7 February, b) 16 February, c) 1 March, and d) 5 March. Note that a positive value indicates that Exp. PQO931 has a lower MAE than Exp. Control+ and thus is an improvement over Exp. Control+. 59

Fig. 36 Time series of the difference in MAE between Exp. Control+ and Exp. PQO931 for non-surface observations between 0 and 1000 m AGL for a) temperature and b) dewpoint. A count of the number of observations used to create the MAEs is shown for c) temperature and d) dewpoint. 60

Fig. 37 Time series of the difference in MAE between Exp. Control+ and Exp. PQO931 for non-surface observations between 0 and 1000 m AGL for a) wind speed and b) wind direction. A count of the number of observations used to create the MAE's is shown for c) wind speed and d) wind direction. Note that positive values indicate that Exp. PQO931 performed better than Exp. Control+. 61

Fig. 38 Time series of the difference in MAE between Exp. PQO931 and Exp. NudPQO931 for non-surface observations between 0 and 1000 m AGL for a) temperature and b) dewpoint. Note that positive values indicate that Exp. NudPQO931 performed better than Exp. PQO931 62

Fig. 39 Time series of the difference in MAE between Exp. PQO931 and Exp. NudPQO931 for non-surface observations between 0 and 1000 m AGL for a) wind speed and b) wind direction. Note that positive values indicate that Exp. NudPQO931 performed better than Exp. PQO931 63

List of Tables

Table 1 Radii of influence (rounded to nearest integer) used by Obsgrid for objective analysis for surface and non-surface observations for each domain and each of the 5 possible scans. An "—" indicates that the scan was skipped due to the number of gridpoints within the radius of influence dropping below the minimum allowed value. 7

Table 2 Experimental design for developmental testing. The table indicates whether the Ungrib bug fix is included in each experiments (Ungrib Fix), as well as if surface pressure quality control (PSFC QC), surface pressure objective analysis (PSFC OA) for each domain (27, 9, 3, and 1 km), and observation nudging are used (nudging). 13

Table 3 Experimental design for testing of the methodology. The table indicates whether the Ungrib bug fix is included in each experiments (Ungrib Fix), as well as if surface pressure quality control (PSFC QC), surface pressure objective analysis (PSFC OA) for each domain (27, 9, 3, and 1 km), and observations nudging are used (nudging). 14

Acknowledgments

Bob Dumais is acknowledged for helpful feedback as the research was in progress. AirDat LLC provided Tropospheric Airborne Meteorological Data Reporting observational data, which expanded the above-surface data available for data assimilation and verification. This study was made possible in part due to the data made available to the National Oceanic and Atmospheric Administration by various providers for inclusion in the Meteorological Assimilation Data Ingest System (MADIS). The parallel Real-Time Mesoscale Analysis "use" and "reject" lists were provided by Steve Levine at the National Weather Service's National Centers for Environmental Prediction – Environmental Modeling Center and greatly facilitated making full use of the MADIS observational data set.

INTENTIONALLY LEFT BLANK.

1. Introduction

An important factor in the accuracy of forecasts produced by numerical weather prediction models is how well the model's initial conditions match the actual conditions. In general, more accurate initial conditions should lead to a more accurate forecast. Therefore, various methodologies have been developed with the goal of providing the model the best possible initial conditions.

Model initial conditions are often generated from the output of a separate model integration, either by using that model output alone or combining it in some manner with observations. Intermittent assimilation techniques apply the observations at discrete times, whereas continuous assimilation techniques apply the observations over some time period. Intermittent techniques include 3-dimensional variational (3DVAR) and objective analysis techniques such as the Cressman scheme. Continuous techniques include 4-dimensional variation (4DVAR) and observation nudging. In this study, an objective analysis is used to incorporate the observations at the beginning of the model integration, and then in some experiments, observation nudging is applied during a pre-forecast time period in order to provide better conditions at the beginning of the model forecast.

Unexplained structures in initial conditions created by an objective analysis of observations onto a coarser model background field prompted the current research. The structures were found to occur in locations where the objective analysis of a layer other than the surface was applied to the model surface by the numerical weather prediction model. The surface objective analysis was not applied at the surface because the pressure associated with the surface objective analysis differed from the model surface pressure. This mismatch occurs largely because the coarse model's surface pressure field is associated with the surface objective analyses of other fields such as temperature because no analysis is completed for surface pressure. This study investigates the potential utility of an objective analysis of surface pressure replacing the coarse model surface pressure field as the pressure associated with the surface objective analysis.

Section 2 details the numerical weather prediction model and associated objective analysis technique used in this study, as well the configuration thereof. Section 3 describes the cases used by this investigation, while Section 4 discusses the methodologies used. Section 6 contains the results of this study, and a summary, conclusions, and discussion are provided in Section 7.

2. Model Description and Configuration

The Advanced Research version of the Weather Research and Forecasting model (WRF-ARW) V3.6.1 (Skamarock et al. 2008) is applied with 56 vertical layers, and 27-, 9-, 3-, and 1-km horizontal grid spacing domains centered over San Francisco, California (Figs. 1–3). The terrain height of the 1-km domain is shown in Fig. 4. Next, 24-h model integrations are carried out from 12 Coordinated Universal Time (UTC) to 12 UTC for the 5 case days described in Section 3.

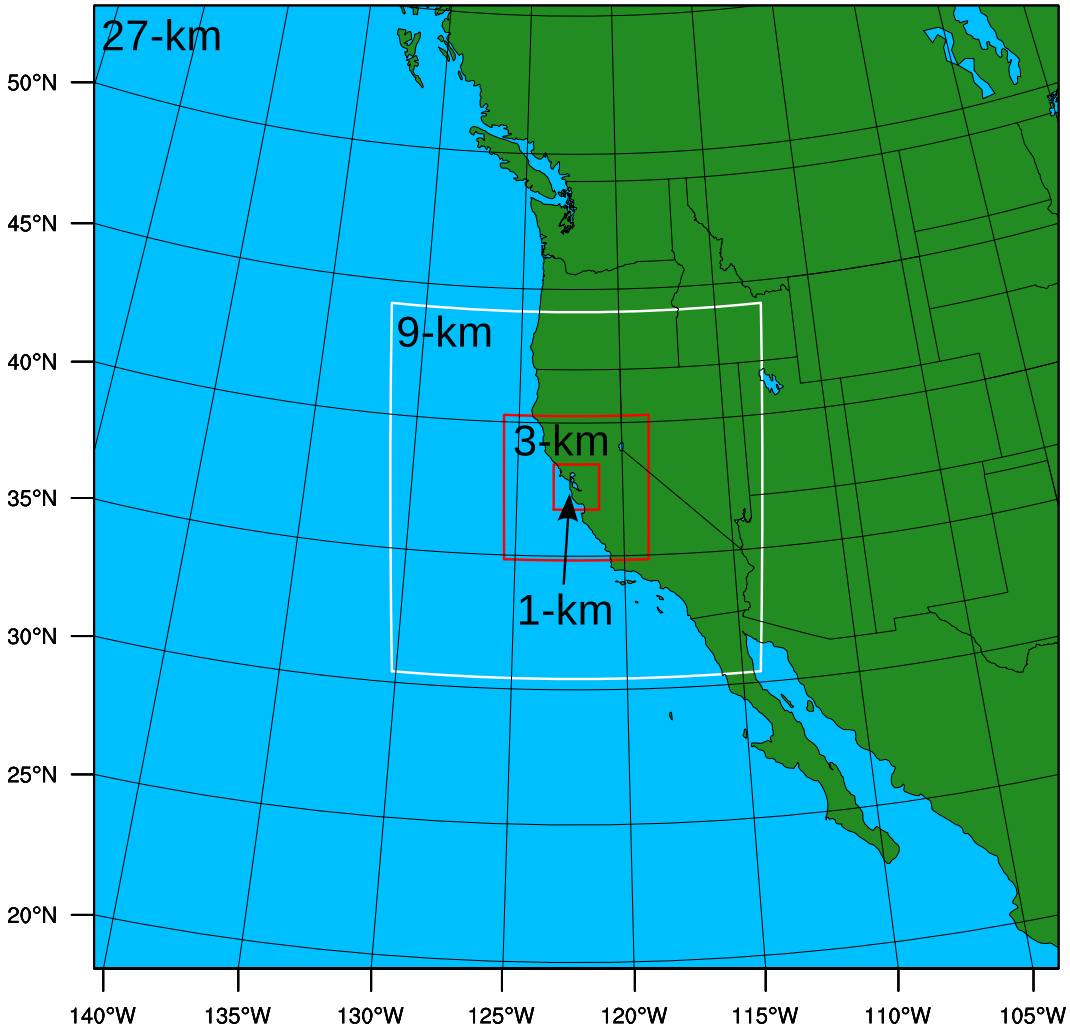

Fig. 1 WRF domain configuration consisting of nested 27-, 9-, 3-, and 1-km horizontal grid spacing domains

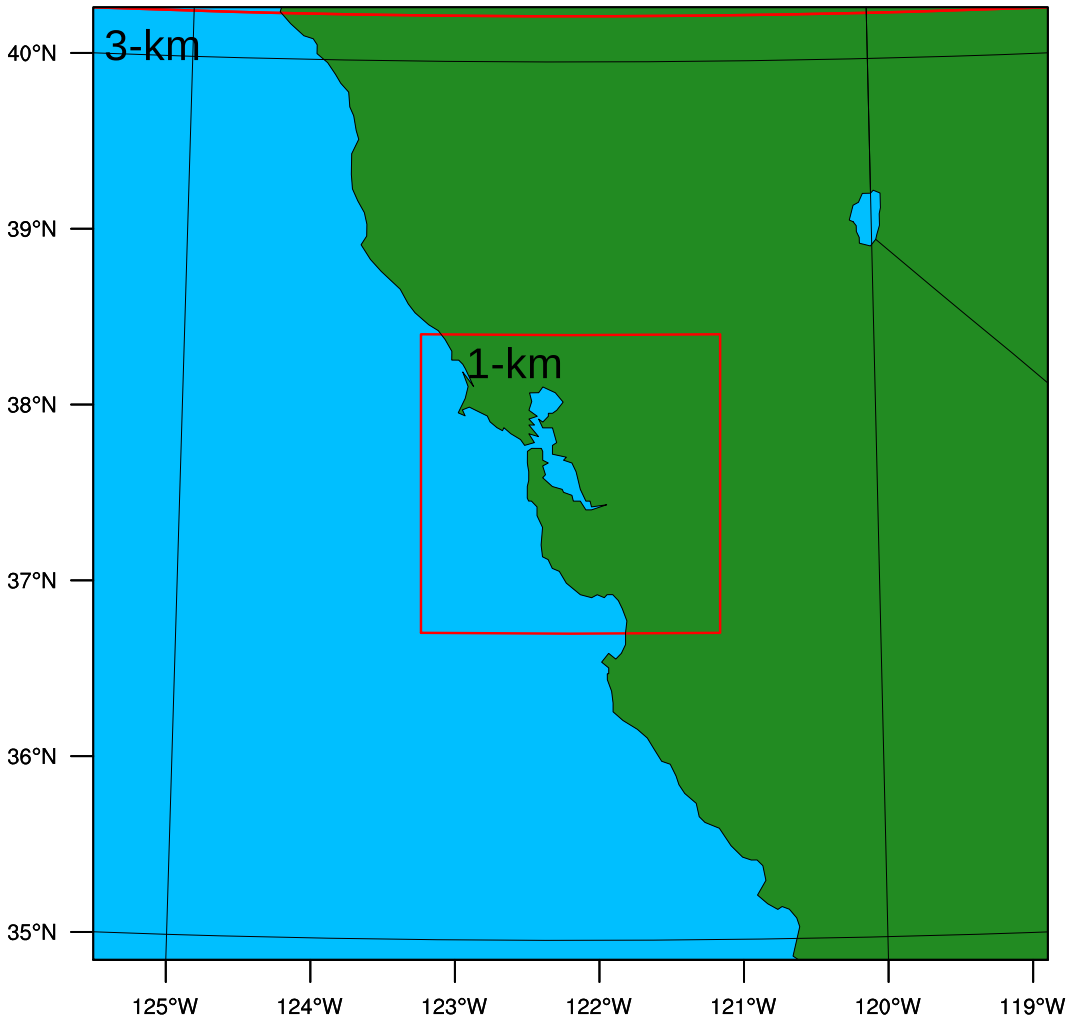

Fig. 2 The 2 innermost WRF domains: 3- and 1-km horizontal grid spacing domains centered over San Francisco, California

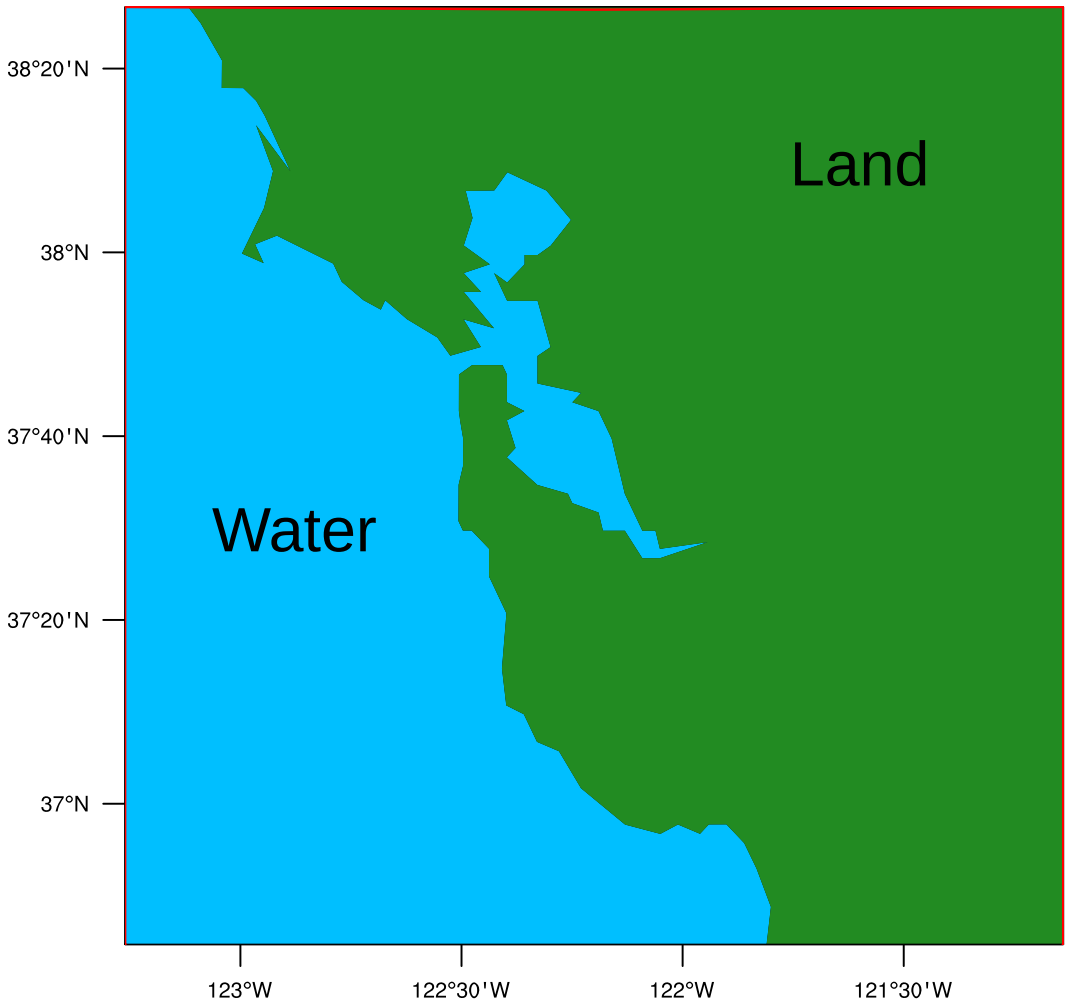

Fig. 3 The land/water layout of the innermost WRF domain (1-km)

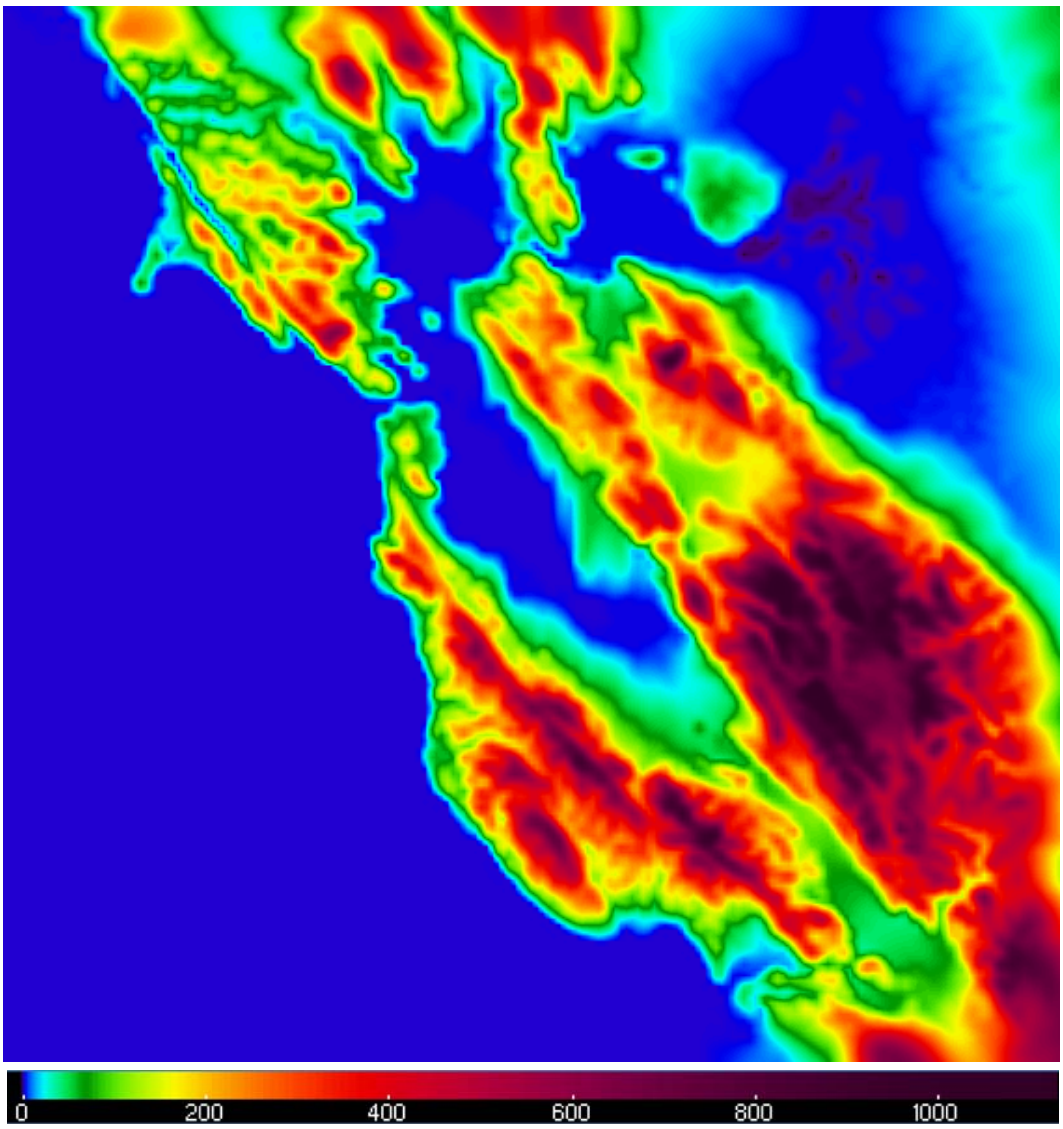

Fig. 4 Terrain height of the innermost WRF domain (1 km)

2.1 Initial Condition Sources

Global Forecast System (GFS) 0.5° horizontal resolution output (≈55 km) is used in the process of creating initial and boundary conditions. Sea surface temperature was from the 1/12° horizontal grid spacing Real Time Global Sea Surface Temperature product (Genmill et al. 2007) from the National Centers for Environmental Prediction, Marine Modeling and Analysis Branch. The snow fields from GFS are replaced with 1-km fields from National Operational Hydrologic Remote Sensing Center (NOHRSC) Snow Data Assimilation System (SNODAS) (National Operational Hydrologic Remote Sensing Center 2004) from the National Weather Service.

2.2 Obsgrid

Obsgrid performs quality control of observations and creates objective analyses by combining observations and coarse grid model data (here, GFS); it is part of the WRF software suite. Obsgrid is modified as described in Reen et al. (2014a) as well as described later in this report; other modifications are outside the scope of this report. Obsgrid is used to enhance the model initial and boundary conditions as well as perform quality control on the observations used for observation nudging and verification.

Obsgrid quality control includes gross error checks, checks against a first-guess field (here, GFS), and checks against nearby observations (buddy check). Obsgrid performs quality control of temperature, wind, relative humidity, and sea-level pressure. The modifications described in Reen et al. (2014a) add quality control of dewpoint.

Obsgrid objective analysis uses either a Cressman scheme or a multiquadric method; this investigation uses the Cressman scheme. The Cressman scheme in Obsgrid uses multiple scans and, for wind and relative humidity, is flow dependent. For this case, Obsgrid was configured to complete 5 scans using the default Obsgrid method for calculating the radius of influence used for these scans; this method assumes an average spacing of 325 km between upper air observations. For surface observations, this version of Obsgrid is modified to use radii of influence that are 40% of the upper air radii of influence to account for the smaller error correlation length scales at the surface. However, the surface observations are limited to a radius of influence between 4.5 and 100.0 model grid cells. The lower bound is to prevent the analysis from introducing "spots" (local values significantly different than surrounding grid points). If the calculated radius of influence for a given scan falls below this threshold, then the current scan is not carried out. The upper bound is to prevent surface observations from influencing too large an area. If the calculated radius of influence on the first scan is above this threshold, then the radius of influence is multiplied by the number needed to decrease it to the threshold; the radius of influence of all subsequent scans is also multiplied by this number. The resulting radii of influence for the 4-domain configuration used here are shown in Table 1.

Table 1 Radii of influence (rounded to nearest integer) used by Obsgrid for objective analysis for surface and non-surface observations for each domain and each of the 5 possible scans. An "—" indicates that the scan was skipped due to the number of gridpoints within the radius of influence dropping below the minimum allowed value.

Domain (km)	Surface Ob?	Radius of Influence (km)				
		Scan 1	Scan 2	Scan 3	Scan 4	Scan 5
27	No	540	378	270	189	135
9	No	522	369	261	189	135
3	No	522	366	258	183	129
1	No	520	364	255	179	126
27	Yes	216	151	—	—	—
9	Yes	209	148	104	76	54
3	Yes	209	146	103	73	52
1	Yes	100	70	49	34	24

The objective analysis uses the coarse grid model (here, GFS) as the first-guess field and then analyzes the observations onto this first-guess field. The objective analyses are used by WRF in determining the initial conditions for the model.

2.3 WRF-ARW

WRF-ARW is configured here to use the Mellor-Yamada-Janjić (MYJ) scheme (Janjić 2001) to parameterize the atmospheric boundary layer (ABL). It predicts turbulent kinetic energy (TKE) and is a Mellor-Yamada Level 2.5 turbulence closure model. As in Lee et al. (2012) and Reen et al. (2014b), the background TKE is decreased to better simulate conditions with low TKE and the ABL depth diagnosis is altered.

The WRF single-moment, 5-class microphysics parameterization (Hong et al. 2004) is used for all domains and, for the 27- and 9-km domains, the Kain-Fritsch cumulus parameterization (Kain 2004) is employed. For radiation, the Rapid Radiative Transfer Model (RRTM) (Mlawer et al. 1997) is used for longwave and the Dudhia scheme (Dudhia 1989) for shortwave. The Noah land surface model (Chen and Dudhia 2001) is used to represent land surface processes.

For some experiments, the observation nudging capability of WRF (Deng et al. 2009) is used to incorporate observations into the model via a 6-h pre-forecast

(12 to 18 UTC). During this pre-forecast, the model is gradually nudged toward observations of temperature, moisture, and wind. A nudging weight of 8×10^{-4} s^{-1} was used with the radius of influence set to 180, 180, 90, and 45 km for the 4 domains, respectively, for observations just above the surface. The radius of influence increases linearly with pressure up to 500 hPa and remains constant above this. For surface observations, the radius of influence is 70% that of observations just above the surface. The innovations calculated from the observations were applied with constant weight between 0.75 h prior to the observation until 0.75 h after the observation, with weight linearly decreasing with time between 0.75 h before (after) and 1.50 h before (after). For surface observations the time window is 75% as long.

The WRF program Real is used to place the input conditions onto the WRF vertical levels. A few WRF configuration options are particularly relevant to how this process takes place near the surface. In this study, *force_sfc_in_vinterp* was set to "6" (levels), which means that data from all non-surface GFS-derived levels with pressures greater than or equal to the pressure at model level 6 and less than the pressure at the GFS-derived surface pressure are ignored. The aim of this setting is to allow surface observations to affect a potentially deeper layer in the model since many more observations go into the surface analysis than other levels. The setting *zap_close_levels* was set to "500" (Pa), meaning that any GFS-derived levels within 500 Pa (5 hPa) of the pressure from the GFS-derived surface level are ignored. Some interpolation methods perform poorly if 2 layers involved in the interpolation are very close to each other relative to the distance between other levels involved in the interpolation. The setting *lowest_lev_from_sfc* was set to ".false."; if it were set to ".true.", it would force the GFS surface value to be used at the lowest level of the model. Note, however, that setting this to ".true." only forces the lowest model level to use the GFS surface level; it does not change the values at any other model level. This means that WRF model levels near the lowest WRF model level will not necessarily be affected by the GFS surface value (e.g., forcing the GFS surface value to be the WRF model initial condition value at the lowest WRF model level will not force that value to be used in interpolation to any other WRF level no matter how close that level is to the WRF surface). Finally, *use_levels_below_ground* defaulted to ".true.", which allows GFS levels whose pressure is higher than the GFS surface level to be used.

3. Case Description

The 5 cases considered here are identical to those used in Reen and Dumais (2014) and so the description of those 5 cases is repeated here. Five 24-h periods in early 2012 over the southwestern United States were modeled with each starting at 12 UTC: 7 February, 9 February, 16 February, 1 March, and 5 March. The case days were chosen to include days with active weather and those with more benign weather. On 7 February a trough moved onshore and led to widespread precipitation in the region. More quiescent weather was in place for the 9 February case with a 500-hPa ridge centered over central California at 12 UTC. On 16 February, an upper-level low was near the California/Arizona border with Mexico at 12 UTC bringing precipitation to that portion of the domain. The area of low pressure and the associated precipitation moved to the south and then east as the case day progressed. For 1 March, a weak shortwave trough at the beginning of the period resulted in precipitation in northern California that spread to Nevada and then moved southward and decreased in coverage. There was widespread high-level cloudiness for the 5 March case due to weak, upper-level low pressure but very limited precipitation.

For data assimilation (both the objective analysis performed by Obsgrid and the observation nudging) and verification, observations from the Meteorological Assimilation Data Ingest System (MADIS) dataset were used in addition to Tropospheric Airborne Meteorological Data Reporting (TAMDAR) observations (Daniels et al. 2004) obtained directly from AirDat LLC. The portions of the MADIS dataset applied here include standard surface, mesonet surface, profilers, Aircraft Communications Addressing and Reporting System (ACARS), and surface airways observations (SAOs). In addition to the quality control applied by Obsgrid, use/reject lists designed for the Real-Time Mesoscale Analysis (RTMA) (De Pondeca et al. 2011) are applied to the mesonet observations to deal with data quality issues in mesonet observations (e.g., from poor siting).

4. Methodology

4.1 Ungrib Vertical Interpolation Bug Fix

The WRF preprocessor Ungrib ingests gridded binary (GRIB) formatted data (such as GFS) and converts it to a format called the WRF intermediate format, which is used by other WRF preprocessor programs. The version of Ungrib used in this study can vertically interpolate the input GRIB dataset to additional user-defined pressure levels (a feature not available in the standard version of Ungrib). These modifications were originally created by the National Center for Atmospheric

Research in an earlier version of Ungrib but have never been incorporated into the version released publicly. This vertical interpolation capability is used to decrease the maximum pressure difference between a given observation and the GFS data used as a first-guess field against which quality control is performed. However, during the course of this investigation it was found that the Ungrib interpolation code contained an error wherein the weighting of the 2 levels used in the interpolation is switched so that the closer level is weighted more lightly and the more distant level is weighted more heavily. This bug exists in the standard Ungrib code, but is less likely to be problematic there since the standard version of Ungrib only uses the interpolation to fill in levels with missing data rather than to create new levels. The bug was fixed by switching the weights used in the interpolation so that they were associated with the proper levels. The bug fix has been reported to the WRF developers and has been incorporated into the WRF preprocessor Ungrib starting in version 3.7.

4.2 Surface Pressure Estimation

The version of Obsgrid used in this study will estimate the pressure of any observation for which the pressure is either missing or whose pressure has a quality control flag indicating that it was estimated using a standard atmosphere (the current standard version of Obsgrid does not create a new estimate in the latter situation). Note that the modifications to Obsgrid used in this study have been submitted to the National Center for Atmospheric Research for possible inclusion in a future release of Obsgrid. Pressure is estimated in Obsgrid by interpolating within the non-surface levels of the first-guess field (here, GFS). In other words, it will take the height of the observation and use the relationship between height and pressure in the GFS data to determine an estimated pressure for the observation. If the height of the observation is above the highest non-surface first-guess level, then Obsgrid will use the height of the observation along with the standard atmosphere to calculate the pressure of the observation. If the height of the observation is below the lowest non-surface level in the first-guess, then the standard version of Obsgrid will use the height of the observation to calculate the estimated pressure of the observation using the standard atmosphere. This latter case is altered here to minimize reliance on the standard atmosphere and more fully utilize the first-guess fields.

Observations whose pressure is missing or is marked as having been derived from the standard atmosphere and whose height is below the lowest non-surface level in the first-guess are now calculated in a different manner. If the height of the observation indicates that it is at or above sea level, the pressure is found by interpolating between the first-guess sea-level pressure and the pressure in the first

guess at the lowest non-surface level. If the height of the observation indicates that it is below sea level, then we find the temperature at the height of the observation, use this with the standard lapse rate to get the temperature at sea level, and then use the hypsometric equation to find pressure at the height of the observation. To obtain temperature at the height of the observation, the observed temperature is used if available. If this is not available, then the algorithm will use the temperature of the first-guess field interpolated to this point. If this is not available, then the algorithm will find the temperature at the height of the observation using the standard atmosphere.

4.3 Surface Pressure Quality Control

In order to use the surface pressure observations for an objective analysis, it is desirable to quality control these observations. Without quality control of surface pressure observations, erroneous or unrepresentative surface pressure observations could significantly degrade the quality of the surface pressure analysis. The standard version of Obsgrid does not have the ability to quality control surface pressure observations and so the capability was added to Obsgrid. Quality control of surface pressure is difficult due to its strong dependence on terrain height. The first-guess field (e.g., GFS) used by Obsgrid to determine if an observation is reasonable may be from a model with relatively coarse horizontal resolution; this can lead to substantial mismatches between the actual terrain height of the observation and the terrain height assumed by the first-guess field at that location. This, in turn, can lead to substantial differences in surface pressure solely due to the inability of the source of the first-guess fields to resolve the terrain. Therefore, quality control of surface pressure against the first-guess field is problematic, especially if the first-guess field has coarse horizontal resolution and the actual terrain is not close to uniform. Similarly, nearby observations used to perform the buddy check may be at locations with a substantially different terrain height. This can lead to non-trivial differences in surface pressure among nearby observations solely due to terrain variability.

Due to the difficulties in performing quality control on surface pressure, surface pressure was converted to sea-level pressure and quality control was carried out on sea-level pressure. The maximum allowed differences between the sea-level pressure derived from surface pressure observations and both the first-guess field and nearby observations are based on the maximum allowed difference the user specifies for pressure. Assumptions must be made to translate surface pressure to sea-level pressure, and the depth over which these assumptions must be made is the terrain height of the observation. Therefore, a multiplicative factor is added to increase the maximum allowed sea-level pressure difference based on the terrain

height of the observation (based on the observed increase in the pressure mismatch with terrain height, the standard allowed pressure difference is multiplied by the quantity 1 plus the terrain height of the elevation in meters divided by 2000). After quality control is carried out on the sea-level pressure derived from the surface pressure, the resultant quality control flags are applied to the surface pressure fields (i.e., the derived sea-level pressure is only used to determine the quality control flags that are applied to the surface pressure).

4.4 Surface Pressure Objective Analysis

The current standard version of Obsgrid does not perform objective analysis on surface pressure. It takes the surface pressure provided by the first-guess source (e.g., GFS) and makes some adjustments based on the sea-level pressure analysis. However, it does not analyze surface pressure observations onto the first-guess surface pressure field. The adjustments based on the sea-level pressure analysis will only account for errors in the first guess due to errors in the meteorological features (e.g., the strength of an area of high pressure), but will not account for the coarseness of the first-guess field results in its surface pressure not being representative of the actual terrain (or the terrain of the WRF model domain). Obsgrid was thus modified to perform an objective analysis of surface pressure using the same methods it uses to perform objective analyses of other variables.

5. Experimental Design

The experimental design consists of 2 parts: 1) development and initial testing of the methodology using a single case day, and 2) evaluation of the added value of the addition of surface pressure quality control and objective analysis on 4 case days.

5.1 Developmental Testing

Initial development and testing of the inclusion of surface pressure objective analyses and all of the associated techniques was carried out for the 9 February 2012 case described in the case description in Section 2. Exp. Ungrib includes the Ungrib vertical interpolation bug fix described in Section 4.1 for comparison against the control experiment (Exp. Control). Exp. PQ implements the improved surface pressure estimation technique described in Section 4.2 and the surface pressure quality control described in Section 4.3 in addition to using the Ungrib vertical interpolation bug fix. Objective analysis of surface pressure is added to the Exp. PQ configuration in Exp. PQO. Exp. PQO931 is identical to Exp. PQO except that surface pressure objective analysis is not applied to the 27-km domain.

Observation nudging experiments are completed, which are analogous to the non-nudging experiments already described. They include Exp. Nud (analogous to Exp. Control), Exp. NudUngrib (analogous to Exp. Ungrib), Exp. NudPQO (analogous to Exp. PQO), and Exp. NudPQO931 (analogous to Exp. PQO931). A summary of the experiments is shown in Table 2.

Table 2 Experimental design for developmental testing. The table indicates whether the Ungrib bug fix is included in each experiments (Ungrib Fix), as well as if surface pressure quality control (PSFC QC), surface pressure objective analysis (PSFC OA) for each domain (27, 9, 3, and 1 km), and observation nudging are used (nudging).

Name	Ungrib Fix	PSFC QC	PSFC OA				Nudging
			27	9	3	1	
			(km)				
Control							
Ungrib	X						
PQ	X	X					
PQO	X	X	X	X	X	X	
PQO931	X	X		X	X	X	
Nud							X
NudUngrib	X						X
NudPQO	X	X	X	X	X	X	X
NudPQO931	X	X		X	X	X	X

5.2 Evaluation of Methodology

Evaluation of the added value of the addition of surface pressure quality control and objective analysis is carried out on 4 case days in 2012: 7 February, 16 February, 1 March, and 5 March. While the single case day developmental testing was based on Obsgrid V3.4, this 4 case day segment of the research includes updates from the next released version, Obsgrid V3.7. Additionally, new Obsgrid modifications created after the experiments in the previous section were configured are applied to the 4 case days. The purpose of this group of experiments is to determine the added value of performing quality control and objective analysis on the surface pressure observations using the most up-to-date version of Obsgrid.

The experiments are summarized in Table 3 and are similar to the experiments used on the single case day described in Section 5.2. Exp. PQO931 uses surface pressure quality control on all domains and surface pressure objective analysis on the finest three domains and is compared to Exp. Control+, which has neither of these. However, Exp. Control+ differs from the Exp. Control used on the single case day in that Exp. Control+ includes the Ungrib bug fix as well as improvements to the method for estimating surface pressure; neither of these were used in Exp. Control. For the 4 case days, the focus is on the utility of adding surface pressure quality

control and objective analysis, rather than the value of the Ungrib bug fix or improved methods of estimating pressure.

Table 3 Experimental design for testing of the methodology. The table indicates whether the Ungrib bug fix is included in each experiments (Ungrib Fix), as well as if surface pressure quality control (PSFC QC), surface pressure objective analysis (PSFC OA) for each domain (27, 9, 3, and 1 km), and observations nudging are used (nudging).

Name	Ungrib Fix	PSFC QC	PSFC OA (km)				Nudging
			27	9	3	1	
Control+	X						
PQO931	X	X		X	X	X	
Nud+	X						X
NudPQO931	X	X		X	X	X	X

6. Results

6.1 Developmental Testing

6.1.1 Motivation

In Exp. Control, unusual patterns occurred in the surface initial conditions on the 1-km domain. For example, the water vapor mixing ratio indicates an area with moister conditions in the southeast quadrant of the domain with sharp gradients on both the outside edge and inside edge of this feature (Fig. 5). A similar feature can been seen in both the WRF v-wind component (Fig. 6) and the potential temperature (Fig. 7). The features appear unrealistic and thus an effort was launched to better understand the source of this structure and how it might be removed from the initial conditions.

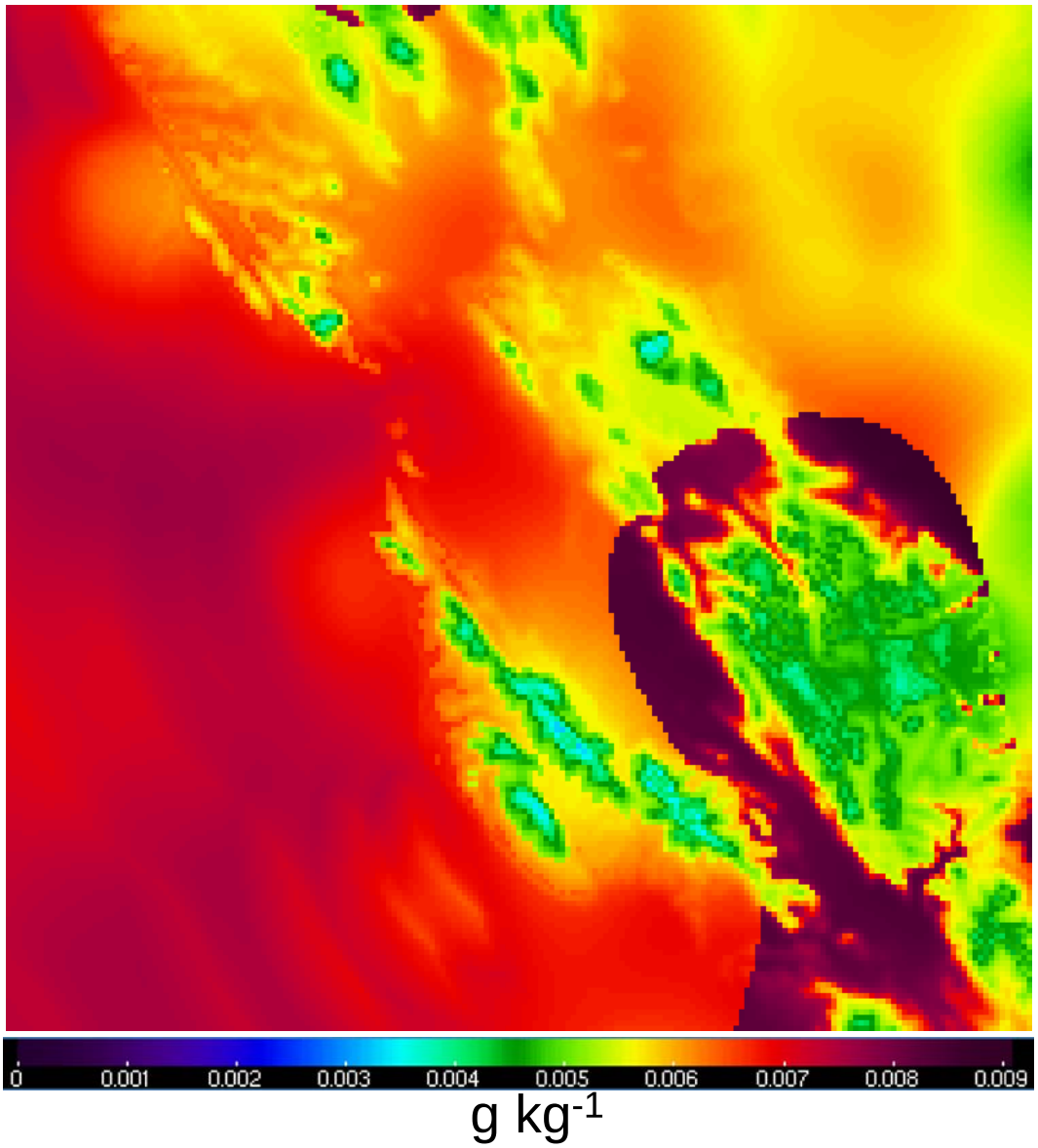

Fig. 5 WRF water vapor mixing ratio at the lowest prognostic model level (≈12 m above ground level [AGL]) at the initial time (12 UTC) for Exp. Control

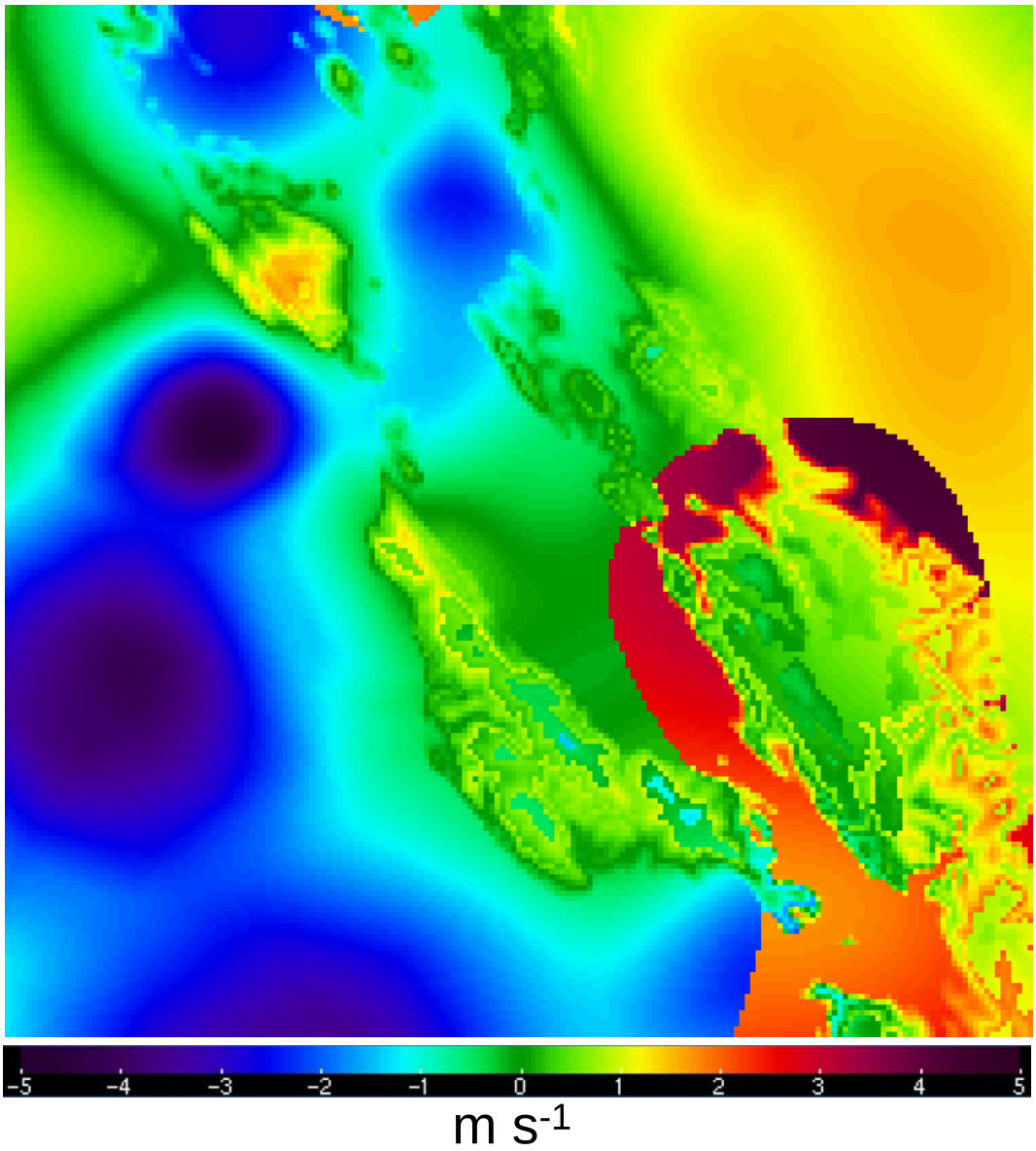

Fig. 6 WRF v-wind component at the lowest prognostic model level (≈12 m AGL) at the initial time (12 UTC) for Exp. Control

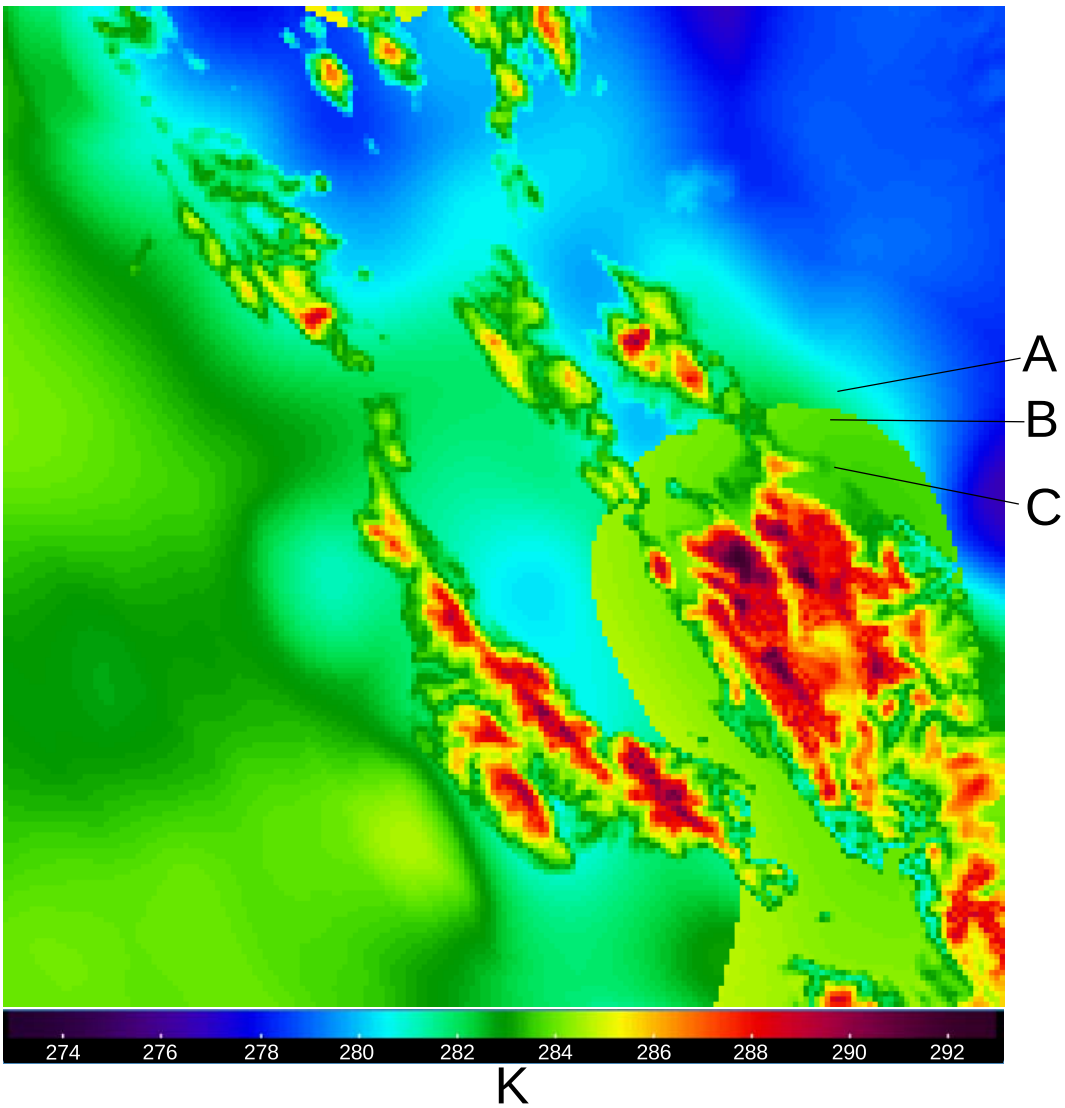

Fig. 7 WRF potential temperature at the lowest prognostic model level (≈12 m AGL) at the initial time (12 UTC 9 February 2012) for Exp. Control. Three locations discussed in the text are labeled "A", "B", and "C".

The details of how the model determined the potential temperature were investigated (Fig. 8) at the 3 grid points labeled in Fig. 7; these points include a point outside the feature (point A), a point within the feature (point B), and a point on the inner edge of the feature (point C). Across the entire domain, Obsgrid will output levels at both 1000 and 975 hPa, because these levels are in the GFS-derived data passed into Obsgrid. Obsgrid will also have a surface level whose pressure varies across the domain. At point A, the surface is at 997 hPa (Fig. 8). Because the 1000-hPA level is within 5 hPa of the surface, this level is omitted from consideration (due to the WRF setting *zap_close_levels*). Therefore, the 997-hPa Obsgrid surface level is used to determine the WRF surface data at its surface of

1025 hPa. At point B (which is within the unrealistic feature), Obsgrid has a surface pressure of 993 hPa; since this is greater than 5 hPa from the 1000-hPa level, the 1000-hPa level is not omitted in this case. The WRF surface is at 1024 hPa, and so uses the closest Obsgrid output level of 1000 hPa to determine the WRF surface values. At point C, the Obsgrid surface remains at 993 hPa, but the WRF surface is 981 hPa. The 975- and 950-hPa levels are removed from consideration because these 2 pressures fall within the first 6 WRF layers above the surface (due to the WRF setting *force_sfc_in_vinterp*), and so the WRF surface value is determined via a combination of the Obsgrid 925-hPa level and surface level (993 hPa). Therefore, the areas in the surface fields (e.g., Fig. 7) that appear relatively smooth with generally small gradients (e.g., point A) are points where WRF is directly using the Obsgrid surface values. The areas with the unrealistic looking feature (e.g., point B) are those where the WRF surface is below the lowest pressure level in the Obsgrid output, and the Obsgrid surface level is neither below the lowest Obsgrid pressure level nor close enough to that level in order to have the lowest Obsgrid pressure level omitted. The areas with the detailed structure (e.g., point C) are those where an interpolation between 2 Obsgrid levels is used to construct the surface data.

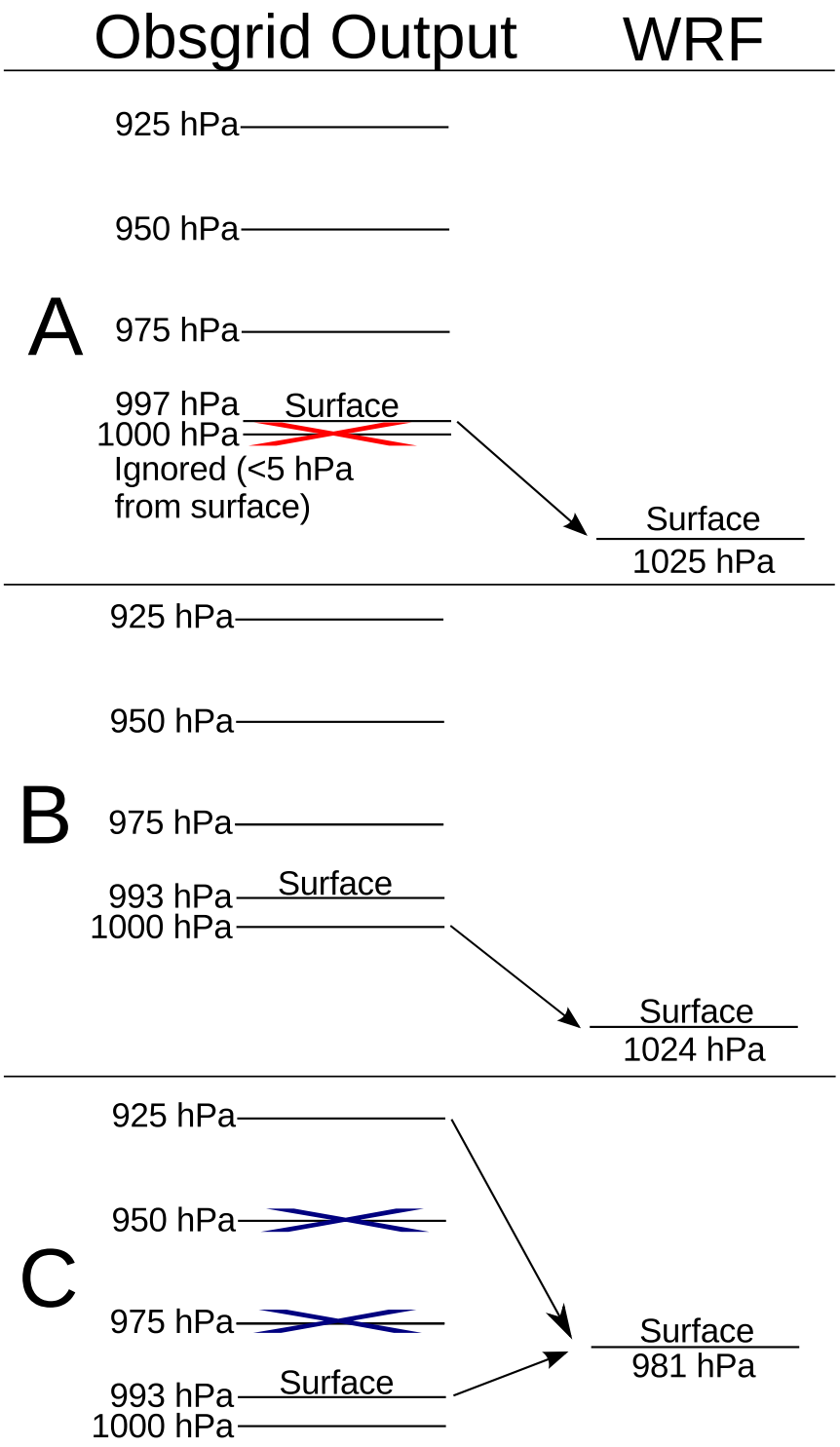

Fig. 8 Diagram of the near-surface levels in the Obsgrid output at 12 UTC 9 February 2012 showing which of these levels is used to construct the WRF surface value for Exp. Control. A red X indicates levels removed from consideration due to being within 5 hPa of the Obsgrid output surface; a blue X indicates levels removed from consideration due to having a pressure greater than that of the sixth WRF model layer.

If the pressure of the Obsgrid surface level better matched the WRF surface pressure, then there would be fewer instances where the Obsgrid surface level is not used in determining the WRF surface values (e.g., point B) and the Obsgrid surface level would tend to be weighted more heavily when it and another Obsgrid level are used to interpolate to create the WRF surface value (e.g., point C). This would decrease the occurrence of the unrealistic looking structure of which point B is a part and should reduce the variation within the highly variable region of which point C is a part. The pressure of the Obsgrid surface level by default does not reflect the pressures of the observations used to derive the Obsgrid surface level fields and so the pressure of the Obsgrid surface level should be enhanced to better represent the pressure of the observations. Adding a surface pressure objective analysis should decrease the differences between the Obsgrid surface pressure and the WRF surface pressure.

Therefore, surface pressure objective analysis was implemented in Obsgrid as described in Section 4.4. However, this effort led to the discovery of further changes that were needed in order to fully benefit from the surface pressure objective analysis.

First, the results of the modifications tested in this study are examined from a more qualitative approach (however, quantification of changes are included). Secondly, verification of the results against observations will be undertaken.

6.1.2 Pre-Verification Evaluation

6.1.2.1 Ungrib Interpolation Bug Fix

The error in the Ungrib interpolation described in Section 4.1 was discovered when surface pressure quality control indicated unexpected patterns. Further investigation revealed that the Metgrid output files showed unexplained vertical structure, which led to the unexpected patterns (Metgrid takes the output of Ungrib as an input and horizontally interpolates the data to the WRF grids for ingestion by Obsgrid). For example, the lowest 21 levels of the temperature field (Fig. 9a) show a pattern where temperature drops at a level, followed by very little change for a few levels, followed by another notable temperature drop. After Ungrib vertically interpolates the GFS data to a given pressure level, that interpolated value can be used as an input to a vertical interpolation to another pressure level. This combined with the vertical interpolation bug in Ungrib led to the vertical pattern in Fig. 9a (Exp. Control). Correcting the bug leads to a much smoother vertical profile in Exp. Ungrib (Fig. 9b).

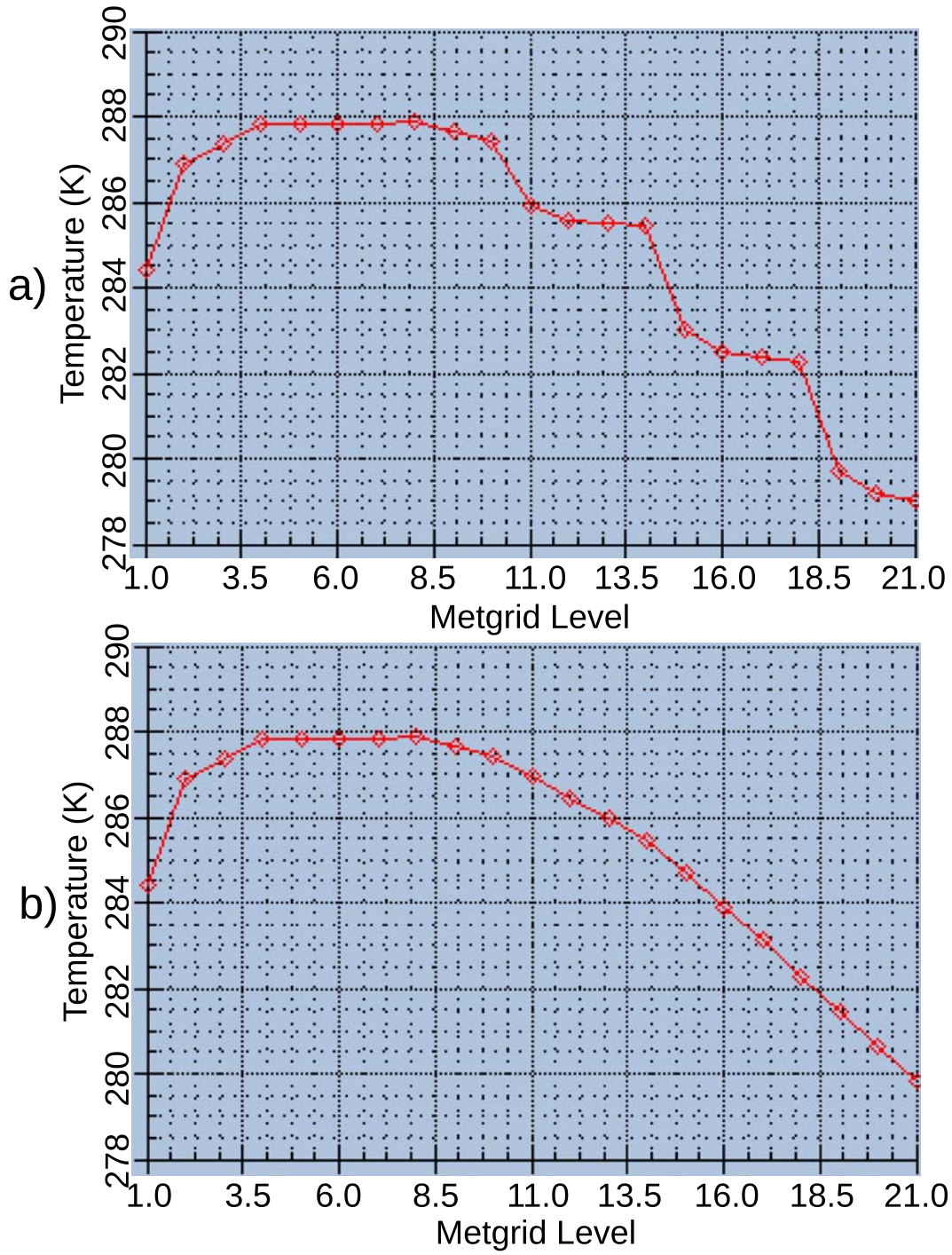

Fig. 9 Temperature profile (K) for the first 21 levels in the Metgrid output for a) Exp. Control and b) Exp. Ungrib

The Ungrib vertical interpolation bug fix can affect the estimation of surface pressure for surface observations missing this quantity. The GFS data vertically interpolated by Ungrib are used to estimate the height-pressure relationship, which is used to estimate surface pressure for observations missing this quantity. The

surface pressure for approximately 59% of surface observations available over the 27-km grid are affected by this update from Exp. Control to Exp. Ungrib (there are about 10100 observations available at the 12 UTC time; some locations contribute multiple observation during this hour). A histogram of the changes (Fig. 10) shows that although the bins with the most observations are those showing little to no change in surface pressure with the vertical interpolation bug fix, there is a fairly broad distribution of pressure decreases. The median change is –7.0 hPa, the mean change is –9.5 hPa, while the largest change is –26.6 hPa.

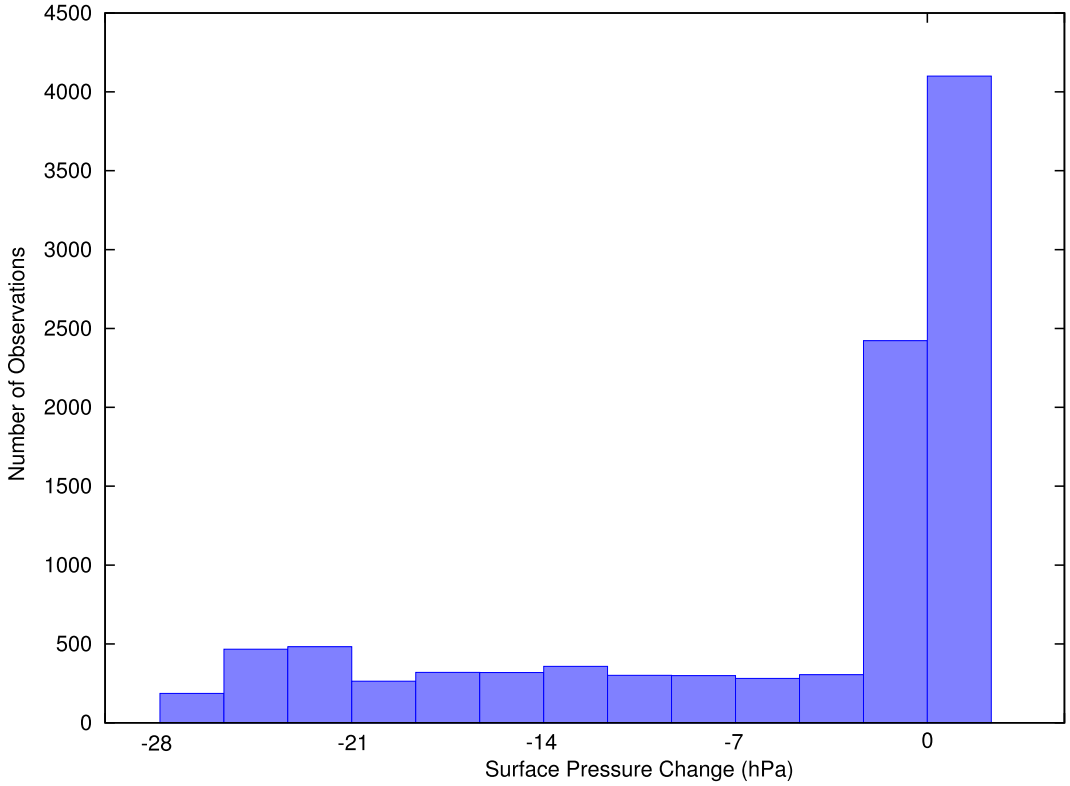

Fig. 10 Histogram of the change in estimated surface pressure of observations at 12 UTC 9 February 2012 as a result of fixing the bug in the Ungrib vertical interpolation (Exp. Ungrib vs. Exp. Control). Note that all observations whose surface pressure did not change are in the rightmost column.

6.1.2.2 Surface Pressure Estimation

Quality control of surface pressure (via converting it to sea-level pressure) revealed unexpectedly high surface pressure "errors" (deviations from the first-guess field or nearby observations). Due to this, the surface pressure estimation techniques described in Section 4.2 were implemented to minimize the use of the standard atmosphere in the estimation process. The new technique altered the surface pressure estimate for about 10% of the observations (1013 out of 10100) on the 27-km domain at 12 UTC. Considering only these 1013 observations the median

pressure change was 10.7 hPa, with changes ranging from –2.2 to 17.6 hPa. The distribution of these changes (Fig. 11) shows a peak in the 9.75 to 11.25 hPa bin.

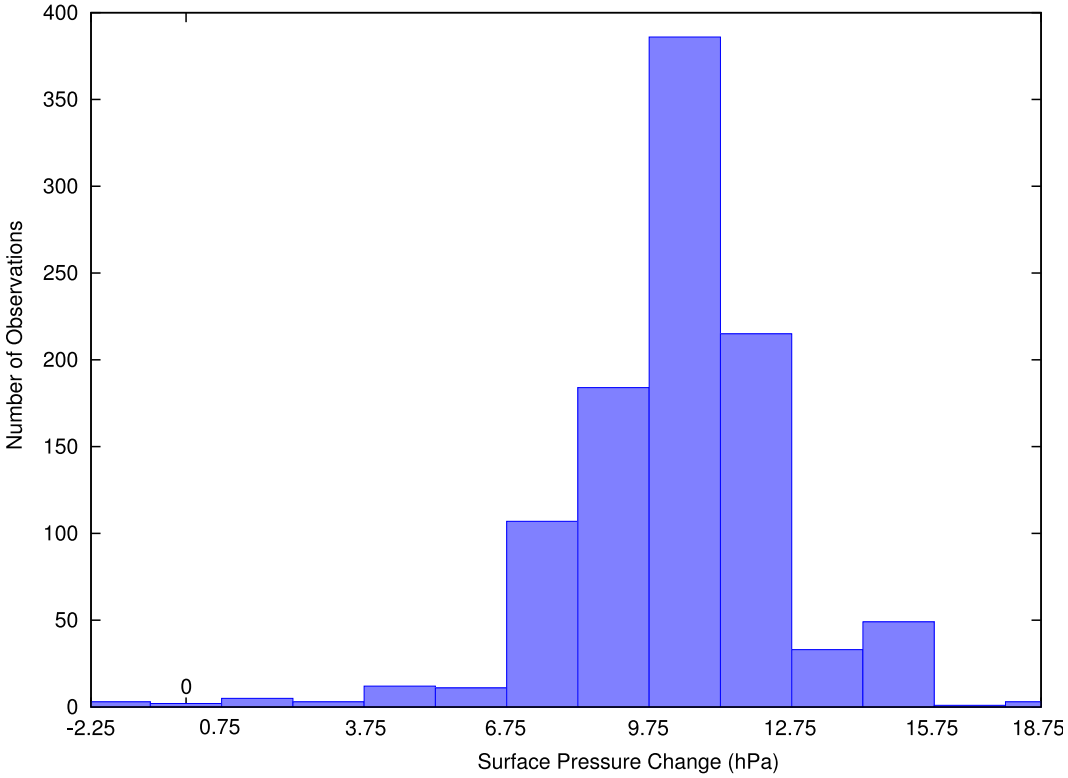

Fig. 11 Histogram of the change in estimated surface pressure of observations at 12 UTC 9 February 2012 as a result of enhancing the surface pressure estimation technique for observations below the lowest first-guess level. Note that observations whose surface pressure did not change are omitted from this figure.

6.1.2.3 Surface Pressure Analysis

Compared to the default Obsgrid capability of using an objective analysis of sea-level pressure analysis to enhance surface pressure (Exp. PQ; Fig. 12a), completing an objective analysis of surface pressure (Exp. PQO; Fig. 12b) creates a more detailed surface pressure field. Note that this is not the surface pressure field used by WRF for its initial condition, but rather the surface pressure used to determine how the surface analysis of other fields should be applied to the WRF model. The actual initial condition surface pressure used by the model for both Exp. PQ and PQO (Fig. 12c) shows more detailed structure than either Obsgrid surface pressure fields, since WRF uses the terrain height for the current domain to calculate surface pressure. However, the objective analysis of surface pressure allows the Obsgrid surface pressure field to better match WRF's initial pressure field (i.e., Fig. 12b better matches Fig. 12c than does Fig. 12a). This is because the observations provide information on the actual terrain that the much coarser GFS cannot resolve.

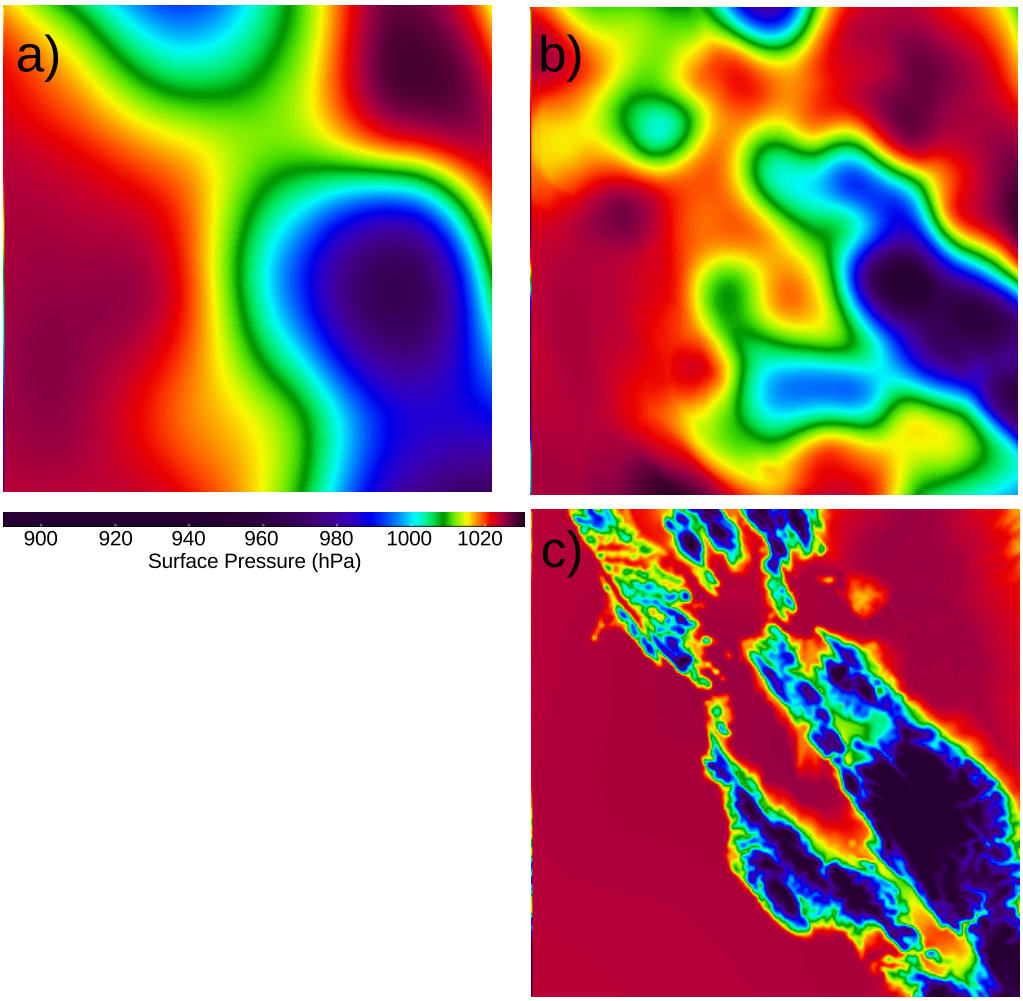

Fig. 12 Surface pressure at 12 UTC 9 February 2012 for 1-km domain output by Obsgrid for a) Exp. PQ, and b) Exp. PQO, compared to c) the WRF initial condition surface pressure for both experiments

The WRF initial condition lowest prognostic model layer potential temperature constructed using the surface pressure objective analysis (Fig. 13b; Exp. PQO) differs from the field created without invoking surface pressure analysis (Fig. 13a; Exp. PQ). Without the surface pressure analysis, there is an area in the southeast quadrant where the structure appears unrealistic due to the very small gradients within the region and large gradients along the edge of the region. The use of surface pressure objective analysis appears to have removed the unrealistic looking potential temperature structure in the southeast quadrant of the domain. In other words, assuming that the potential temperature analysis is valid at the pressure given by the surface pressure analysis (created by analyzing surface pressure observations onto the GFS surface pressure field) removes the unrealistic structure that occurs when one assumes the potential temperature analysis is valid at the GFS surface pressure field.

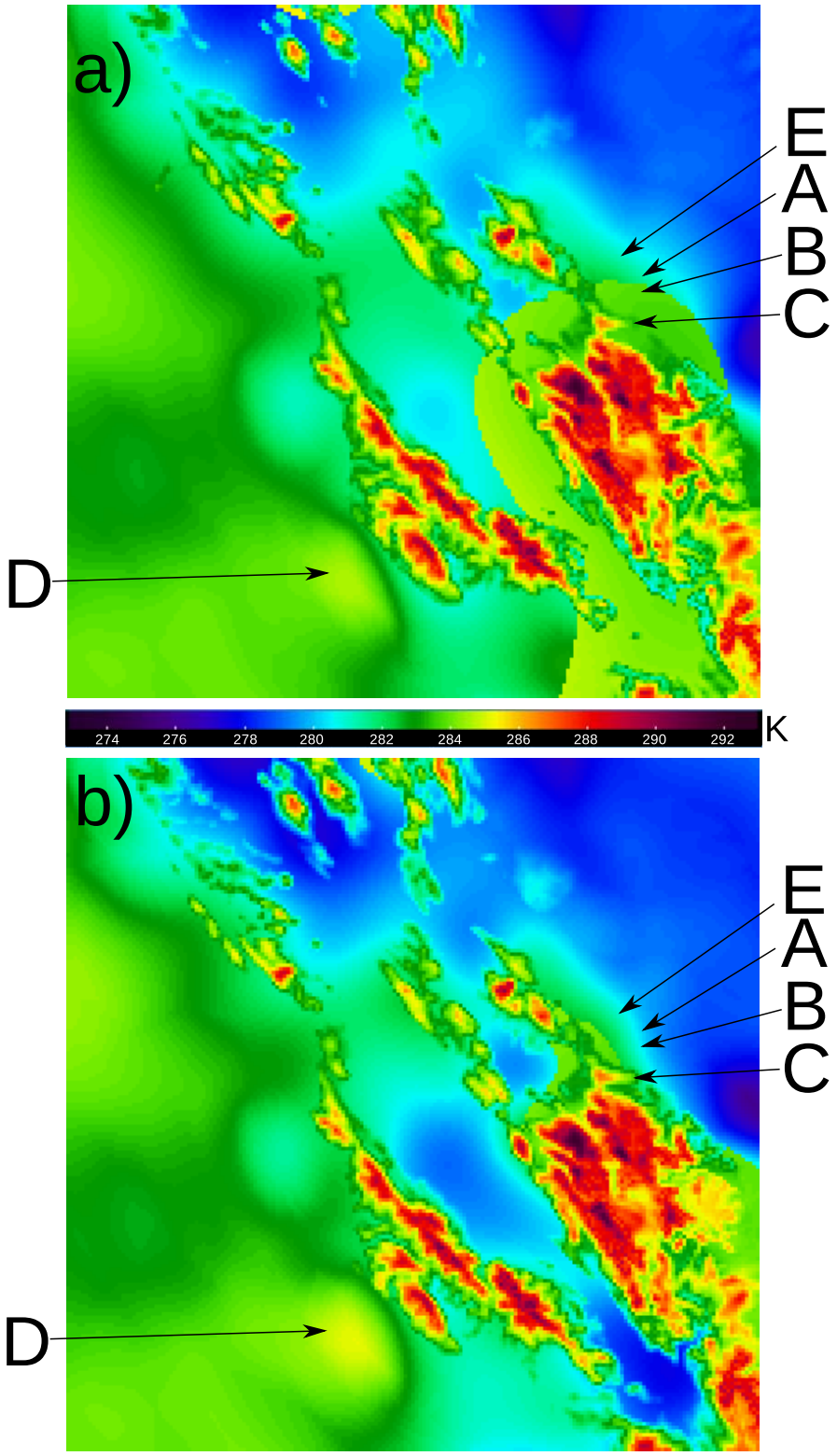

Fig. 13 WRF potential temperature at the lowest prognostic model level (≈12 m AGL) at the initial time (12 UTC 9 February 2012) for a) Exp. PQ and b) Exp. PQO. The five locations discussed in the text are labeled "A", "B", "C", "D", and "E".

The differences between how the WRF surface potential temperature is determined in Exp. PQ versus PQO is explored (Fig. 14) for the same 3 locations (A, B, and C) examined earlier in this report for Exp. Control; these locations are labeled in Fig. 13). As described in Section 6.1.1 for Exp. Control, the surface potential temperature field in Exp. PQ appears to have 3 difference fields overlaid, with each field applied in non-contiguous areas: 1) a field with relatively small gradients (e.g., point A), 2) a field with very small gradients (e.g., point B), and 3) a field with large gradients (detailed structure, e.g., point C). The combination of input fields that led to this structure in Exp. Control were described in Section 6.1.1; the surface potential temperature field in Exp. PQ is the same as Exp. Control and thus this same combination of input fields lead to the structure in Exp. PQ (Fig. 13a). Fig. 14 compares the formation of the surface potential temperature field in Exp. PQ (same as Exp. Control in Fig. 8) to that in Exp. PQO.

Location A is in an area with small horizontal gradients for both Exp. PQ (Fig. 13a) and Exp. PQO (Fig. 13b), and in both, the WRF surface potential temperature is derived from the Obsgrid surface value (Fig. 14). However, in Exp. PQ the 1000-hPa level was actually closer to the WRF surface value (1025 hPa) than the Obsgrid surface level (997 hPa) and thus the 1000-hPa level would have been used for the surface had not it been within 5 hPa of the Obsgrid surface value (WRF does not consider pressure levels within 5 hPa of the Obsgrid surface pressure in determining the surface potential temperature here due to the *zap_close_levels* setting). In Exp. PQO, the Obsgrid surface level (1012 hPa) was closer to the WRF surface than the 1000-hPa level, and thus does not need to rely on the discarding of all levels within 5 hPa of the surface field. For location A, although the inclusion of the surface pressure objective analysis made the Obsgrid surface pressure much more closely match that of WRF (difference decreased from 28 to 13 hPa), it made little difference on the surface potential temperature.

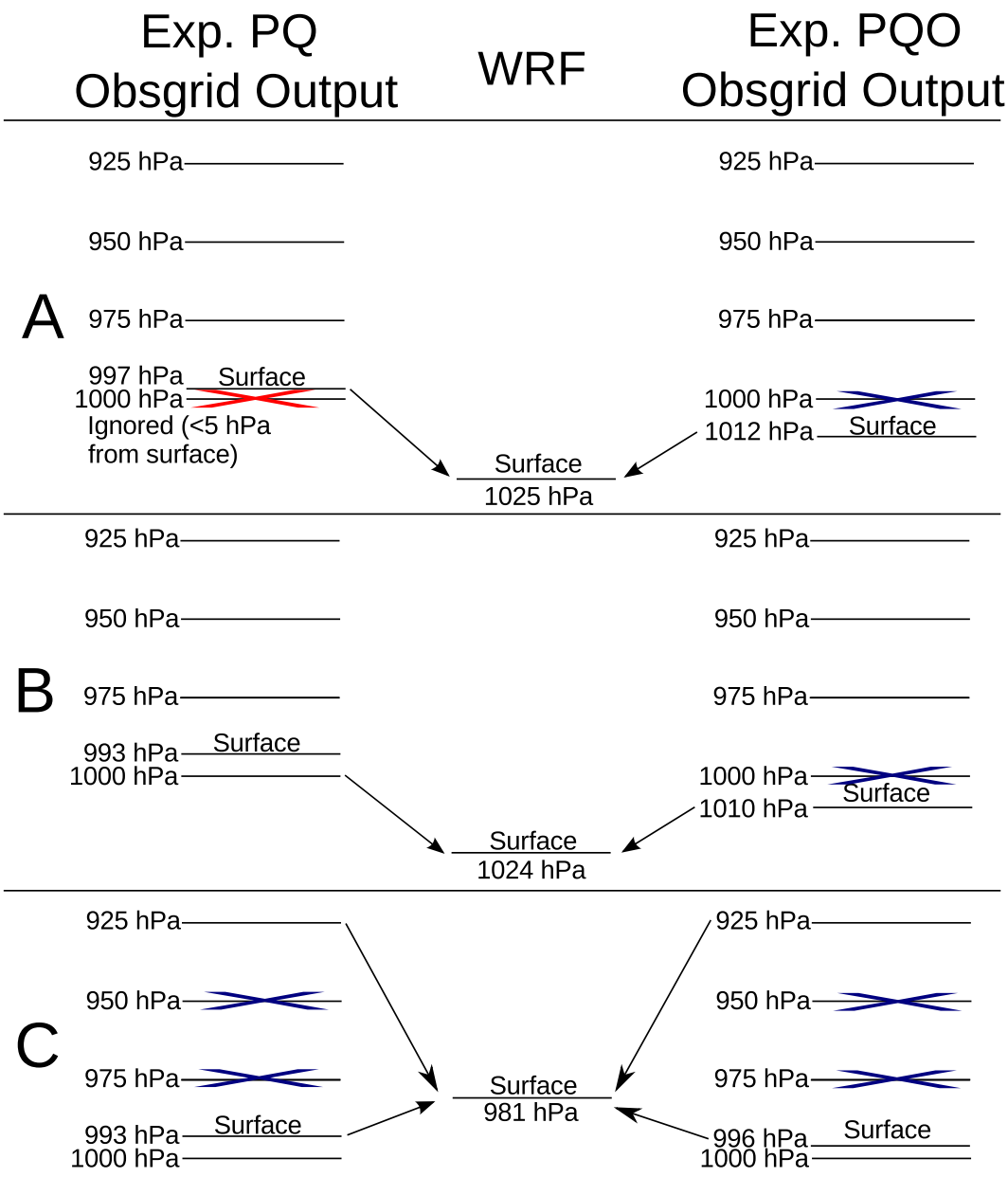

Fig. 14 Diagram of the near-surface levels in the Obsgrid output at 12 UTC 9 February 2012 and which of these levels is used to construct the WRF surface value for Exp. PQ and Exp. PQO. A red X indicates levels removed from consideration due to being within 5 hPa of the Obsgrid output surface; a blue X indicates levels removed from consideration due to having a pressure greater than that of the sixth WRF model layer.

Location B is in the area with very small horizontal gradients for Exp. PQ, and thus within the area where the potential temperature field appears unrealistic, whereas in Exp. PQO location B is in an area with small horizontal gradients of potential temperature. Whereas in Exp. PQ the WRF surface (1024 hPa) potential temperature was obtained from the 1000-hPa level Obsgrid data (the Obsgrid surface pressure was 993 hPa), in Exp. PQO the WRF surface potential temperature

is from the Obsgrid surface level (1010 hPa). Thus the inclusion of the surface pressure analysis results in a surface pressure value that better matches that derived by WRF (13-hPa difference compared to the 31-hPa difference with Exp. PQ), which allows the Obsgrid surface potential temperature field to be used to determine the WRF surface potential temperature.

Location C is in the area with very detailed structure (large potential temperature gradients) for both Exp. PQ and PQO, and in both cases the Obsgrid 925 hPa and surface values are combined to determine the potential temperature at the WRF surface (981 hPa). In Exp. PQO, the Obsgrid surface pressure differs slightly more from the WRF surface pressure than in Exp. PQ (15-hPa difference vs. 12-hPa difference), so the weighting of the Obsgrid 975 hPa and surface values will change somewhat between the experiments, but the resulting potential temperature should be similar.

The use of a surface pressure analysis (Exp. PQO) results in a surface pressure field that more closely matches the observations and more closely matches the surface pressure field used by WRF. Thus, in Exp. PQO, the surface analyses of other fields are more fully utilized in creating WRF initial conditions at the surface than in Exp. PQ. This greatly diminishes the unrealistic "structure" in the initial condition potential temperature field where there are very small horizontal gradients.

Similar reductions in unrealistic looking horizontal structures through the use of the surface pressure analysis occur for other fields as well. The surface v-wind component shows a structure in the southeast quadrant in Exp. PQ (Fig. 15a), the same shape as the structure in the potential temperature field (Fig. 13a); just as with potential temperature (Fig. 13b), the use of the surface pressure objective analysis in Exp. PQO basically eliminates the unrealistic structure (Fig. 15b). The surface water vapor mixing ratio field also shows the same elimination of the unrealistic-looking structure via use of the surface pressure objective analysis (Fig. 16a vs. Fig. 16b).

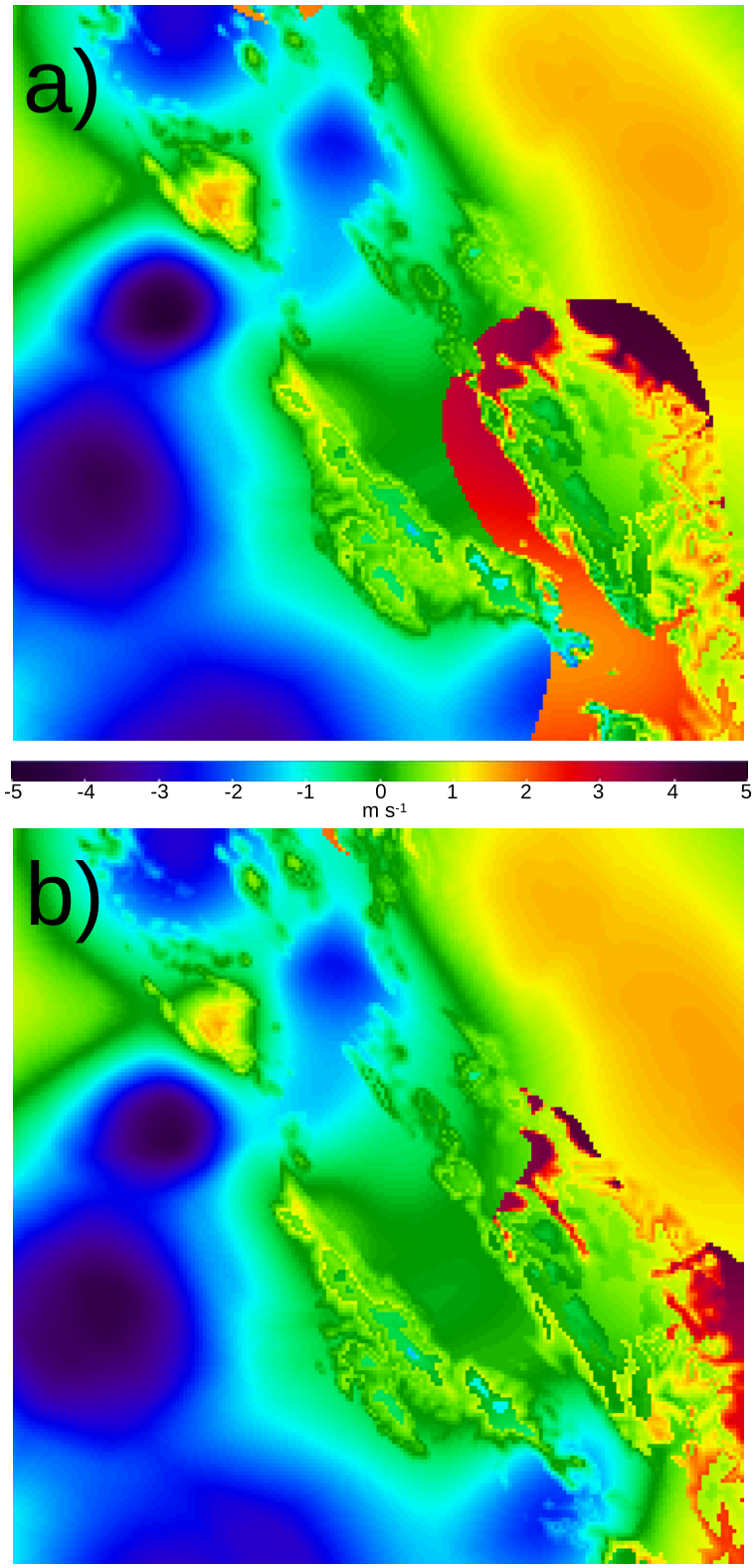

Fig. 15 WRF v-wind component at the lowest prognostic model level (≈12 m AGL) at the initial time (12 UTC 9 February 2012) for a) Exp. PQ and b) Exp. PQO

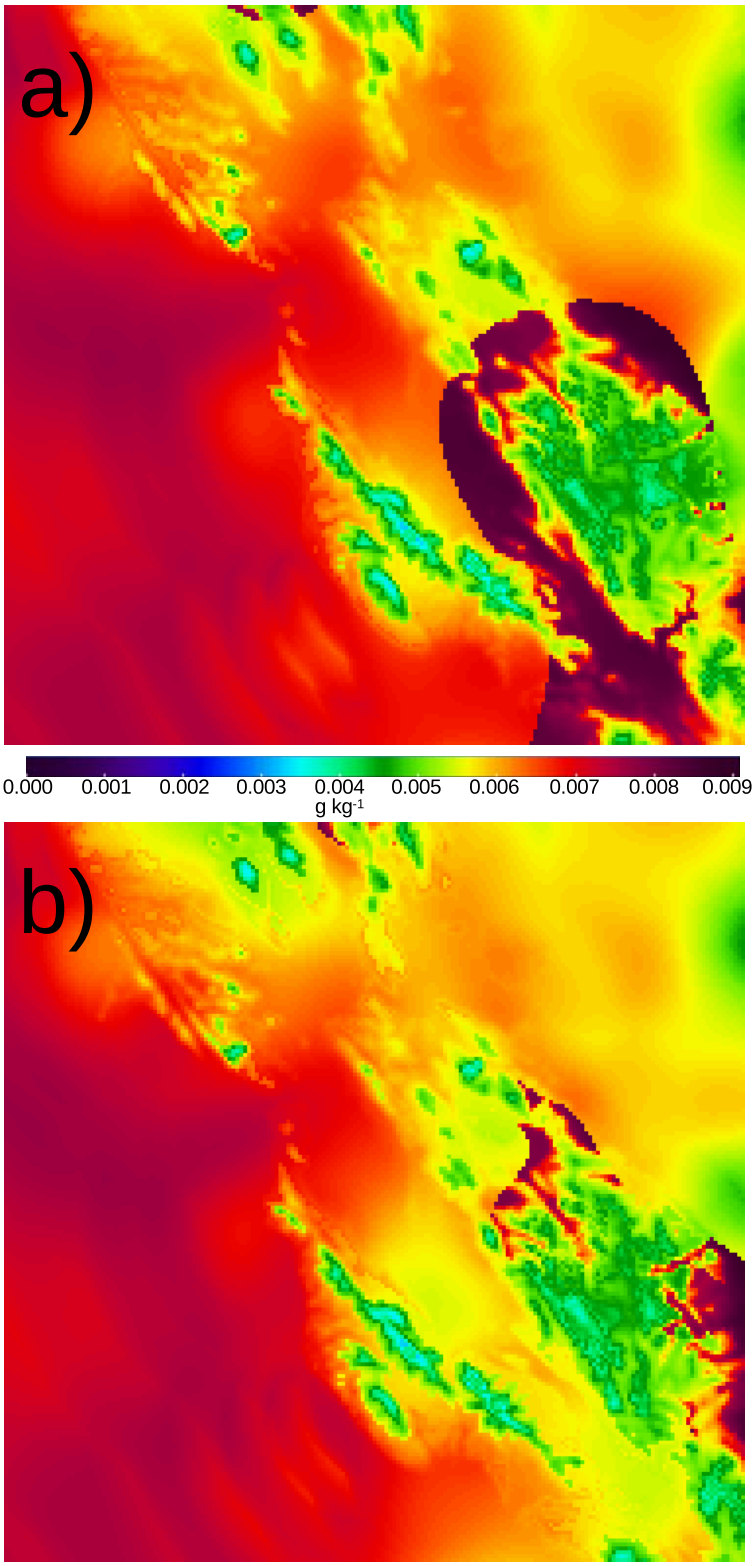

Fig. 16 WRF water vapor mixing ratio at the lowest prognostic model level (≈12 m AGL) at the initial time (12 UTC 9 February 2012) for a) Exp. PQ and b) Exp. PQO

6.1.3 Verification

The use of the surface pressure objective analysis in applying the surface analyses of other fields to WRF has a notable impact on the initial conditions. Each surface temperature observation was evaluated against the lowest prognostic model level temperature (≈12 m AGL) and the absolute error was calculated for each observation. The modeled 2-m diagnostic temperature was not used, because in the output created at the initial time, it has not yet been fully calculated. These absolute errors were then compared between Exp. PQ and Exp. PQO to calculate whether the addition of the surface pressure objective analysis improved the model prediction at that location. Histograms of this comparison (Fig. 17) are used to show the distribution of changes in the fit of the initial conditions to the observations for each domain. For the 1-km domain (Fig. 17d), the bins with the largest number of observations are the 2 bins highlighted in black, which represent changes not exceeding 0.5 K. However, there are also observations in the bins representing improvements up to 7.0 K, but limited number of observations in bins representing degradations >0.5 K. The increased fit of the model initial conditions to the observations is seen most clearly on the finest domain (1-km, Fig. 17d) with the benefits decreasing as the coarseness of the grid increases. On the coarsest domain, degradations appear to potentially outweigh improvements (27-km, Fig. 17a). Overall at 12 UTC, the change in temperature mean absolute error (MAE) when going from Exp. PQ to Exp. PQO for the 27-, 9-, 3-, and 1-km domains are 0.0, 0.5, 0.5, and 0.7 K, respectively.

The time series of MAE indicates the effects of the various initialization strategies on how well the model integration matches observations. For the time series of temperature and dewpoint, the model 2-m diagnostic values are used and the results at the initial time (12 UTC) are omitted since the diagnostic values are not fully calculated for output in the initial time.

Time series of surface temperature MAE for the finest domain (1-km horizontal grid spacing) are shown in Fig. 18a. The non-nudging experiments show no difference between Exp. Control, Ungrib, and PQ; this is not surprising since Exp. Ungrib only changes the vertical interpolation of GFS data used for observational quality control and Exp. PQ only adds surface pressure quality control checks to the observations, while none of these experiments nudges toward the observations. Using the surface pressure objective analysis (Exp. PQO) does show a small improvement for the first couple hours (13–14 UTC) compared to Exp. PQ, consistent with the improvement in the initial conditions demonstrated for comparisons between 2-m observations and lowest prognostic level model data. The use of nudging (compare Exp. Nud to Exp. Control or Exp. NudPQO to Exp. PQO) decreases surface temperature model error through approximately

2200 UTC, even though nudging is completely disengaged by 1900 UTC. The use of the surface pressure objective analysis appears to have slightly degraded the model surface temperature for the nudging case (e.g., compare Exp. Nud and Exp. NudPQO).

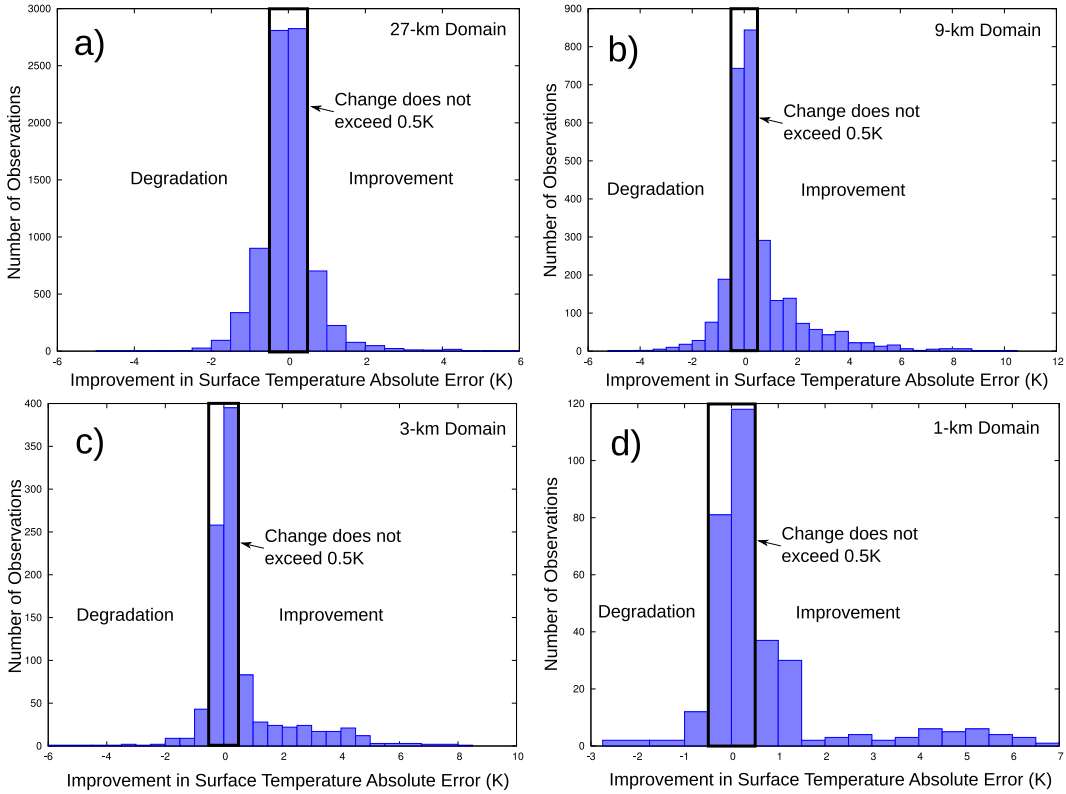

Fig. 17 Histogram of change in absolute error of initial condition surface temperature resulting from the use of a surface pressure objective analysis (Exp. PQ vs. Exp. PQO) for the a) 27-km, b) 9-km, c) 3-km, and d) 1-km domains. Note that the lowest diagnostic level temperature (≈12 m) was evaluated against 2-m observations.

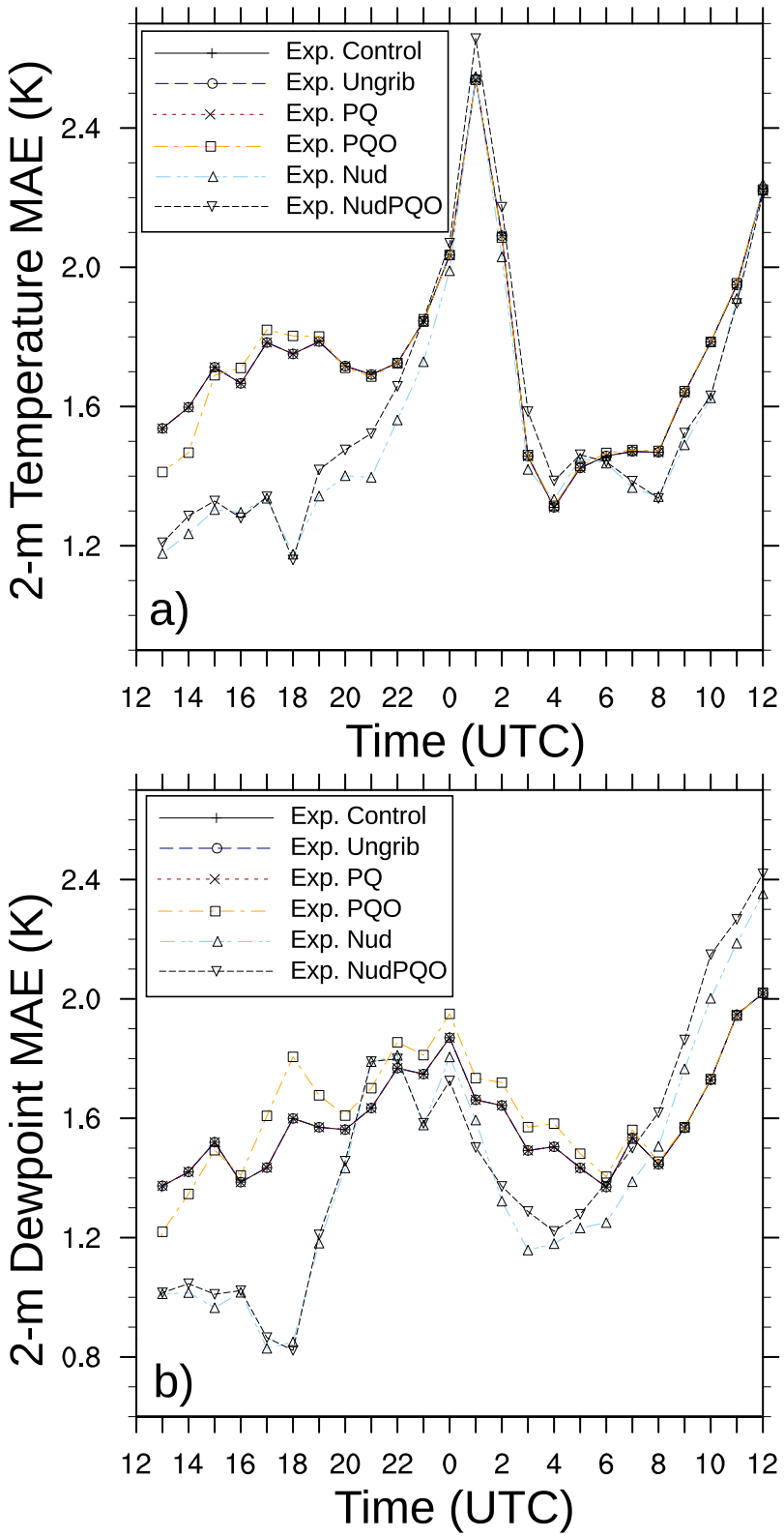

Fig. 18 Time series of MAE of WRF 1-km domain a) 2-m temperature and b) 2-m dewpoint both evaluated against the model 2-m diagnostic values

The improvements in the model surface temperature from applying the surface temperature analysis based on an objective analysis of surface pressure for the non-nudging experiments (Exp. PQ vs. Exp. PQO in Fig. 18a for 13-14 UTC) appear to be in conflict with the slight degradation for the same change in the nudging experiments (Exp. Nud vs. Exp. NudPQO). The surface pressure objective analysis allows a larger area of the surface analyses of fields such as temperature to be used in the WRF initial conditions, and thus surface observations are more fully reflected in the WRF initial conditions. However, this change does not affect the ability of these observations to be nudged toward with observation nudging. Apparently, nudging toward the observations during the first portion of the model integration is able to compensate for the lesser utilization of the surface observations in the initial conditions.

Time series of the verification of other surface fields on the 1-km domain either supports the conclusions gleaned from surface temperature or are inconclusive. Surface dewpoint (Fig. 18b) results are similar to surface temperature results but the benefits of nudging last only through about 2000 UTC. The wind verification (not shown) is slightly more difficult to interpret on the 1-km domain; quality control removes more wind observations than temperature/moisture, and thus perhaps the verification results are less robust and more likely to have temporal variability.

For the coarsest domain (27-km horizontal grid spacing), the nudging experiments indicate that the addition of the Ungrib bug fix, quality control for surface pressure observations, and an objective analysis of surface pressure all combined (Exp. Nud vs. Exp. NudPQO) improves the model surface temperature throughout the model integration (Fig. 19a). This is in contrast to the 1-km domain where this comparison suggested a slight degradation. Because there are multiple differences between the configuration of Exp. Nud and Exp. NudPQO, an additional experiment was formulated that differed from Exp. Nud only in that it incorporated the Ungrib bug fix (Exp. NudUngrib). The temperature MAE time series from this experiment (not shown) revealed that most of the differences between Exp. Nud and Exp. NudPQO appear to be due to the fix of the Ungrib interpolation bug. The Ungrib interpolation is used to create additional pressure levels for quality control of observations. These pressure levels are also used when estimating surface pressure for observations that are missing surface pressure or whose surface pressure has previously been estimated using a standard atmosphere. This means that fixing the Ungrib interpolation bug also improves the estimation of surface pressure. This is important for observation nudging because WRF uses the observed surface pressure to convert the observed temperature into potential temperature for nudging.

In the nudging experiments, on the 27-km domain, the combined effect of the changes (Exp. Nud vs. Exp. NudPQO) on fields other than temperature are more mixed than for temperature. For surface dewpoint (Fig. 19b), a small degradation is seen in the middle of the integration (≈17–23 UTC), but a small improvement was seen for the last ≈10 h of the simulation (≈2–12 UTC). For wind speed, there is a very small improvement during parts of the simulation (Fig. 20a), but wind direction (Fig. 20b) has very small improvements at the beginning of the simulation, transitioning to small degradations during the middle portion of the integration (22 to 03 UTC).

For surface temperature (Fig. 19a) and dewpoint (Fig. 19b), the non-nudging experiments indicate the use of the surface pressure objective analysis degraded the 27-km domain model values during the first few hours (approximately 13–17 UTC; Exp. PQ vs. Exp. PQO); this is in contrast to the 1-km domain but consistent with the earlier evaluation of the model initial condition lowest prognostic level temperature against surface observations. However, the surface pressure objective analysis has little effect on how closely the model matches observed wind speed (Fig. 20a) and direction (Fig. 20b) for the non-nudging 27-km domain.

The 27-km domain is similar in resolution to the 0.5° GFS data (≈55-km grid spacing) used as the first guess for the surface pressure objective analysis and thus modifying the 27-km surface pressure field based on observations is less likely to improve the surface pressure field than when the methodology is applied to a finer domain (e.g., 1-km domain). The analysis may in fact degrade how well the Obsgrid-created surface pressure field represents the actual terrain. Therefore, Exps. PQO931 and NudPQO931, based on the non-nudging Exp. PQO and the nudging Exp. NudPQO, respectively, were formulated that omitted the surface pressure objective analysis from the 27-km domain only. For surface temperature, on the 27-km domain the non-nudging Exp. PQO931 is equivalent to Exp. PQ, and thus the degradation in the first few hours due to the use of the surface pressure objective analysis (Exp. PQ vs. Exp. PQO) is removed by using Exp. PQO931 (Fig. 21a). In the nudging Exp. NudPQO931, the surface temperature MAE time series very closely matches that of Exp. NudPQO; this means that improvements previously seen from changing from Exp. Nud to Exp. NudPQO are not lost. This is because, as previously shown, on the 27-km domain the benefits from changing from Exp. Nud to Exp. NudPQO are mostly due to the Ungrib vertical interpolation bug fix, and thus removing the surface pressure objective analysis from the 27-km domain (Exp. NudPQO931) does not degrade the results.

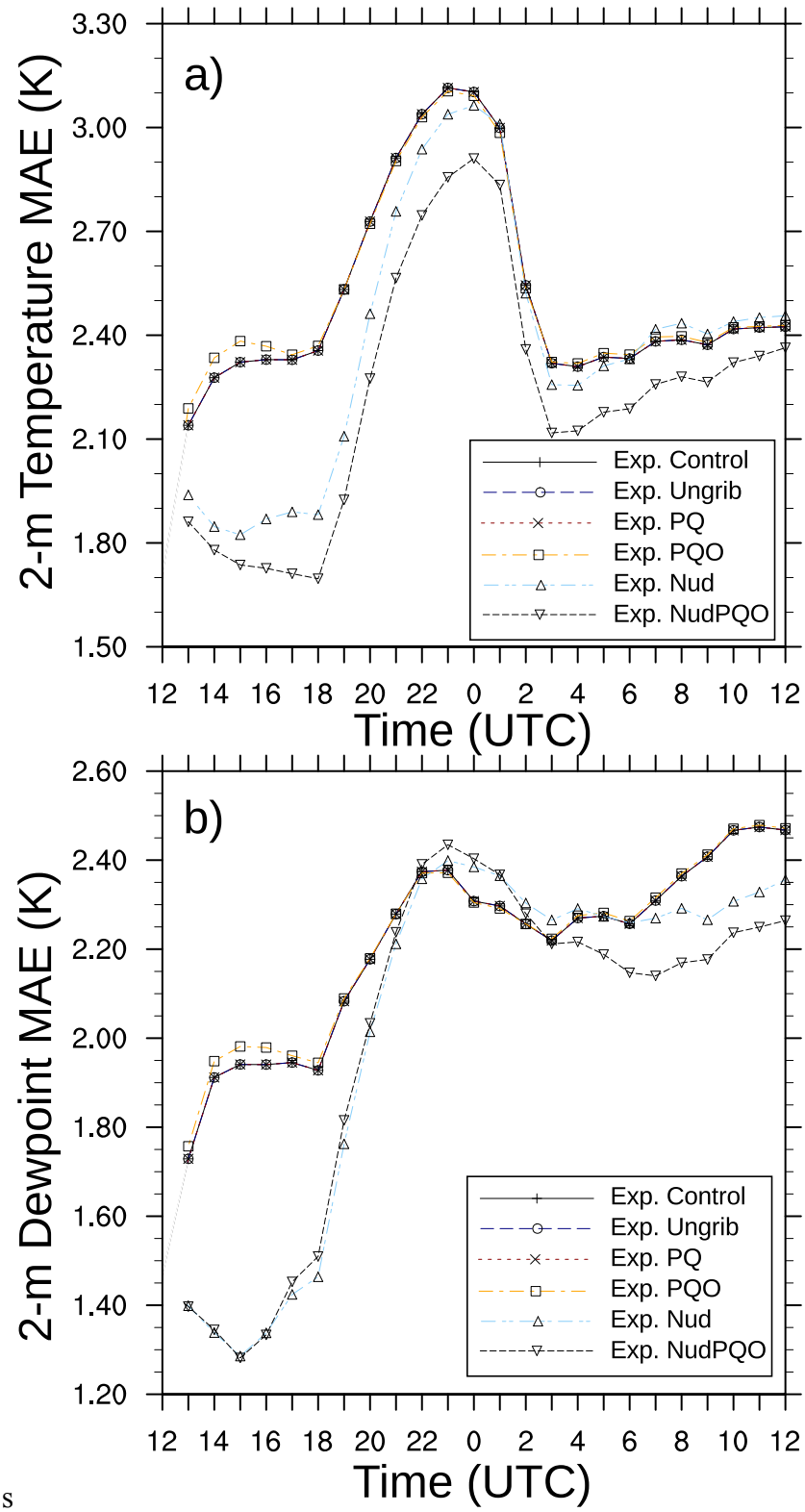

s

Fig. 19 Time series of MAE of WRF 27-km domain a) 2-m temperature and b) 2-m dewpoint both evaluated against the model 2-m diagnostic values

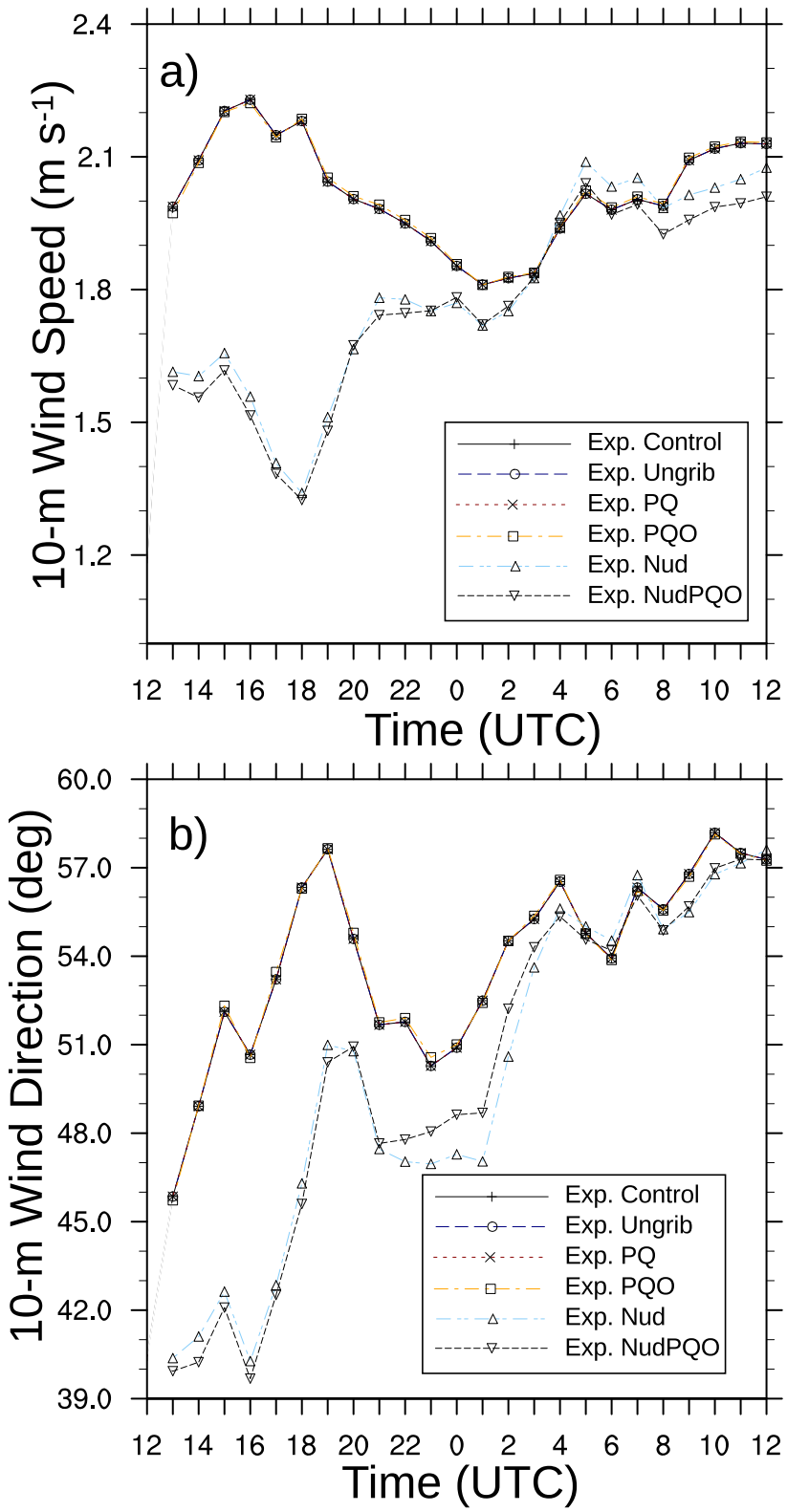

Fig. 20 Time series of MAE of WRF 27-km domain a) 10-m wind speed and b) 10-m wind direction both evaluated against the model 10-m diagnostic values

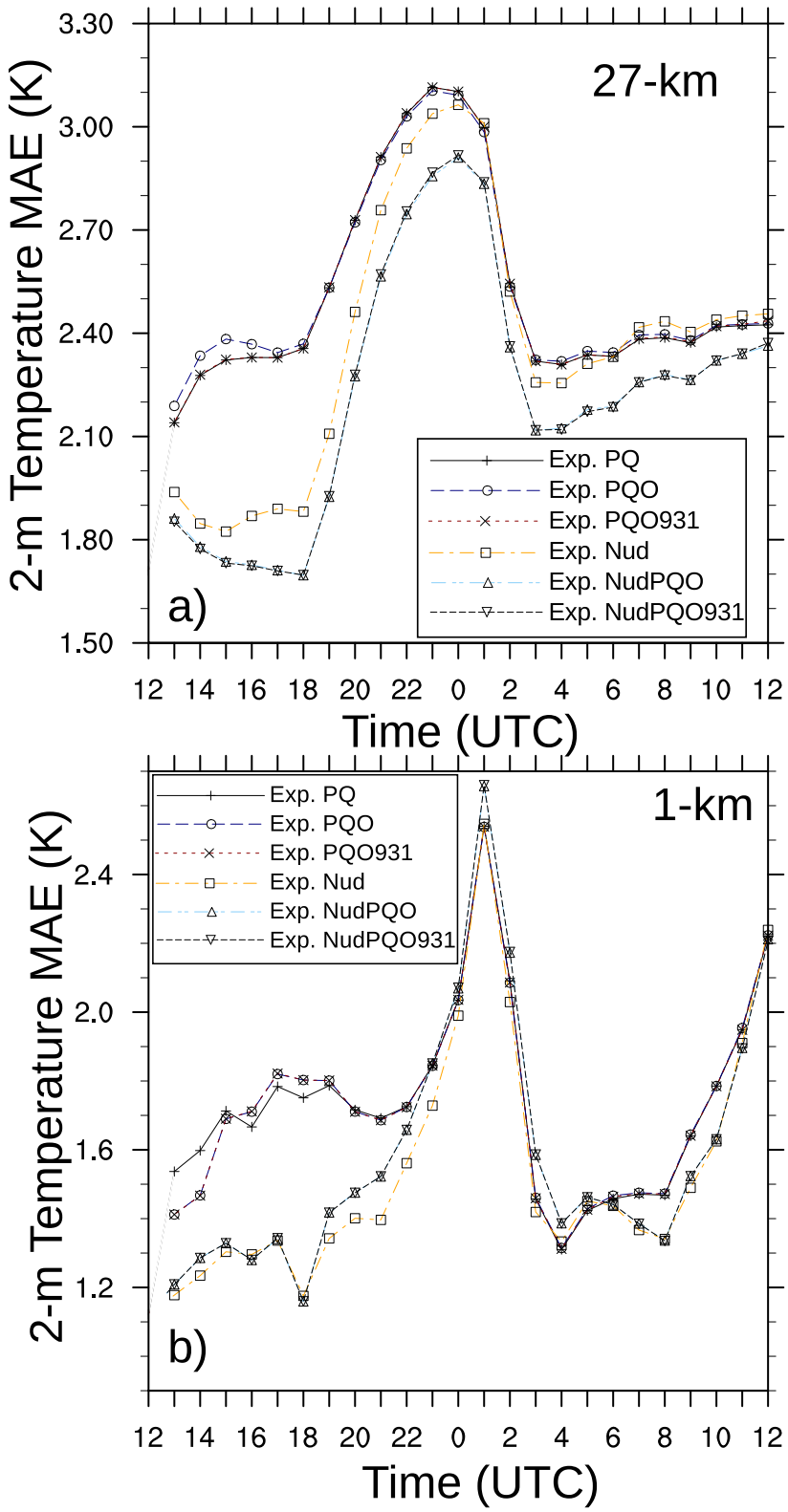

Fig. 21 Time series of MAE of WRF 2-m temperature evaluated against the model 2-m diagnostic values for the WRF a) 27-km and b) 1-km domains

Although Exp. PQO931 and NudPQO931 do not change the configuration of the 1-km domain compared to Exp. PQO and NudPQO, changes can be effected through the boundary conditions the 27-km domain provides to the 9-km domain, which, in turn, provides boundary conditions to the 3-km domain, which finally provides boundary conditions to the 1-km domain. However, the surface temperature MAE time series suggests any effects of removing the surface pressure objective analysis from the 27-km domain on the 1-km domain are very minor, at least in terms of surface temperature (Fig. 21b). The domain-average surface temperature MAE of Exp. PQO very closely matches that of Exp. PQO931, and the same for Exp. NudPQO and Exp. NudPQO931.

Based on the evaluations shown here, Exp. PQO931 and Exp. NudPQO931 appear to be the experiments that perform best. These experiments are used in the evaluation of the benefits of the surface pressure quality control and objective analysis over additional case days.

6.2 Evaluation of Methodology

Based on the detailed examination of the 9 February 2012 case day model simulations, the experiments described in Section 5.2 were formulated to test the potential utility of surface pressure quality control and objective analysis over 4 additional case days.

6.2.1 Initial Conditions

The improvement in WRF initial condition surface temperature due to the use of the surface pressure objective analysis is shown in Fig. 22. For each of the 4 case days examined in this section, the observations are binned by the change in the absolute temperature error caused by the inclusion of the surface pressure objective analysis (Exp. Control+ vs. Exp. PQO931). The lowest model prognostic level air temperature (≈12 m AGL) is used since the model diagnostic 2-m air temperature is not fully calculated in the initial conditions. There is generally more improvement than degradation for each of the case days. However, there are notable differences among the 4 days. On 7 February, the number of observations with degradation >1.0 K is higher than the other 3 days, and there are very few observations with improvements >3.0 K. The case of 5 March is on the opposite end, wherein there are multiple observations with improvements fitting in each bin, including the bin representing improvements between 9 and 10 K.

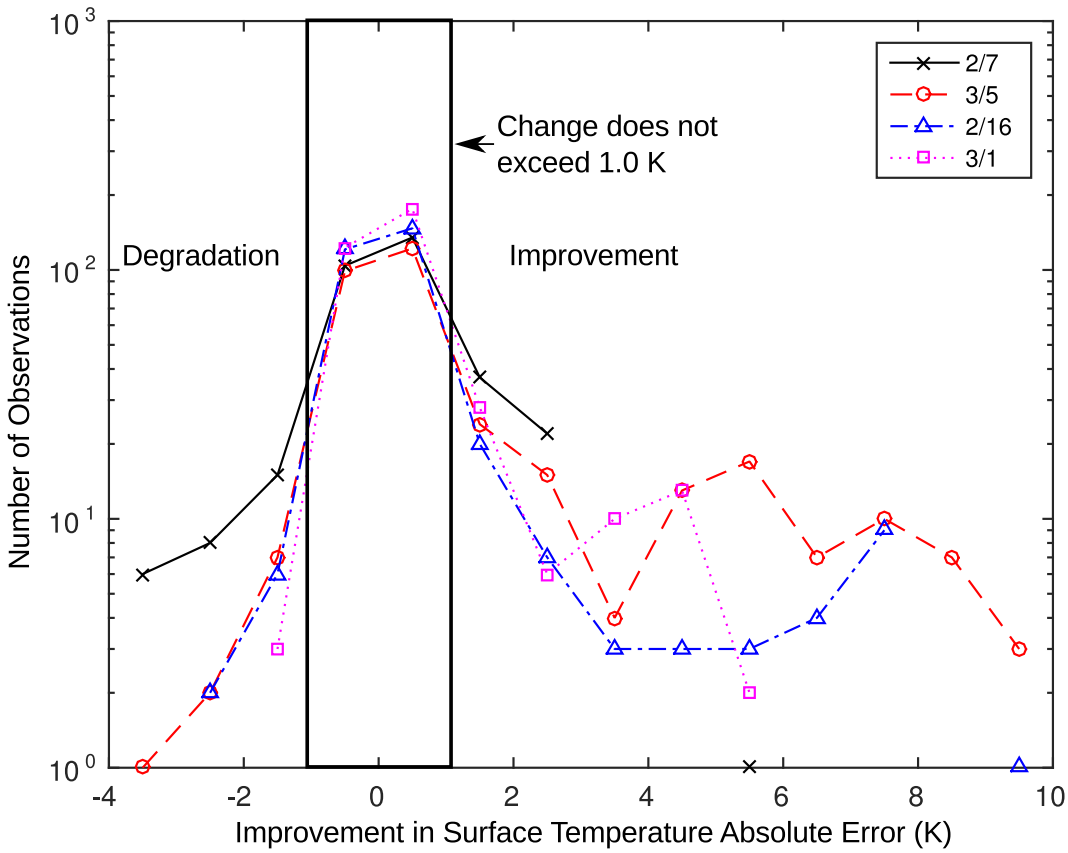

Fig. 22 Histogram of the change in absolute error of initial condition (12 UTC) surface temperature resulting from the use of a surface pressure objective analysis (Exp. Control+ vs. Exp. PQO931) for 4 case days. Note that the lowest diagnostic level temperature (≈12 m AGL) was evaluated against 2-m AGL observations. The symbols are plotted in the center of each 1-K-wide bin on the x-axis. The number of observations in each bin is plotted logarithmically.

A comparison of the surface temperature (lowest prognostic level, ≈12 m AGL) in the WRF initial conditions without the surface pressure objective analysis (Exp. Control+) and with the surface pressure objective analysis (Exp. PQO931) is shown for the 4 cases in Fig. 23 (7 February), Fig. 24 (16 February), Fig. 25 (1 March), and Fig. 26 (5 March). Recall that in the 7 February case, the histogram indicated a larger number of observations where adding the surface pressure objective analysis degraded the initial conditions compared to the other 3 case days. As in the 9 February case (Fig. 7) investigated earlier in this study, the surface temperature field for the 7 February case (Fig. 23a) appears to consist of 3 fields overlaid. Part of the domain has relatively small horizontal gradients (e.g., the southwestern third and the northeast corner), part of the domain has relatively large horizontal gradients (e.g., the structures oriented roughly southeast to northwest), and finally part of the domain has very small gradients (e.g., the large area with a potential temperature of approximately 287.5 K mostly in the southeast quadrant of the domain). The area with very small gradients was referred to in Section 6.1.1 as

the unrealistic-looking structure, and was found for the 9 February case to be regions where the GFS surface temperature was not used to determine the WRF initial condition surface temperature because the GFS surface pressure differed too much from the WRF initial condition surface pressure. The size of this unrealistic looking feature is larger in this 9 February case (Fig. 23a) than in the 7 February case (Fig. 7). Also, much more of the structure remains in the 7 February case after the addition of the surface pressure objective analysis (Fig. 23b vs. Fig. 13b), and some additional areas are added to this structure by adding the surface pressure objective analysis.

The reasons that the "unrealistic structure" is less effectively removed (and the structure is actually introduced in some portions of the domain) in the 9 February case compared to the 7 February case is due to differences in the surface pressures on the 2 days and how they relate to the pressure levels available from the GFS output.

To illustrate the reason for the additional area covered by the unrealistic structure, consider the point labeled D in Fig. 23. In Exp. Control+ this is not part of the unrealistic structure (Fig. 23a), while in Exp. PQO931 the unrealistic structure now includes this area (Fig. 23b). The reason that this occurs is demonstrated in the diagram at the top of Fig. 27. The WRF surface pressure is 1006.8 hPa, while the Obsgrid surface pressure in Exp. Control+ is 1001.6 hPa. This means that the surface level is the level in the Obsgrid output whose pressure is closest to the WRF surface (and there are no levels in the Obsgrid output with a pressure higher than 1001.6 hPa) and thus the Obsgrid surface fields are used as the WRF surface fields. However, in Exp. PQO931, the Obsgrid surface pressure has decreased to 994.5 hPa, presumably due to surface pressure observations over land where the being spread over the ocean. The question then arises as to why this issue was not seen in our earlier comparisons with (Exp. PQO; Fig. 13b) and without the surface pressure objective analysis (Exp. PQ; Fig. 13a) for 9 February. The diagram in Fig. 27 shows that for that case the Obsgrid surface pressure also decreased at point D by using the surface pressure objective analysis (from 1018.5 hPa to 1014.6 hPa); however, with the WRF surface pressure being 1024.2 hPa, in that case the closest Obsgrid level to the WRF surface in terms of pressure is the Obsgrid surface level (and there are no Obsgrid levels with a pressure exceeding that of the Obsgrid surface level). Therefore, for 9 February, the Obsgrid surface level is used as the WRF surface both with and without the surface pressure objective analysis.

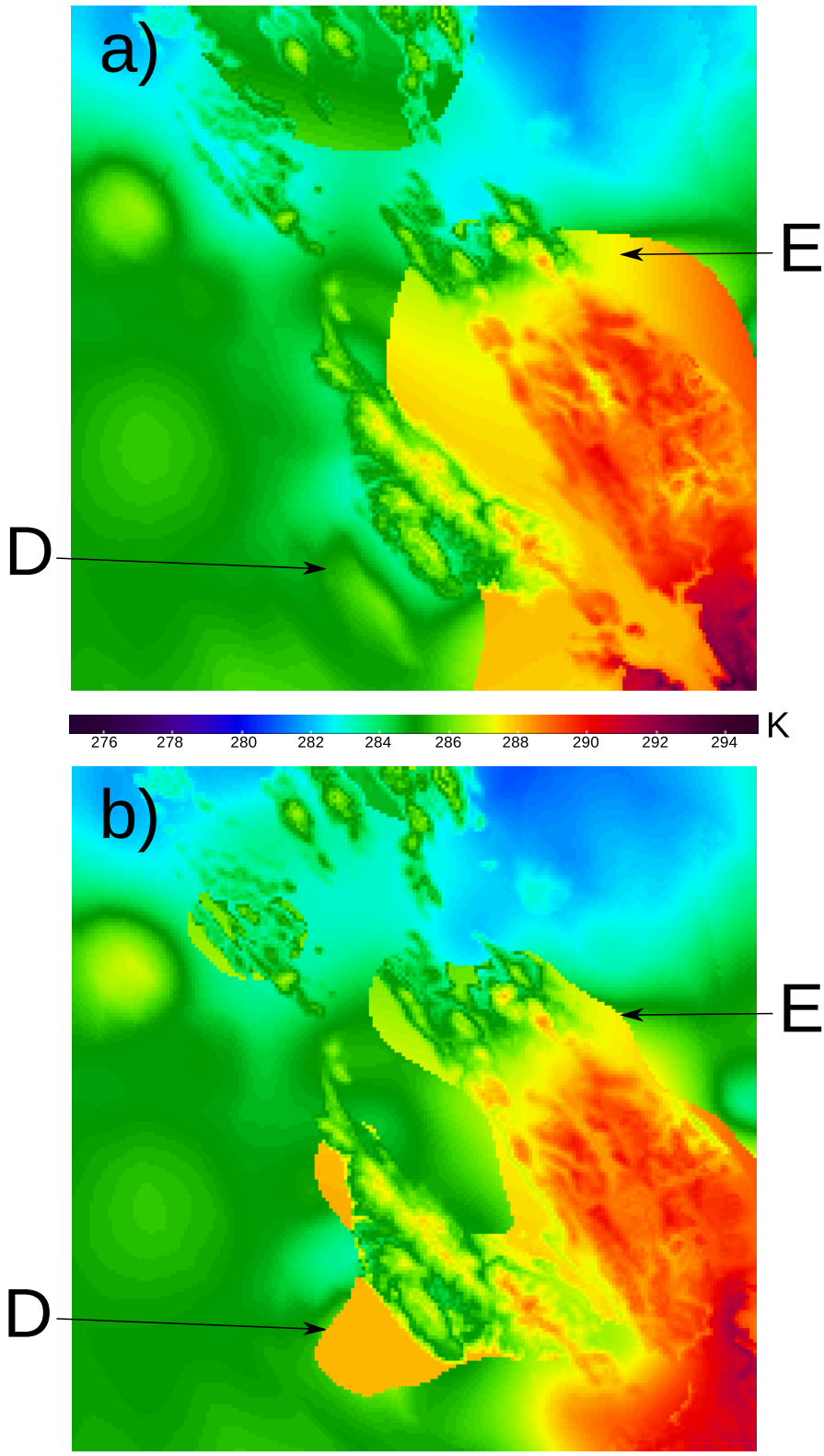

Fig. 23 WRF potential temperature at the lowest prognostic model level (≈12 m AGL) at the initial time (12 UTC) on 7 February 2012 for a) Exp. Control+ and b) Exp. PQO931. The location of points D and E discussed in the text are also shown.

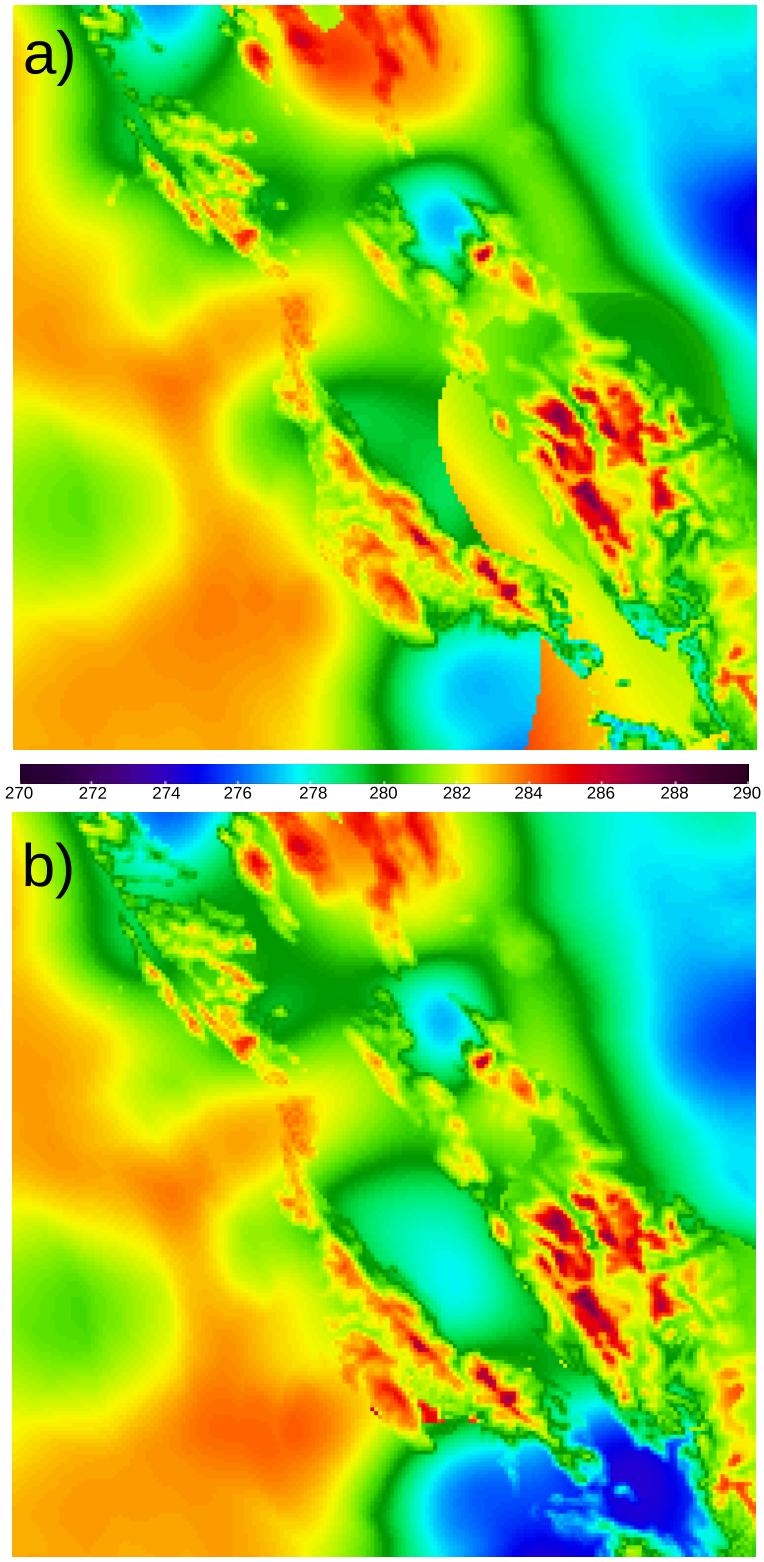

Fig. 24 WRF potential temperature at the lowest prognostic model level (≈12 m AGL) at the initial time (12 UTC) on 16 February 2012 for a) Exp. Control+ and b) Exp. PQO931

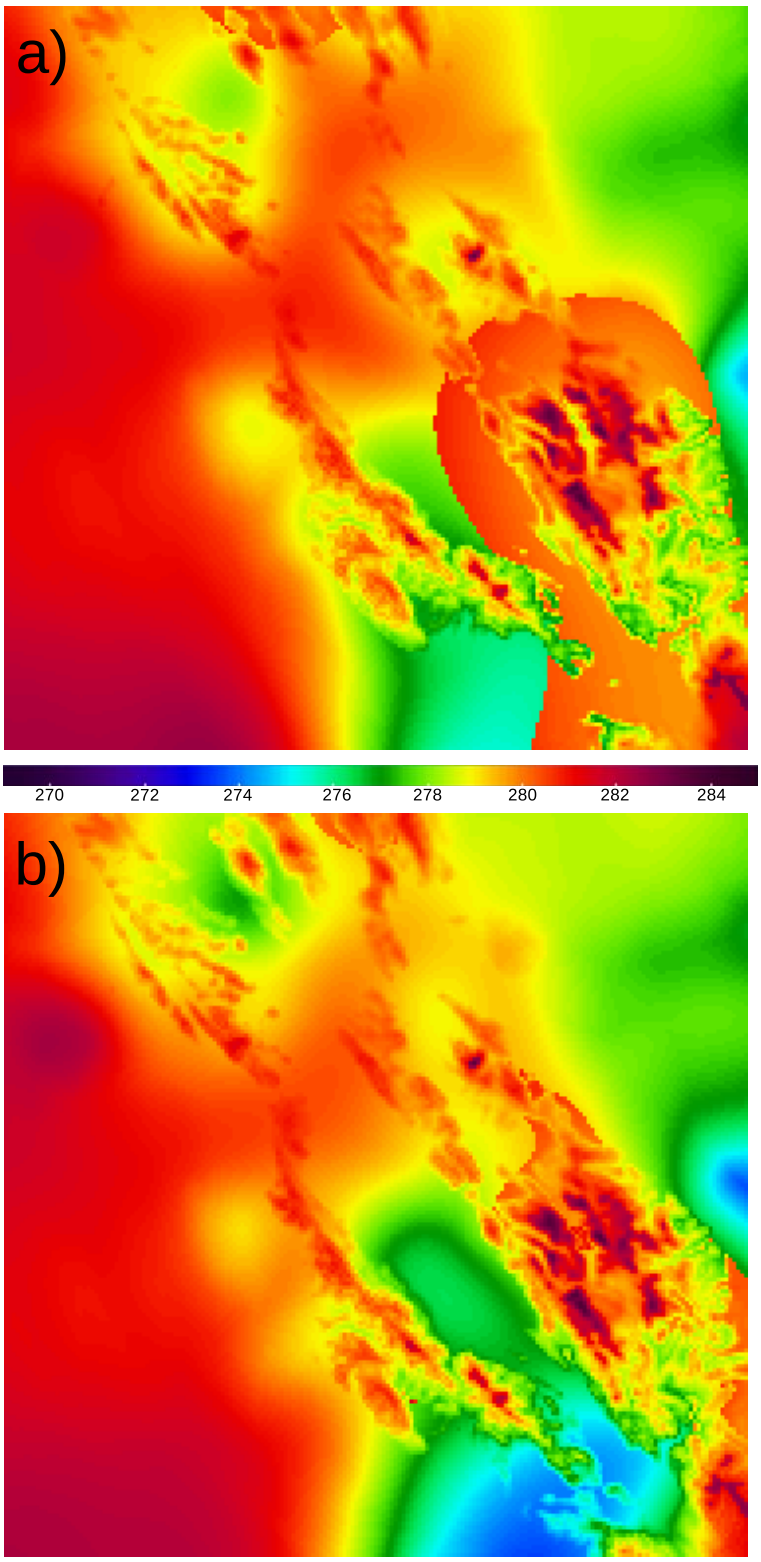

Fig. 25 WRF potential temperature at the lowest prognostic model level (≈12 m AGL) at the initial time (12 UTC) on 1 March 2012 for a) Exp. Control+ and b) Exp. PQO931

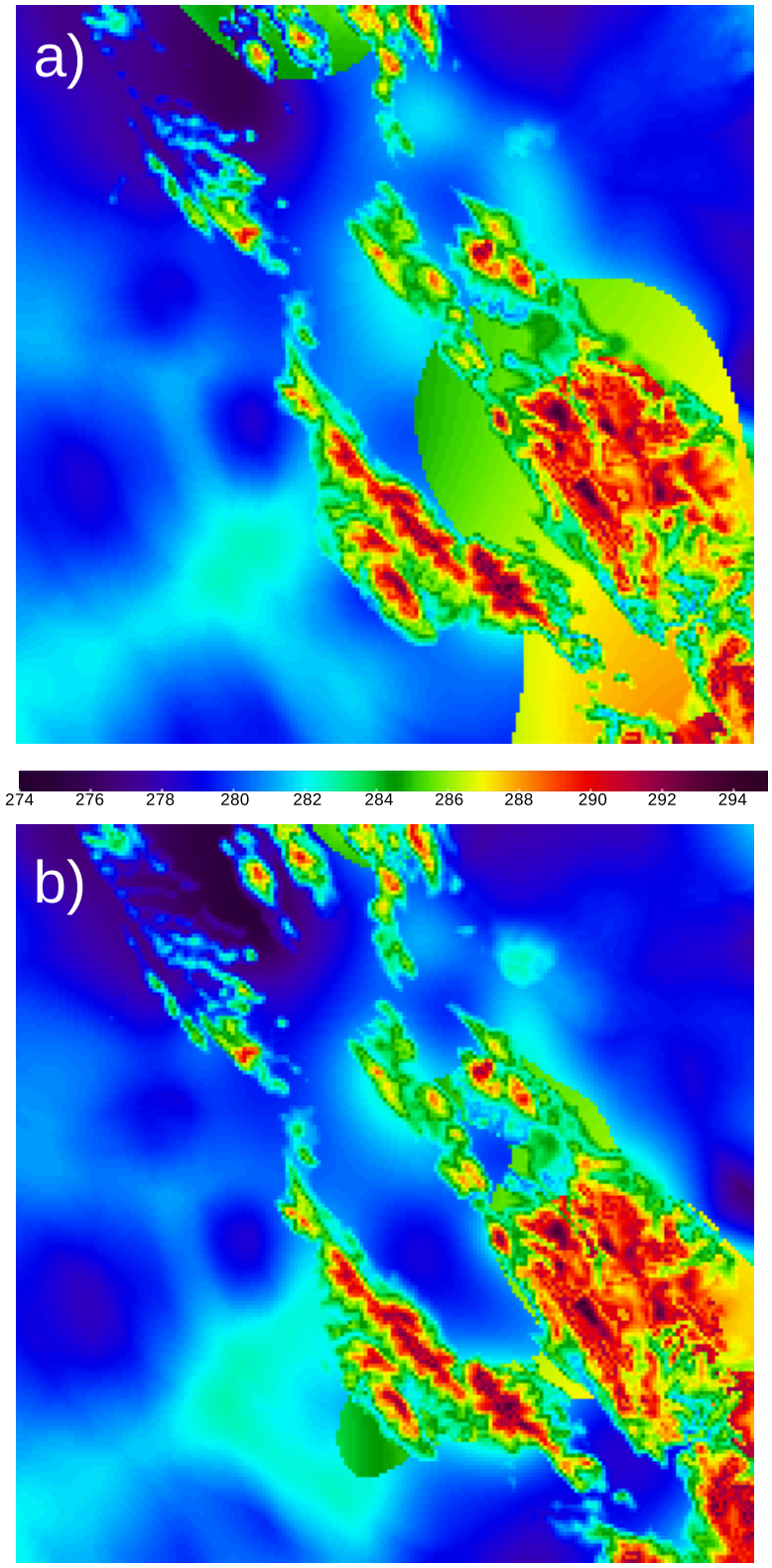

Fig. 26 WRF potential temperature at the lowest prognostic model level (≈12 m AGL) at the initial time (12 UTC) on 5 March 2012 for a) Exp. Control+ and b) Exp. PQO931

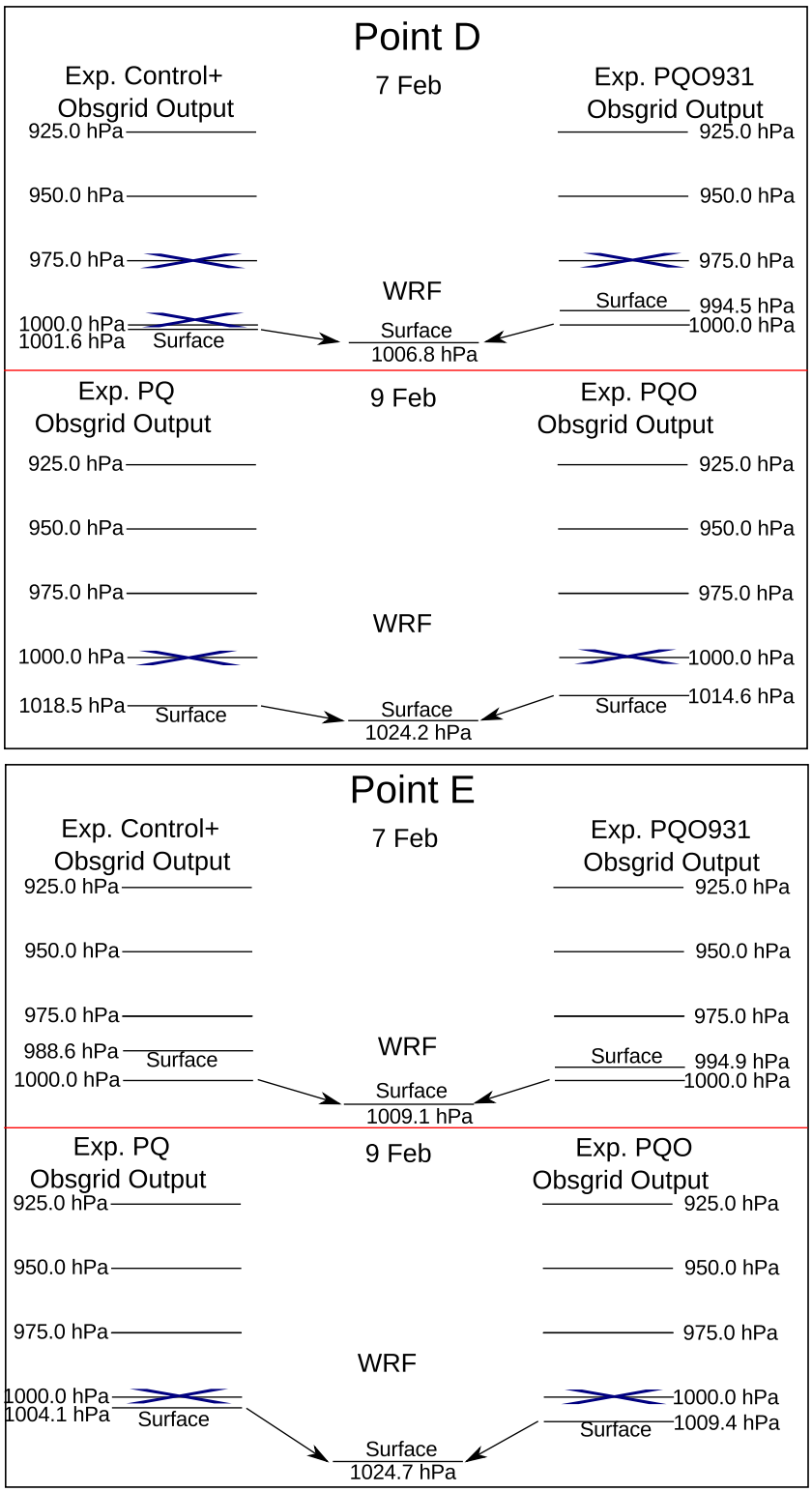

Fig. 27 Diagram of the near-surface levels in the Obsgrid output at 12 UTC on 7 February for Exp. Control+ and Exp. PQO931 and on 9 February for Exp. PQ and Exp. PQO. The locations of points D and E are shown in Fig. 23 for 7 February and in Fig. 13 for 9 February. A blue X indicates levels removed from consideration due to having a pressure greater than that of the sixth WRF model layer.

To investigate the reason for the areas in which the addition of the surface pressure objective analysis does not remove the unrealistic structure, consider the point labeled E in Fig. 23. In Exp. PQO931, this point remains just inside the edge of the unrealistic structure (Fig. 23b). As shown in Fig. 27, on 7 February the WRF surface pressure at point E for both Exp. Control+ and Exp. PQO931 is 1009.1 hPa. For Exp. Control+ the Obsgrid surface pressure is 988.6 hPa, while by adding the surface pressure objective analysis the surface pressure increases 6.3 hPa to 994.9 hPa, closer to the WRF surface pressure. However, for both experiments the 1000-hPa Obsgrid output level lies closer to the WRF surface pressure than the Obsgrid surface level. This results in the 1000-hPa level being used to fill the WRF surface level. The reason that in Exp. PQO931 point E is on the edge of the unrealistic structure is that the Obsgrid output surface pressure is only slightly more than 5 hPa smaller than 1000 hPa. Thus a slight increase in surface pressure would result in the 1000-hPa level being "too close" to the surface level (based on the *zap_close_levels* setting) and thus the 1000-hPa level would be removed from consideration and allow the Obsgrid surface level to be used at the surface. Again, the question arises as to why point E is not in the unrealistic structure for either Exp. PQ (Fig. 13a) or Exp. PQO (Fig. 13b) for the 9 February case. In that case, the WRF surface pressure at that location was 1024.7 hPa, while the Obsgrid surface pressure is 1004.1 hPa in Exp. PQ and 1009.4 hPa in Exp. PQO. As on 7 February, on 9 February the addition of the surface pressure objective analysis increased the surface pressure at point E. However, on 9 February, the Obsgrid surface pressure remained larger than the lowest Obsgrid non-surface pressure (1000 hPa) and thus the Obsgrid surface temperature data were used to construct the WRF surface temperature.

These 2 points (D and E) illustrate that the reason that the surface pressure objective analysis is less effective on 7 February than on 9 February is largely due to how the surface pressures of each day fell in relationship to the pressures of the Obsgrid levels. The generally higher surface pressures on 9 February compared to 7 February resulted in model surface pressures being more likely to remain above 1000 hPa. Since the lowest non-surface Obsgrid output level is 1000 hPa, having the model surface pressure higher than 1000 hPa makes it more likely that the Obsgrid surface level will be used to define the values at the WRF surface level. These results suggest that the maximum pressure difference between a non-surface level and the surface value that results in the non-surface level no longer being considered (*zap_close_levels*) should perhaps be increased. A larger value could allow the Obsgrid surface level data to be used more widely across the domain and decrease the incidence of the unrealistic structure.

6.2.2 Verification of Model Integration

The time series of MAE for Exp. Control+ is compared to Exp. PQO931 for each of the 4 case days in order to determine whether the use of surface pressure quality control and objective analysis improves the model simulation when observation nudging is not used. For surface temperature, the addition of quality control and an objective analysis for surface pressure shows clear benefit on 5 March (Fig. 28a) for the first ≈6 h (note that positive values indicate that Exp. PQO931 performed better than Exp. Control). Decreases in surface temperature MAE shrink from ≈0.25 K at 13 UTC down below 0.10 K by 17 UTC. This case day shows the largest benefit from the surface pressure objective analysis; this is consistent with the histogram of initial condition surface temperature absolute error changes due to the addition of the surface pressure objective analysis (Fig. 22), which indicates 5 March had the largest number of observations with large improvements. It is also consistent with the effectiveness the surface pressure objective analysis has on removing the unrealistic surface temperature structure in the initial conditions (compare Fig. 26a and 26b). However, in contrast to 5 March, the other 3 case days (Fig. 28a) show a slight degradation in surface temperature MAE at 13 UTC (<0.05 K). On 1 March, the degradation transitions to an improvement by 15 UTC; however, for the other 2 case days, it remained a degradation through at 17 UTC (although the magnitude of the degradation does not usually exceed 0.05 K). The 7 February case shows a degradation through the longest period (≈19 UTC), which is consistent with the histogram of initial condition surface temperature absolute errors (Fig. 22) showing the largest degradation among the case days. It is also consistent with the inability of the surface pressure objective analysis to completely eliminate the unrealistic structure in the initial surface temperature (Fig. 23a vs. Fig. 23b); as previously discussed, the unrealistic structure also spreads to some additional areas. For surface temperature in non-nudging experiments, the surface pressure quality control and objective analysis improved 1 case and was fairly neutral for the other 3 cases.

The surface dewpoint MAE difference time series (Fig. 28b) shows that at 13 UTC for 3 of the case days Exp. PQO931 is an improvement over Exp. Control (ranging from ≈0.1 to 0.3 K), and for the fourth case (1 March), there is basically no improvement or degradation. The 1 March case transitions to a degradation by 14 UTC and the 5 March case by 16 UTC. Thus, for surface dewpoint in non-nudging experiments the surface pressure quality control and objective analysis generally improved the model values through the first ≈3 h.

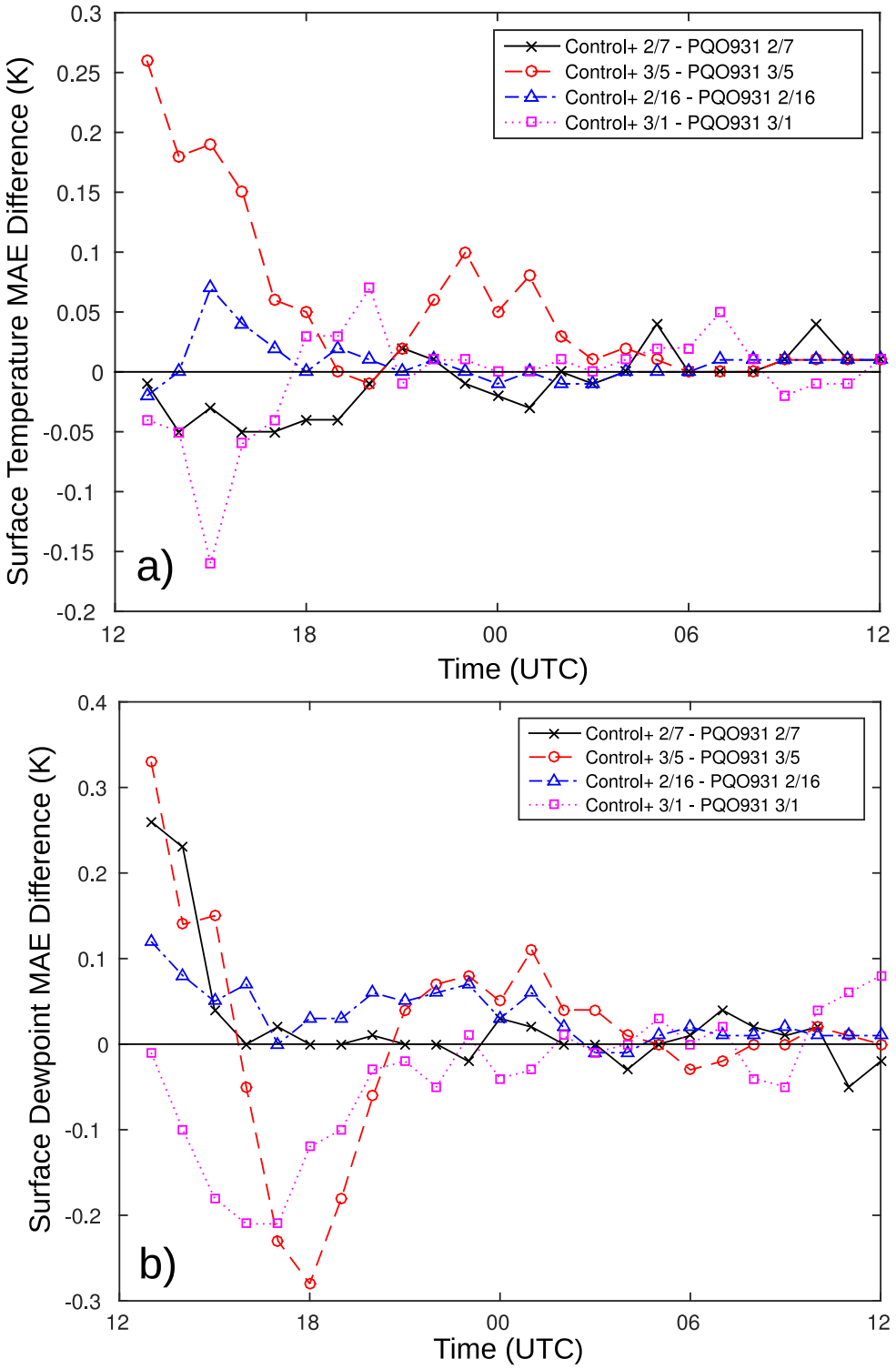

Fig. 28 Time series of the difference in MAE between Exp. Control+ and Exp. PQO931 for surface a) temperature and b) dewpoint. Note that a positive value indicates that Exp. PQO931 has a lower MAE than Exp. Control+ and thus is an improvement over Exp. Control+.

For wind speed (Fig. 29a) and direction (Fig. 29b), the MAE differences are generally quite small (≤0.1 ms^{-1} and ≤5°) and it is difficult to ascertain patterns, particularly for wind speed. As noted earlier, there are notably few wind observations that pass the quality control procedure as compared to temperature and dewpoint.

The equivalent comparison plots for the nudging experiments (Exp. Nud vs. Exp. NudPQO931) are shown in Fig. 30 (surface temperature and dewpoint) and Fig. 31 (surface wind). These generally indicate much smaller MAE differences than the analogous non-nudging plots, which is consistent with the nudging results shown for the initial case day evaluated (9 February). For surface temperature (Fig. 30a), the MAE difference between the nudging experiment without the surface pressure objective analysis (Exp. Nud) and the experiment with it (Exp. NudPQO931) never exceeds 0.04 K in magnitude, so there is very little overall domain mean change in surface temperature verification. At 13 UTC, 3 out of 4 of the cases show degradation, but it is quite small (0.02–0.03 K) and so unlikely to be significant. For dewpoint, the MAE difference never exceeds 0.08 K in magnitude during the length of the model integration among the 4 case days, but at the 13 UTC time, 3 out of 4 the experiments show very small improvements (0.04–0.07 K); however, the magnitude of this is so small that it is difficult to ascribe significance to this. For surface wind speed, the changes are almost always less than 0.2 m s^{-1} in magnitude (Fig. 31a), and are less than 0.1 m s^{-1} at 13 UTC. For wind direction, 3 out of 4 of the cases have a degradation at 13 UTC (≈3° to 9°), but for most of the time over the 4 case days, the magnitude of the MAE change does not exceed 4°. Overall, adding the surface pressure objective analysis has little domain-wide effect for the observation nudging experiments.

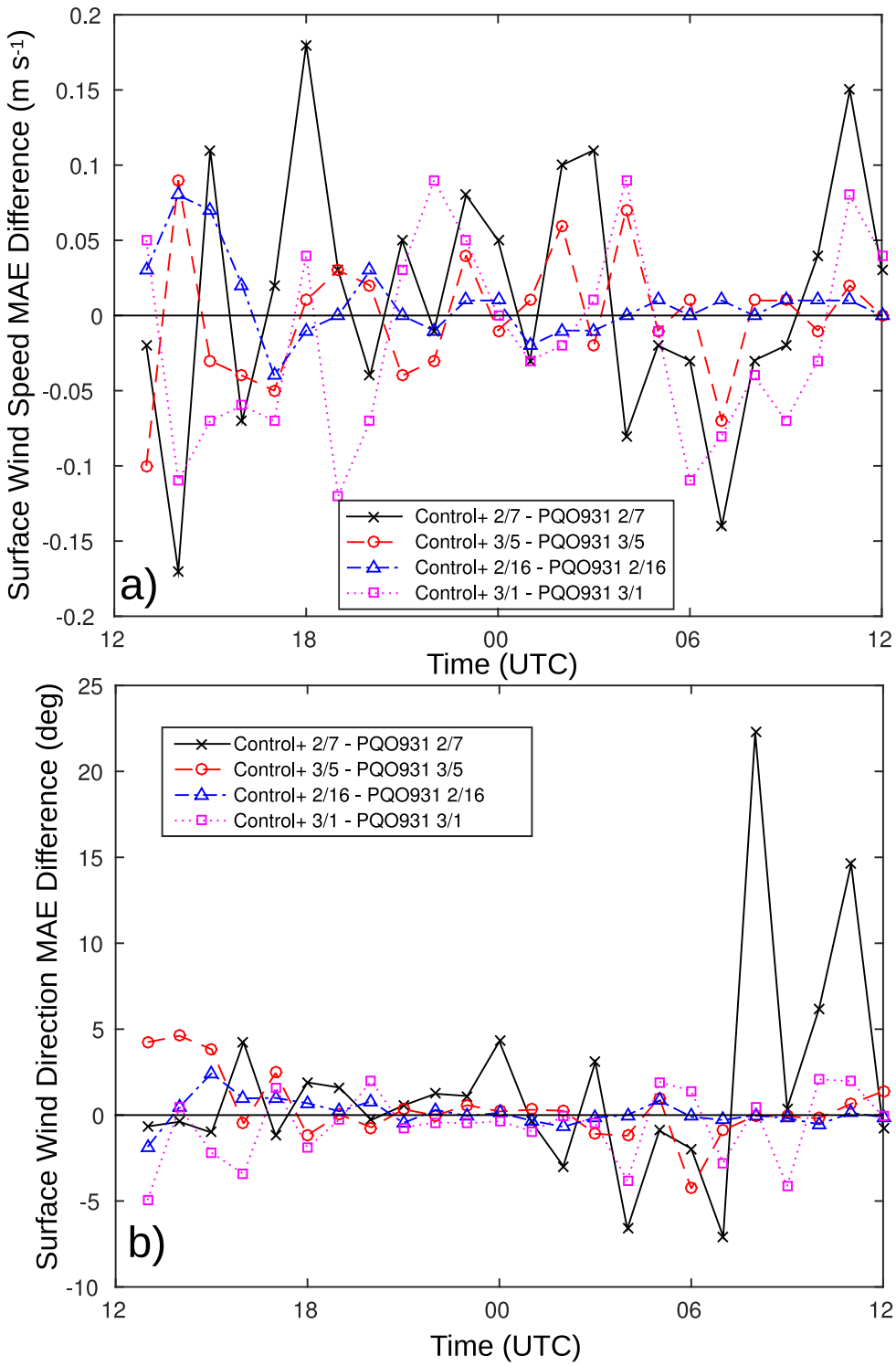

Fig. 29 Time series of the difference in MAE between Exp. Control and Exp. PQO931 for surface a) wind speed and b) wind direction. Note that a positive value indicates that Exp. PQO931 has a lower MAE than Exp. Control+ and thus is an improvement over Exp. Control+.

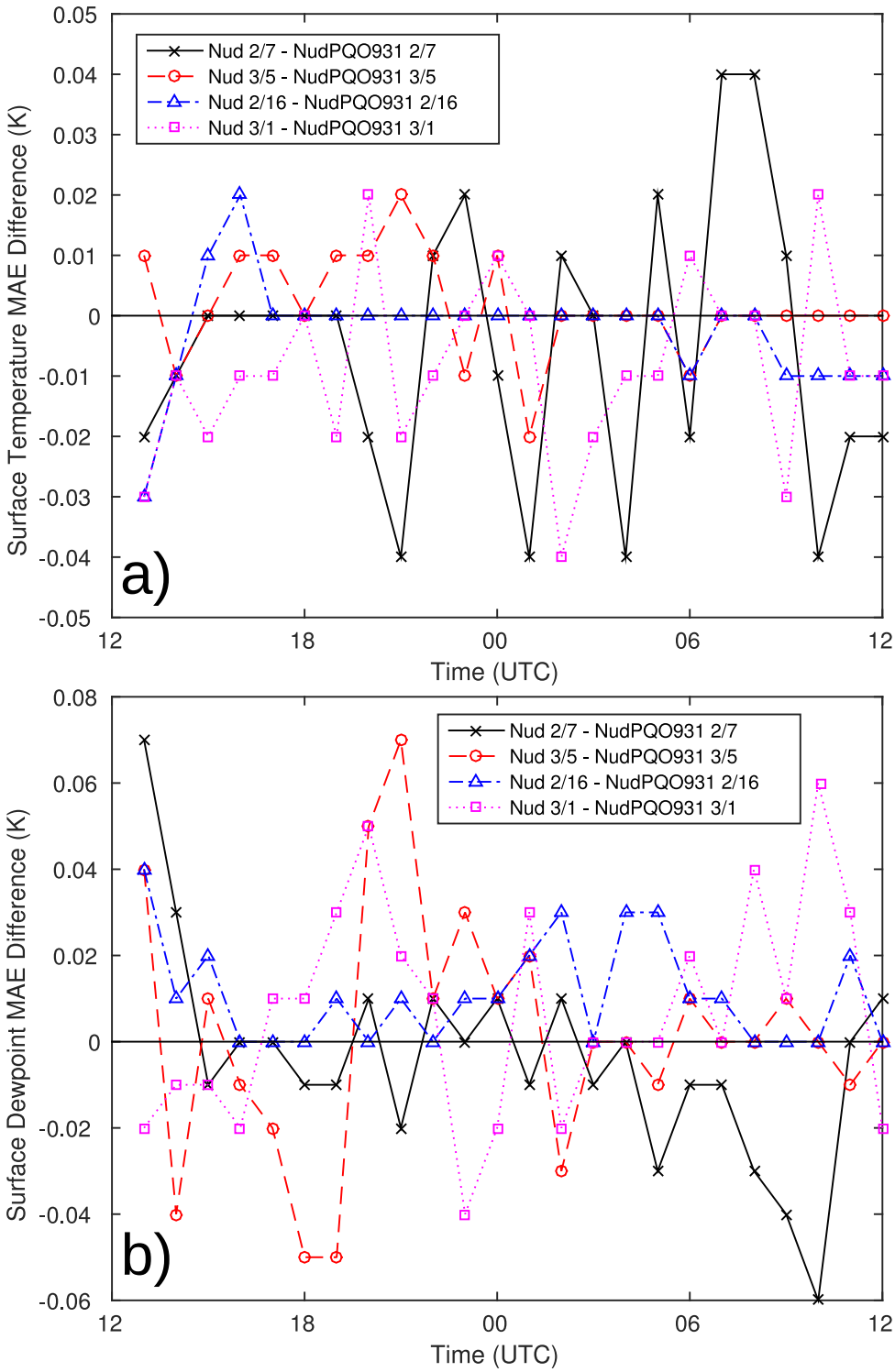

Fig. 30 Time series of the difference in MAE between Exp. Nud and Exp. NudPQO931 for surface a) temperature and b) dewpoint. Note that a positive value indicates that Exp. NudPQO931 has a lower MAE than Exp. Nud and thus is an improvement over Exp. Nud.

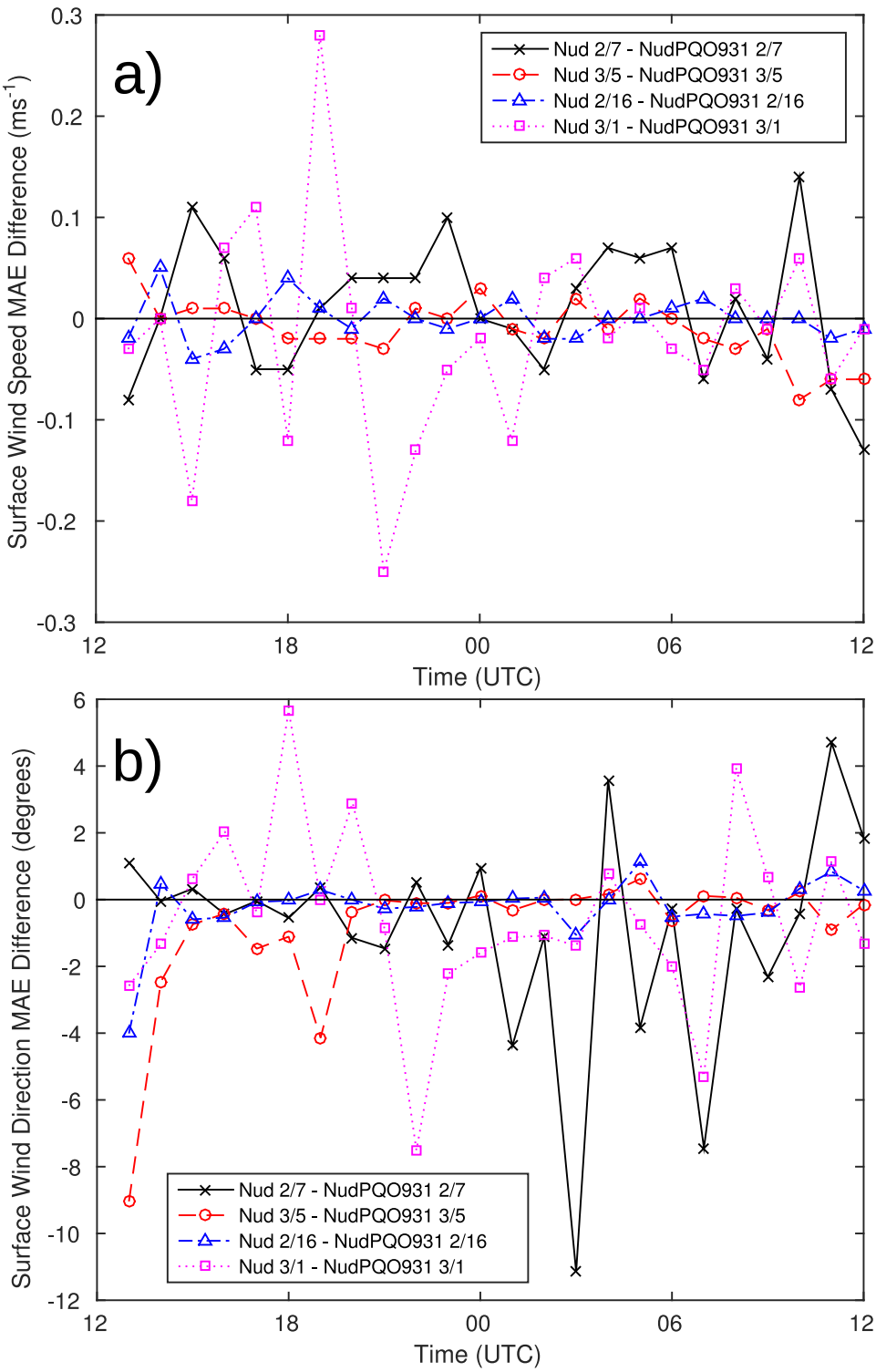

Fig. 31 Time series of the difference in MAE between Exp. Nud and Exp. NudPQO931 for surface a) wind speed and b) wind direction. Note that a positive value indicates that Exp. NudPQO931 has a lower MAE than Exp. Nud and thus is an improvement over Exp. Nud.

Although the focus of this report is on the potential benefits of use of a surface pressure objective analysis, a brief comparison of experiments with and without observation nudging is included in order to provide a fuller context of the results. Figs. 32 and 33 show time series of the MAE difference between Exp. PQO931 and Exp. NudPQO931; both experiments use the surface pressure objective analysis, and thus, the difference between the 2 experiments is that the latter includes nudging while the former does not. All 4 case days show improvements in surface temperature through at least 19 UTC (Fig. 32a), with 3 of the case days showing improvements through at least 22 UTC. The MAE improvements peak between ≈0.5 and ≈1.0 K for the 4 case days. Recall that observation nudging is applied at full strength through 18 UTC, with observations from 18 UTC or earlier permitted to be applied with a linearly decreasing weight with time through 19 UTC. Surface dewpoint similarly shows all 4 case days with MAE improvements through at least 20 UTC (Fig. 32b), with 2 case days showing improvements through 02 UTC, and 1 case day showing improvements throughout the 24-h model integration (16 February). The peak surface dewpoint MAE improvements range between ≈0.6 and ≈0.8 K among the 4 case days. Surface wind speed MAE (Fig. 33a) improves for all 4 case days through only 15 UTC, although it remains improved for 3 of the case days through 18 UTC. The 7 February shows the largest improvements with all but 1 h showing surface wind speed MAE improvements through 07 UTC. Surface wind direction improvements from nudging (Fig. 33b) are more difficult to interpret, but except for 16 UTC on 5 March, none of the 4 case days show non-negligible degradation until 19 UTC. There is a large amount of hour-to-hour variation in the wind direction statistics, which may be related to light and variable winds in some cases. Overall, the addition of observation nudging to the experiments using the surface pressure objective analysis shows improvements in surface fields at least through the data assimilation period and, for temperature and dewpoint, the benefit lasts past the assimilation period.

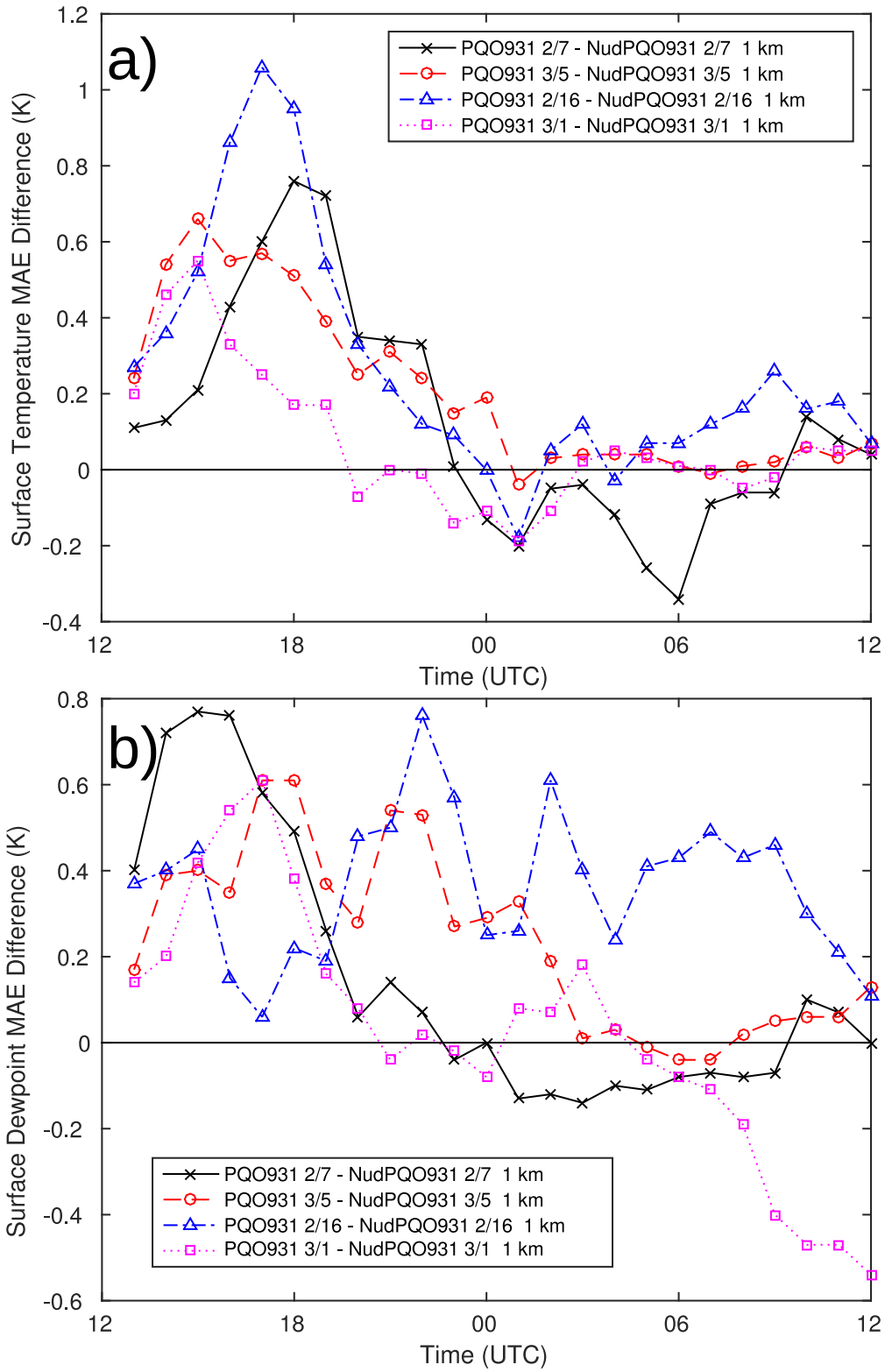

Fig. 32 Time series of the difference in MAE between Exp. PQO931 and Exp. NudPQO931 for surface a) temperature and b) dewpoint. Note that a positive value indicates that Exp. NudPQO931 has a lower MAE than Exp. PQO931 and thus is an improvement over Exp. PQO931.

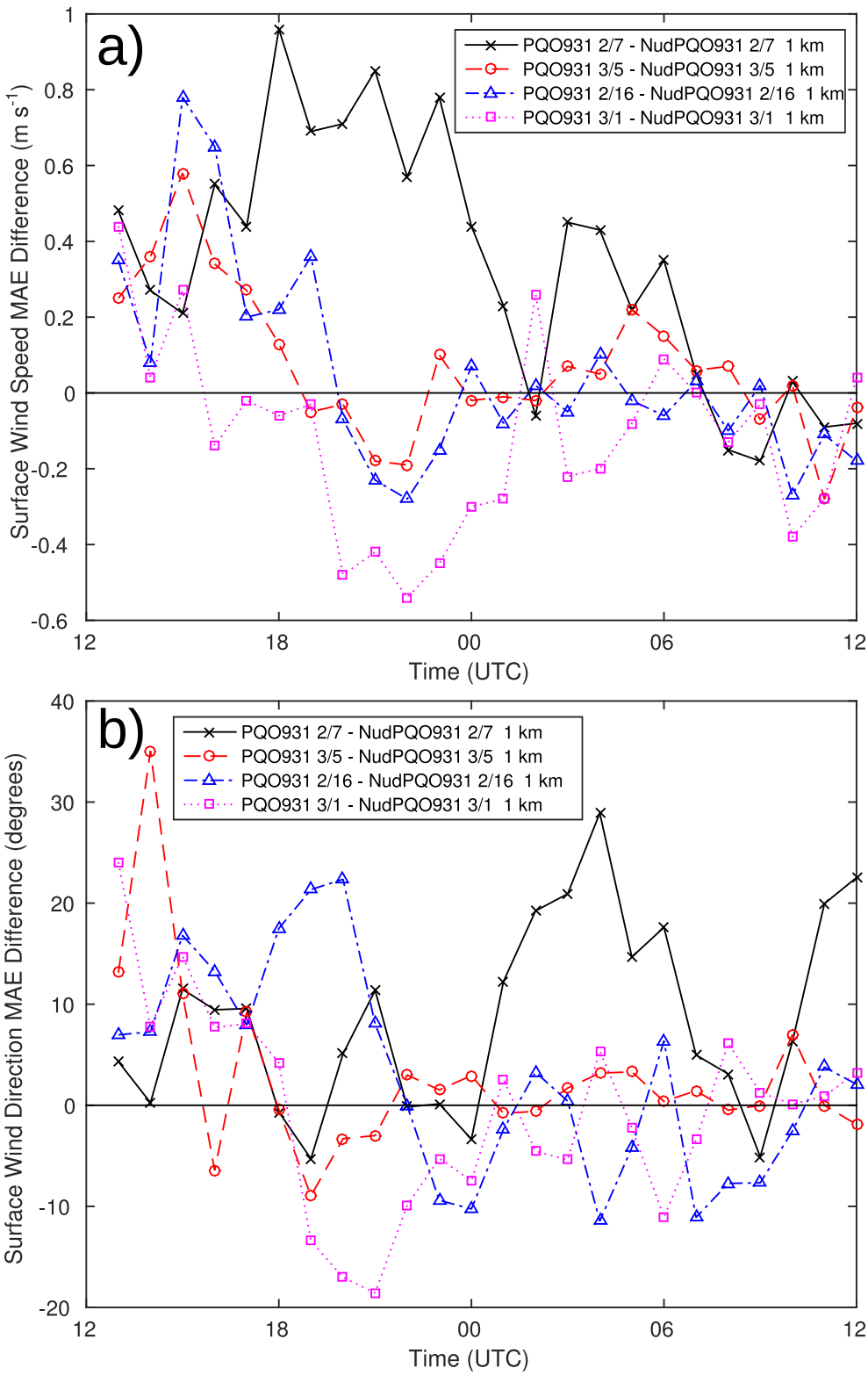

Fig. 33 Time series of the difference in MAE between Exp. PQO931 and Exp. NudPQO931 for surface a) wind speed and b) wind direction. Note that a positive value indicates that Exp. NudPQO931 has a lower MAE than Exp. PQO931 and thus is an improvement over Exp. PQO931.

To investigate how the effects of adding the surface pressure objective analysis vary with horizontal grid spacing, the time series of the differences in the surface temperature MAE between Exp. Control+ and Exp. PQO931 are plotted in Fig. 34 for each of the 4 cases (the results for the 1-km domain alone were previously shown in Fig. 28a). For 7 February (Fig. 34a) the changes in surface temperature MAE are quite small (<0.05 K) and so it is difficult to glean much, but note that other than the 1-km domain the "degradations" never exceed 0.02 K and thus there is no evidence that use of the surface pressure objective analysis degrades any of the coarser grids. Note that the 27-km domain shows no difference between Exp. Control+ and Exp. PQO931, consistent with the surface pressure objective analysis not being applied in Exp. PQO931. For 16 February (Fig. 34b), while the 1-km domain showed a very small degradation at 13 UTC, transitioning to an improvement by 14 UTC, the 3-km domain shows an improvement through ≈18 UTC, and the 9-km domains shows a smaller improvement through ≈16 UTC. For 1 March (Fig. 34c), the finer 3 domains show small degradations at 13 UTC; while the magnitude of the degradation remains small (or becomes a slight "improvement") in the first few hours of the model integration, the degradation increases somewhat on the 1-km domain (exceeding –0.15 K at 15 UTC). Finally, on 5 March (Fig. 34d) improvements are seen on all 3 finer domains, with the magnitude of the improvement decreasing as horizontal grid spacing increases; at 13 UTC the improvement is 0.26 K on 1-km domain, 0.19 K on the 3-km domain, and 0.10 K on the 9-km domain. In general, adding the surface pressure analysis affects the coarser domains less than the 1-km domain; the finer domains are more likely to have surface pressures that differ notably from the GFS surface pressures, since the finer domains can better resolve terrain unresolved in GFS.

An analogous comparison among the domains of the surface dewpoint temperature MAE improvements caused by use of a surface pressure objective analysis is shown in Fig. 35. Over the first few hours of the model integration, the coarser domains generally show a similar but muted response compared to the 1-km domain. For example, on 7 February (Fig. 35a), the 3 finer domains all indicate improvement through use of the surface pressure objective analysis at 13 UTC, with the magnitude of the improvement largest for the 1-km domain and smallest for the 9-km domain. The improvement decreases with time and disappears by 14 UTC for the 9-km domain, 15 UTC for the 3-km domain, and 16 UTC for the 1-km domain. The 16 February (Fig. 35b) and 5 March (Fig. 35d) cases show a similar pattern to that seen in the 7 February case. The 1 March (Fig. 35c) case differs in that all domains show basically no MAE improvement at 13 UTC, but a degradation develops in the subsequent hours that is strongest in the 1-km domain and weakest in the 9-km domain.

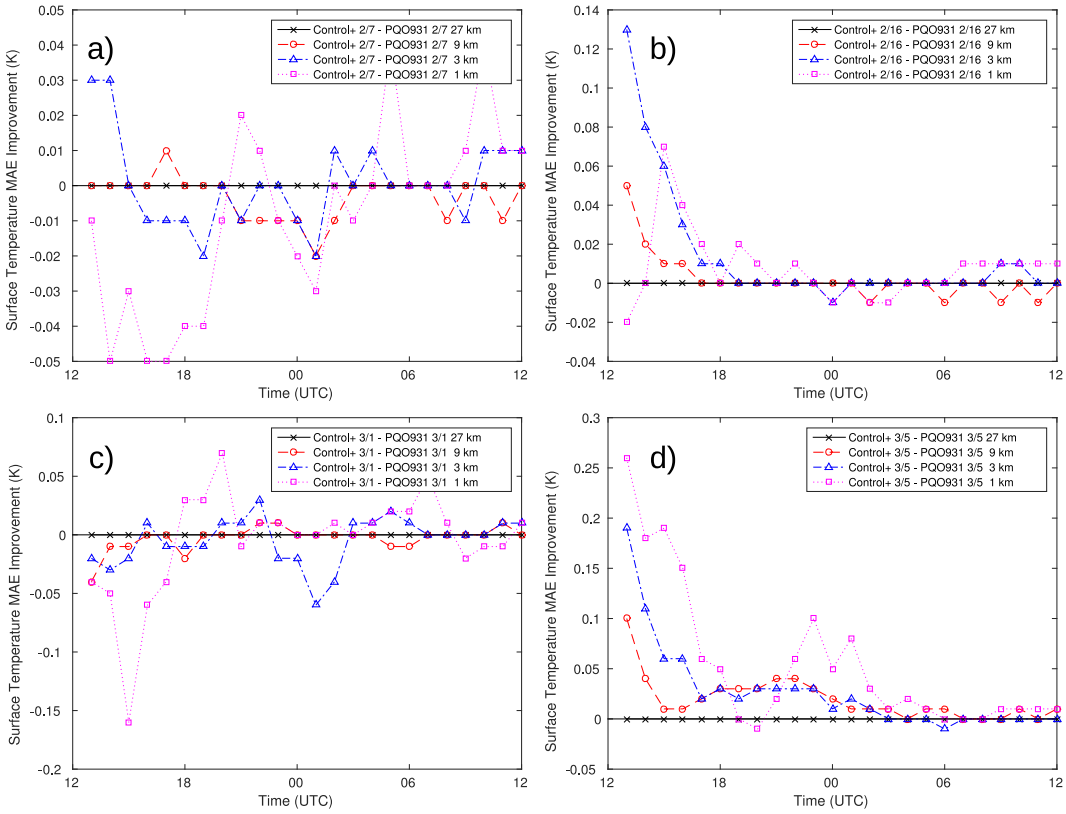

Fig. 34 Time series of the difference in surface temperature MAE between Exp. Control+ and Exp. PQO931 for each of the 4 domains for a) 7 February, b) 16 February, c) 1 March, and d) 5 March. Note that a positive value indicates that Exp. PQO931 has a lower MAE than Exp. Control+ and thus is an improvement over Exp. Control+.

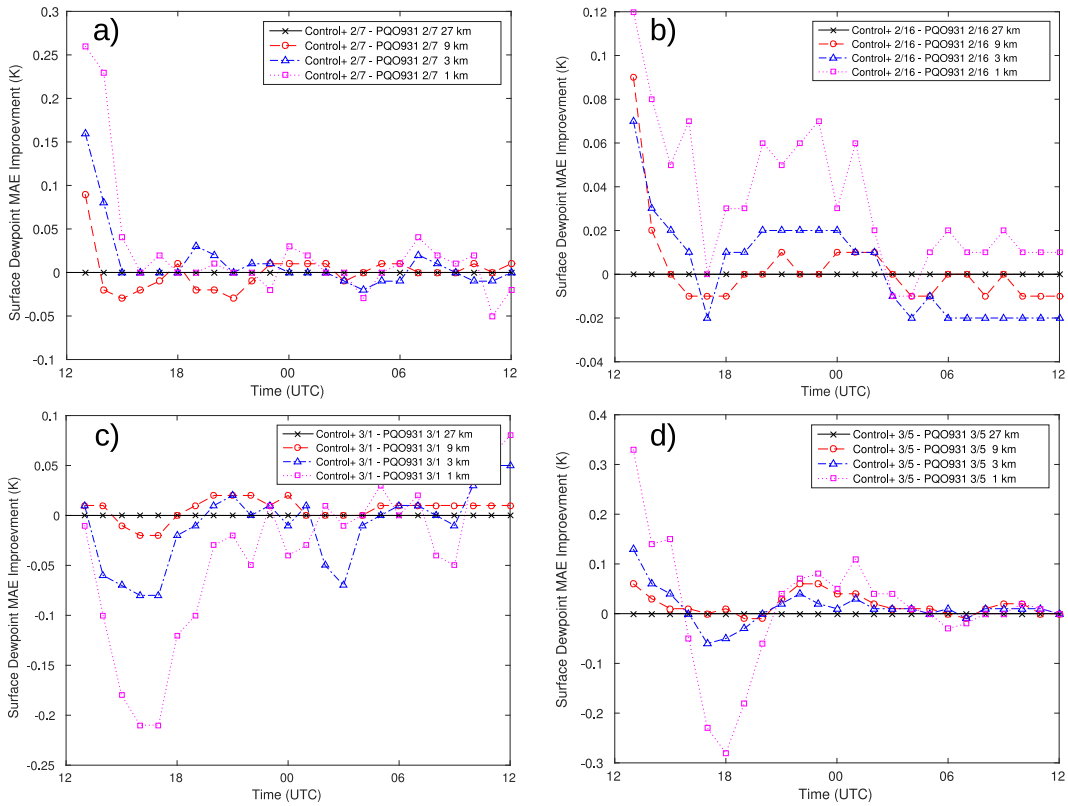

Fig. 35 Time series of the difference in surface dewpoint MAE between Exp. Control+ and Exp. PQO931 for each of the 4 domains for a) 7 February, b) 16 February, c) 1 March, and d) 5 March. Note that a positive value indicates that Exp. PQO931 has a lower MAE than Exp. Control+ and thus is an improvement over Exp. Control+.

Thus far, the verification has focused on surface observations, but next the effects of adding the surface pressure objective analysis on the lowest 1000 m of the atmosphere is discussed. For 0–1000 m AGL air temperature (Fig. 36a) among the 4 case days, there is generally little change in MAE in the first 6 h of the model simulation. However, 7 February shows some degradation, especially at 14 UTC where the magnitude of the degradation exceeded 0.15 K; recall that 7 February showed small degradations in surface temperature as well (although only ≈0.05 K; Fig. 28a). Note that the number of non-surface observations available in the 0–1000 m AGL layer (Fig. 36c) varies strongly by time and case day. At times other than rawinsonde times, the above-surface temperature verification will generally be provided by aircraft-based observations (ACARS and TAMDAR), and the number of flights reporting data to ACARS or TAMDAR within the 1-km domain varies by time and day. This variation in the number of available observations should be used in interpreting above-surface verification, because the number of observations that are used to create a verification statistic can influence one's confidence in that verification statistic. So, for example, the 0–1000 m AGL temperature verification statistics should probably be seen as less significant at

13 UTC and after 07 UTC than at times with a larger number of observations available for use in verification. Note that the spike in the temperature degradation at 14 UTC on 7 February is at a time where only ≈10 temperature observations are available, which may cast doubt on the importance of the spike.

Dewpoint temperature in the lowest 1000 m of the atmosphere (Fig. 36b) shows improvement at some hours for some case days (e.g., improvements of ≈0.2 K on 7 February at 15 UTC and 17 UTC, and ≈0.1 K on 5 March at 16 and 17 UTC), but degradations for other hours and case days (e.g., a degradation of ≈0.4 K on 5 March at 14 UTC, and a degradation of over 0.1 K at 14 and 15 UTC). The variability in the MAE differences from hour to hour and case to case make it difficult to see a clear signal. Part of this may be due to the limited number of dewpoint observations available for the first few hours of the simulation (Fig. 36d).

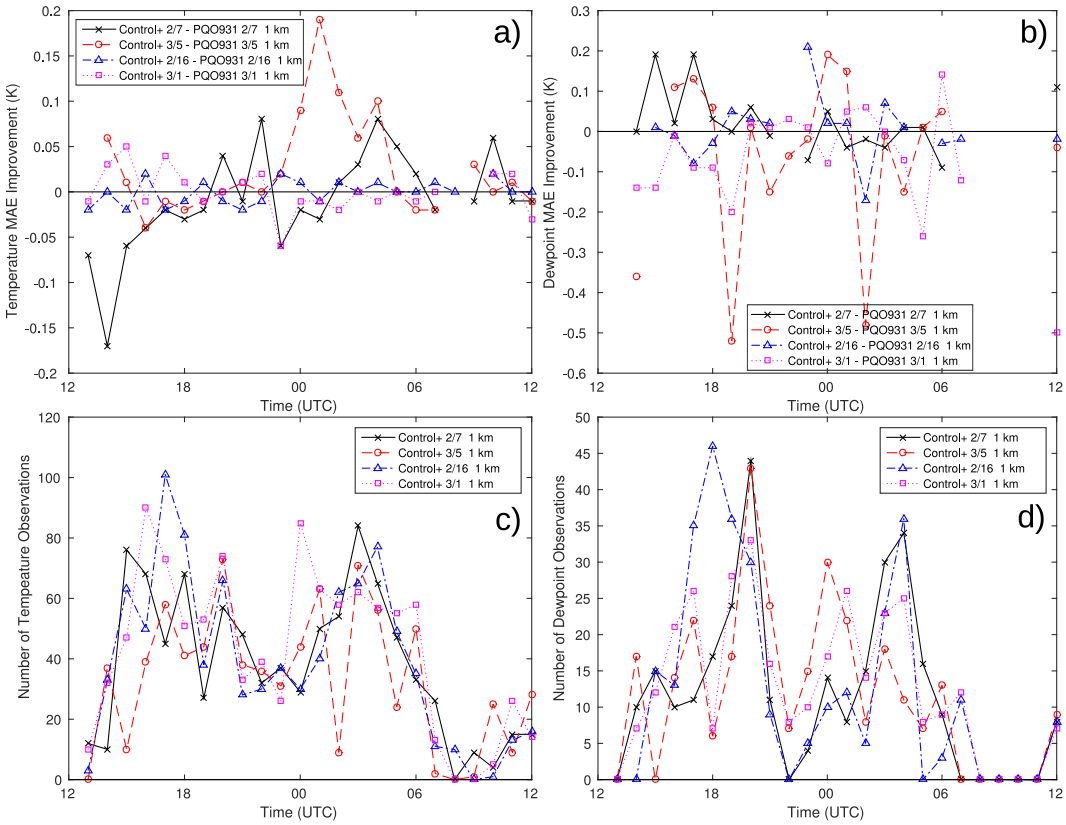

Fig. 36 Time series of the difference in MAE between Exp. Control+ and Exp. PQO931 for non-surface observations between 0 and 1000 m AGL for a) temperature and b) dewpoint. A count of the number of observations used to create the MAEs is shown for c) temperature and d) dewpoint.

For wind speed (Fig. 37a) and wind direction (Fig. 37b) in the 0–1000 m AGL layer, there is limited MAE difference in the first few hours of the simulation. One exception is improvements in wind speed on 7 February of between 0.2 and

0.4 m s^{-1} between 13 and 16 UTC. While there are very few wind speed observations in this layer on 7 February at 14 UTC (<5), at 13 UTC, there are >20, and at both 15 and 16 UTC, there are around 80 observations. This suggests that this wind speed improvement is not an artifact of sampling.

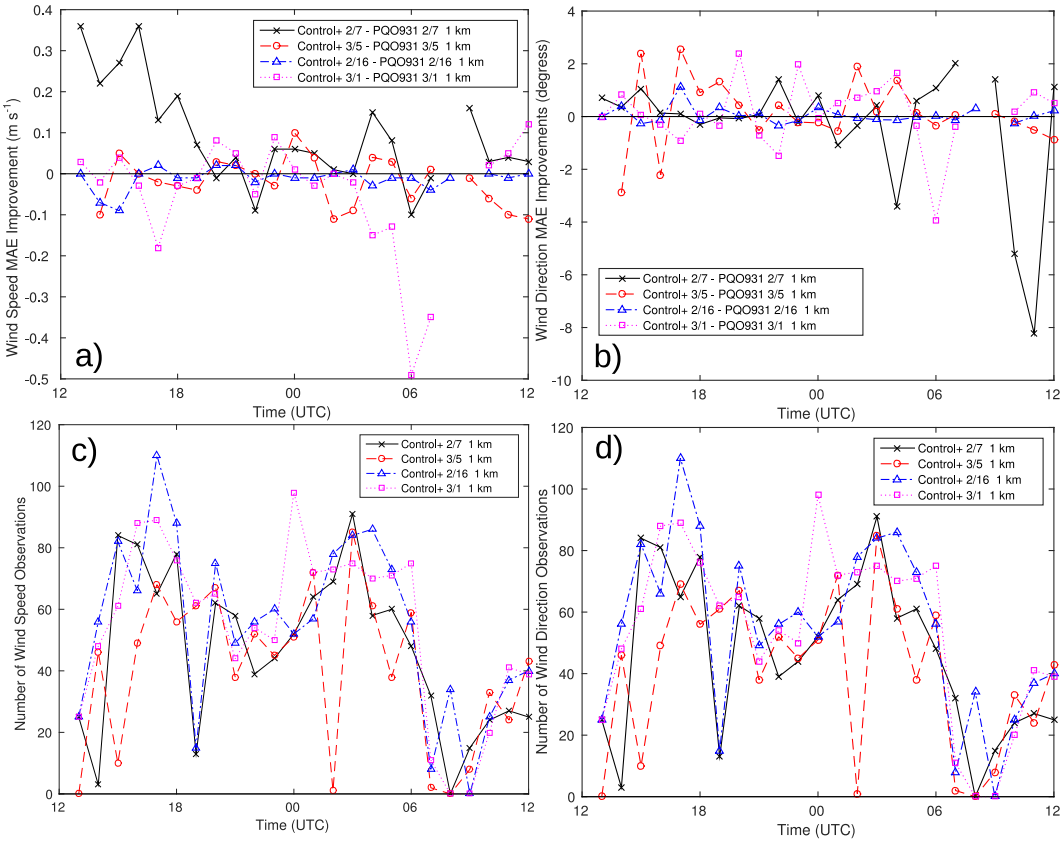

Fig. 37 Time series of the difference in MAE between Exp. Control+ and Exp. PQO931 for non-surface observations between 0 and 1000 m AGL for a) wind speed and b) wind direction. A count of the number of observations used to create the MAE's is shown for c) wind speed and d) wind direction. Note that positive values indicate that Exp. PQO931 performed better than Exp. Control+.

The benefits in the lowest 1000 m of the atmosphere of using observation nudging in experiments using the surface pressure objective analysis are briefly discussed. All 4 case days show at least small improvements in 0–1000 m AGL temperature due to observation nudging (Fig. 38a) through at least 22 UTC except for small degradations (<0.5 K) on 16 February at 13 UTC and 14 UTC on 7 February. The improvements peak between ≈0.5 and ≈1.5 K among the 4 case days. For dewpoint (Fig. 38a), beside 2 small degradations on 5 March, all 4 case days showed improvements through 19 UTC. The maximum improvements varied greatly among the 4 case days between 0.9 K (1 March) and 5.2 K (16 February). During the first 6 h, nudging improves wind speed MAE in the lowest 1 km for 3 of the 4 case days (Fig. 39a), and wind direction is generally improved or has little change

through the assimilation period (Fig. 39b). Overall, adding observation nudging to experiments using a surface pressure objective analysis results in an improvement during the assimilation period, with the benefits after the end of the assimilation period strongest for temperature.

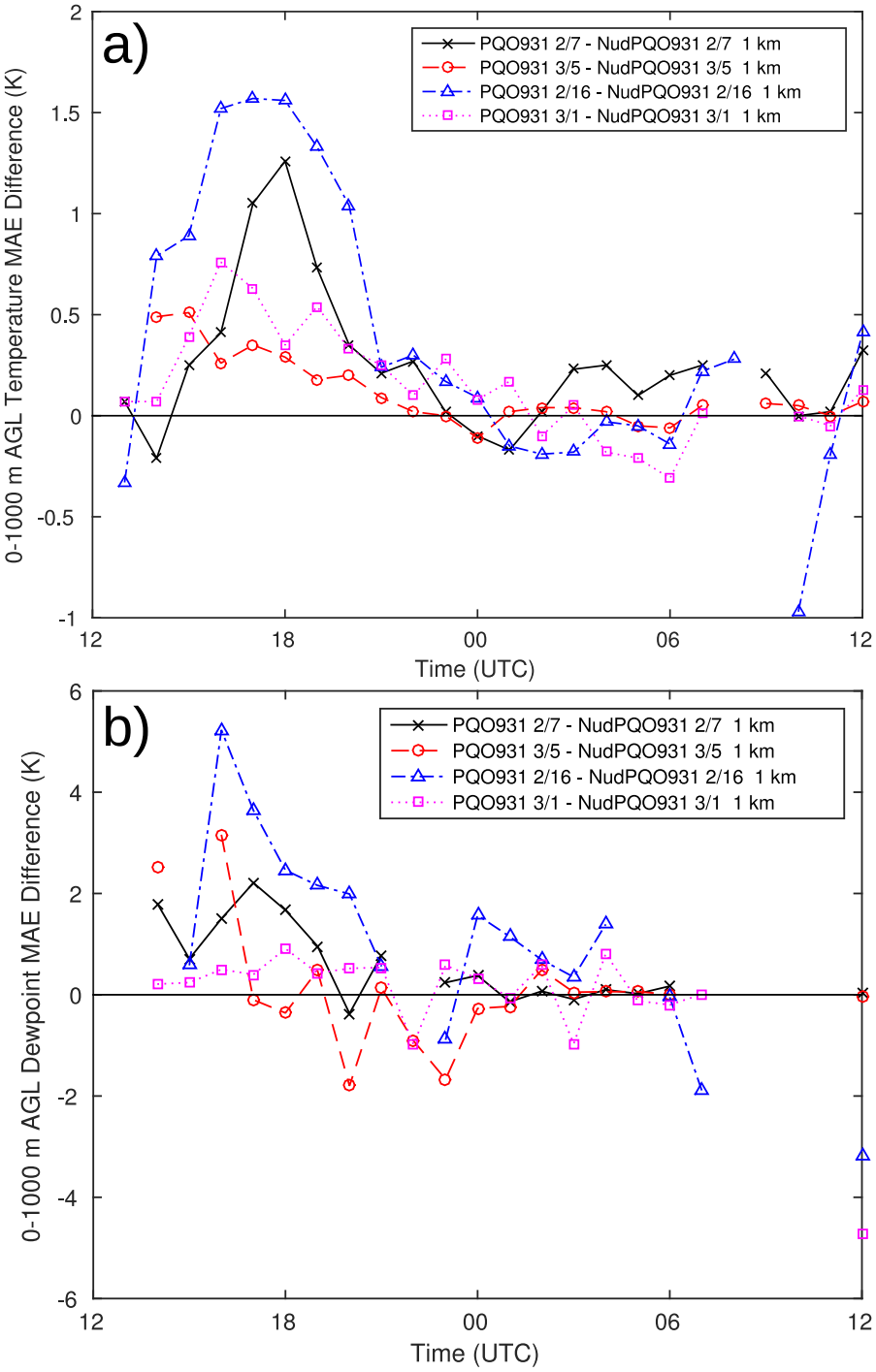

Fig. 38 Time series of the difference in MAE between Exp. PQO931 and Exp. NudPQO931 for non-surface observations between 0 and 1000 m AGL for a) temperature and b) dewpoint. Note that positive values indicate that Exp. NudPQO931 performed better than Exp. PQO931.

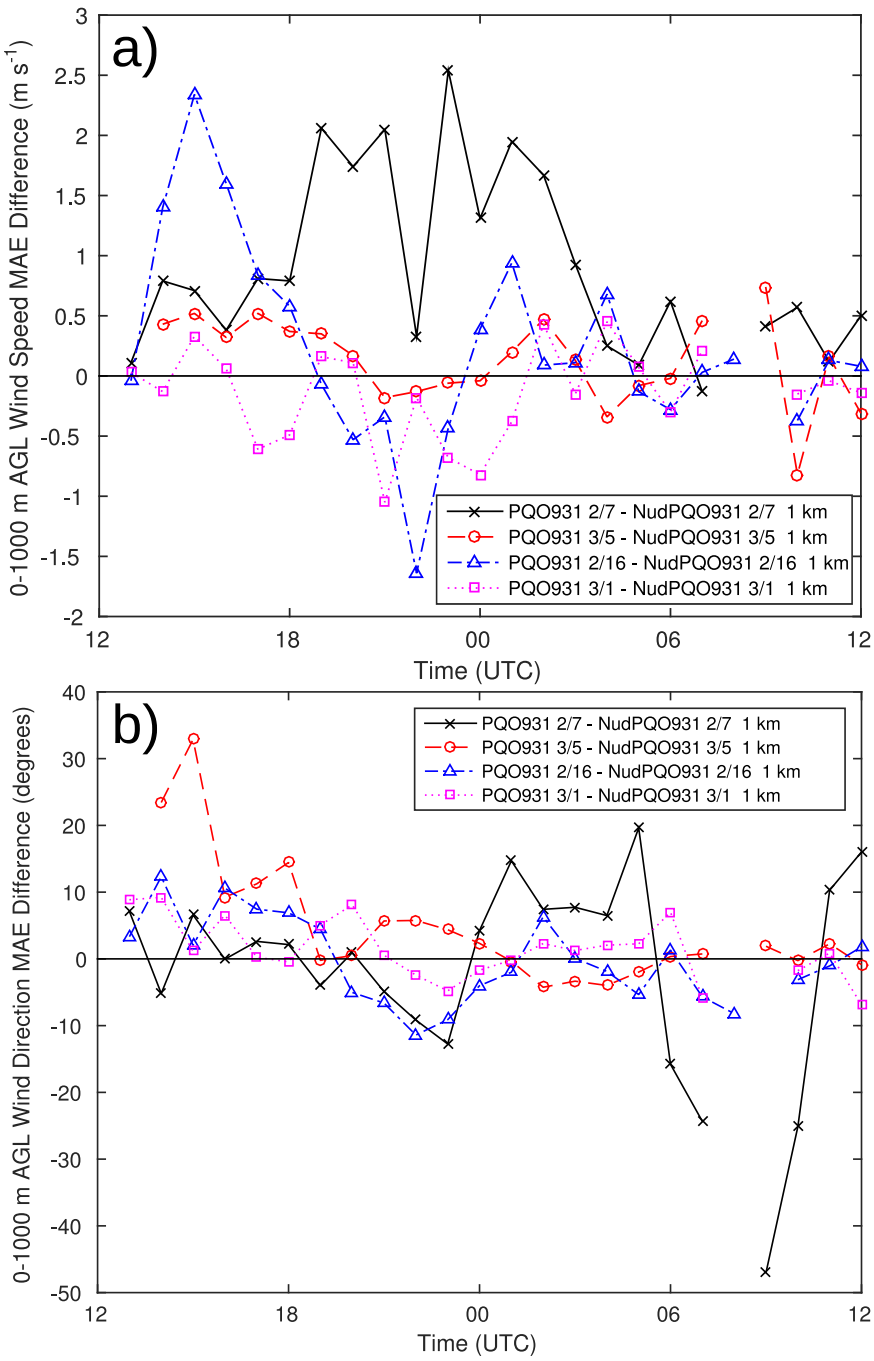

Fig. 39 Time series of the difference in MAE between Exp. PQO931 and Exp. NudPQO931 for non-surface observations between 0 and 1000 m AGL for a) wind speed and b) wind direction. Note that positive values indicate that Exp. NudPQO931 performed better than Exp. PQO931.

7. Summary, Discussion, and Conclusions

Surface fields in WRF initial conditions sometimes include areas with very weak horizontal gradients within the area, but strong vertical gradients along the borders

of this region. The structure does not appear to be physically realistic and occurs even though the software Obsgrid creates a high-resolution surface analysis by blending 0.5° (≈55 km) GFS output with many surface observations and this surface analysis is provided to WRF. The GFS surface pressure field is used as the surface pressure of the other surface analyses. Obsgrid also creates objective analyses at constant pressure levels from GFS pressure level data.

WRF-ARW using 27-, 9-, 3-, and 1-km horizontal grid spacing nested grids was used to investigate this phenomenon first on 9 February 2012 in an area centered over San Francisco. In this case, it was found that these structures occurred on the 1-km grid in fields including potential temperature, water vapor mixing ratio, and wind, in areas where both of the following was true: 1) the WRF surface had a pressure larger than the constant pressure level data provided by Obsgrid with the highest pressure (1000 hPa), and 2) the Obsgrid surface pressure was at least 5 hPa less than that layer. When these conditions are met, the closest Obsgrid data above the WRF surface are the 1000 hPa level and there are no Obsgrid data below the WRF surface so the WRF surface is defined by the 1000 hPa alone. The second criterion uses "5 hPa less" rather than merely "less" because WRF as configured here ignores levels within 5 hPa of the surface pressure (the value is set by *zap_close_levels*) when defining initial conditions.

To ameliorate the issue of the unrealistic structure, Obsgrid was modified to create a surface pressure objective analysis based on a combination of the GFS surface pressure field and the observed surface pressure values. This should be more representative of the pressure at which the surface analyses of other fields are valid at. Given sufficient observations this should also allow the Obsgrid surface pressure field to more closely match that of high-resolution WRF domains and thus allow the surface analyses of other surface fields to be more effectively utilized in the WRF initial conditions.

In implementing the addition of surface pressure objective analysis, it was found that several other modifications were needed. Estimation of surface pressure for observations below the lowest constant-pressure level was improved to more fully utilize the GFS case specific information rather than relying on the standard atmosphere. A bug was found and fixed in the Ungrib code used to vertically interpolate the GFS pressure level data onto additional vertical levels; this improved the surface pressure estimation for observations lacking surface pressures. Quality control of surface pressure was implemented by transforming surface pressure to sea-level pressure; direct quality control of surface pressure is difficult due to differences caused by terrain.

Evaluation of the 1-km domain indicates improvements in surface temperature and dewpoint in the first few hours of the simulation due to the addition of the surface pressure objective analysis in non-nudging experiments, while in nudging experiments the majority of the improvement is due to the Ungrib vertical interpolation bug fix. In the nudging experiments, the lack of the surface pressure objective analysis does not prevent the observations from being assimilated and thus it appears that the omission of these observations from the initial conditions is overcome by their use in the observation nudging. The Ungrib vertical interpolation bug fix benefits the nudging experiments in that the estimated surface pressure relies on the pressure-height relationship in the GFS-derived fields, including those created by vertical interpolation in Ungrib; observation nudging uses the pressure of the observations to convert the temperature observations to the potential temperature needed for observation nudging.

Evaluation of the 27-km domain indicates overall degradation from the surface pressure objective analysis. The 27-km domain is close to the horizontal grid spacing of the GFS input data (~55 km), and thus the surface pressure objective analysis is less likely to add value and may in fact degrade the surface pressure field associated with the surface pressure analyses. Therefore, subsequent experiments removed the surface pressure objective analysis from the 27-km domain.

Following the development of the technique using the 9 February case, experiments were carried out comparing the use of surface pressure objective analysis and quality control in both observation nudging experiments and those without observation nudging for four additional case days in 2012: 7 February, 16 February, 1 March, and 5 March. These experiments, in general, showed the surface pressure objective analysis and quality control having very little impact on the nudging experiments, so this summary focuses on the non-nudging experiments.

The 1-km domains of the non-nudging experiments showed, in general, the temperature of the initial conditions appears to benefit from the surface pressure objective analysis. The 7 February shows the most observations where the modification results in a degradation at the initial time; this appears to be due to the mean surface pressure being lower on this day, resulting in WRF surface pressures being closer to being bracketed by Obsgrid constant pressure level data and thus making it less likely that the Obsgrid surface level will play as strong of a role in defining the WRF surface level fields. Increasing the pressure tolerance surrounding the Obsgrid surface level where constant pressure levels are ignored (*zap_close_levels*) could potentially mitigate this issue. After the initial time, the surface pressure objective analysis shows clear benefit on 5 March, but on the other case days, the effect is more mixed. However, in general any degradations are less than 0.05 K in magnitude, while the improvement at 13 UTC for 5 March exceeds

0.25 K. This suggests that the surface pressure objective analysis helps in some cases but is generally neutral in others; increasing *zap_close_levels* may also improve some days such as 7 February.

Surface dewpoint on the 1-km domain in the non-nudging experiments indicated benefits in the first few hours after the initial time for 3 of the 4 cases (however, 1 of these cases transitions to a degradation by 16 UTC). For wind, the effects are less clear.

Examining the variation of the benefits of using the surface pressure objective analysis among the domains, the benefits or degradations are in general muted as the horizontal grid coarsens for surface temperature and especially surface dewpoint. However, for surface temperature on 16 February, while the 1-km domain showed slight degradation at 13 UTC, transitioning to a benefit by 15 UTC, the 9- and 3-km domains showed improvements at 13 UTC, decreasing with time. Thus, an examination of all domains together suggests that for surface temperature the modifications are a benefit on 2 of the case days, but generally neutral on the other 2 case days.

Examining verification of observations above the surface but in the lowest 1000 m of the atmosphere, it is difficult to obtain a clear signal as to the benefits or degradations of using the surface pressure objective analysis. The variation in the number of observations and their location likely contributes to the difficulty in interpreting the results.

Overall, the use of the surface pressure objective analysis seems to improve model predictions of surface temperature in some cases, while being generally neutral in others, while for surface dewpoint the benefit is clearer. Wind speed and wind direction do not appear to be greatly influenced by these modifications, nor do observations above the surface. The surface pressure objective analysis should not be used on model domains whose horizontal grid spacing approaches that of the coarse grid model used to initialize WRF (e.g., GFS). For observation nudging experiments, the surface pressure objective analysis does not appear to add value. This is apparently because the model will assimilate these observations whether or not a surface pressure objective analysis is completed, and this compensates in these cases for inferior initial conditions. However, although by 13 UTC (1 h into the simulation), the nudging experiments do not have an improvement in the domain mean statistics due to the surface pressure objective analysis, it will take some finite time for the observation nudging to correct for the biases that are corrected before the model integration starts with the addition of the surface pressure objective analysis. Therefore, if the user needs forecasts immediately after the model integration begins, even with nudging the surface pressure objective analysis

should add value. Additionally, although the domain-mean statistics do not show an improvement with the use of the surface pressure objective analysis in the observation nudging cases, there may be regions of the domain where improvements exist.

The pressure tolerance *zap_close_levels*, which determines how close the surface must be to a constant pressure level before that constant pressure level is removed, should likely be increased to allow surface fields to be more widely used in determining the model surface initial condition. One could assign the WRF surface pressure to the Obsgrid surface analyses to allow the Obsgrid surface analysis to be used as the surface value across the WRF grid. This would also allow the Obsgrid surface analysis to be used in vertical interpolation as if it were at the WRF surface pressure. However, this assumes that the surface analyses should be trusted as valid across the domain no matter how the terrain relates to the terrain assumed by the coarse grid model and the observations used to create the analysis. Note that the *lowest_lev_from_sfc* option in WRF will force the lowest model level to use the surface analyses; however, this option does not affect other layers in any way, so this option can lead to strong vertical gradients. Also, note that the *force_sfc_in_vinterp* option as configured here (set to "6") makes it more likely that the surface analyses will be more widely used in the WRF initial conditions, since it removes all pressure level data with pressures that are both lower than the Obsgrid surface pressure and higher than the sixth WRF model layer above the surface. However, the efficacy of this technique may be weakened where Obsgrid surface pressure does not well match WRF surface pressure. Ultimately, these options can be helpful in encouraging the Obsgrid surface analyses to be more fully utilized in WRF, but they function best when the surface pressure of the Obsgrid surface analyses is consistent with the terrain of the WRF domain and consistent with the surface pressure of the observations and first-guess field used to create the surface analyses. Therefore, it is important to ensure that the surface pressure field associated with the Obsgrid surface analyses is not simply the surface pressure of the background field (e.g., GFS), but also represents the surface pressure of the observations used in the analysis.

The modifications made to the WRF initial condition surface temperature might be retained in the simulation longer if the WRF initial condition soil temperature was modified in light of the WRF surface temperature changes. When changes are made solely to the air temperature near the surface, the soil temperature can act to attempt to restore the air temperature to the pre-modified state. Similarly, the benefits of observation nudging surface air temperature may be retained longer if soil temperature were to be nudged in tandem with surface air temperature (e.g., Reen and Stauffer 2010). Future work should consider this option.

8. References

Chen F, Dudhia J. Coupling an advanced land surface–hydrology model with the Penn State–NCAR MM5 modeling system. Part I: Model implementation and sensitivity. Monthly Weather Review. 2001;129:569–585.

Daniels TS, and Coauthors. Validation of Tropospheric Airborne Meteorological Data Reporting (TAMDAR) temperature, relative humidity, and wind sensors during the 2003 Atlantic THORPEX regional campaign and the Alliance Icing Research Study (AIRS II). 11th Conference on Aviation, Range, and Aerospace; 2004; Hyannis, MA, AMS, P8.2.

De Pondeca MSFV, and Coauthors. The real-time mesoscale analysis at NOAA's National Centers for Environmental Prediction: Current status and development. Weather and Forecasting. 2011;26:593–612.

Deng A, and Coauthors Update on WRF-ARW end-to-end multi-scale FDDA system. 10th WRF Users' Workshop; 2009; Boulder, CO, NCAR, 14.

Dudhia J. 1989: Numerical study of convection observed during the winter monsoon experiment using a mesoscale two-dimensional model. Journal of the Atmospheric Sciences. 1989;46:3077–3107.

Genmill W, Katz B, Li X. Daily real-time, global sea surface temperature — high-resolution analysis: RTG_SST_HR. NOAA/NWS/NCEP/MMAB Office Note 260, 39 pp. 2007 [accessed 2015]. http://polar.ncep.noaa.gov/mmab/papers/tn260/MMAB260.pdf

Hong S.-Y, Dudhia J, Chen S.-H. 2004: A revised approach to ice microphysical processes for the bulk parameterization of clouds and precipitation. Monthly Weather Review. 2004;132:103–120.

Janjić Z. Nonsingular implementation of the Mellor-Yamada level 2.5 scheme in the NCEP meso model. NCEP Office Note 437, 61 pp. 2001 [accessed 2015]. http://www.lib.ncep.noaa.gov/ncepofficenotes/files/on437.pdf

Kain JS. The Kain–Fritsch convective parameterization: An update. Journal of Applied Meteorology. 2004;43:170–181.

Lee JA, Kolczynski WC, McCandless TC, Haupt SE. An objective methodology for configuring and down-selecting an NWP ensemble for low-level wind prediction. Monthly Weather Review. 2012;140:2270–2286.

Mlawer EJ, Taubman SJ, Brown PD, Iacono MJ, Clough SA. 1997: Radiative transfer for inhomogeneous atmospheres: RRTM, a validated correlated-k model for the longwave. Journal of Geophysical Research: Atmospheres. 1997;102:16663–16682.

National Operational Hydrologic Remote Sensing Center Snow Data Assimilation System (SNODAS) Data Products at NSIDC 2004 [accessed 2015]. http://dx.doi.org/10.7265/N5TB14TC

Reen BP, Stauffer DR. 2010: Data assimilation strategies in the planetary boundary layer. Boundary-Layer Meteorology. 2010;137:237–269.

Reen BP, Dumais RE., Jr., Assimilating tropospheric airborne meteorological data reporting (TAMDAR) observations and the relative value of other observation Types. Adelph (MD): Army Research Laboratory (US); 2014. Report No.: ARL-TR-7022.

Reen BP, Dumais RE., Jr., Passner JE. Mitigating excessive drying from the use of observations in mesosale modeling. Adelphi (MD): Army Research Laboratory (US); 2014a. Report No.: ARL-TR-6775.

Reen BP, Stauffer DR, Davis KJ. 2014b: Land-surface heterogeneity effects in the planetary boundary layer. Boundary-Layer Meteorology. 2014b;150:1–31.

Skamarock WC, and Coauthors, 2008: A description of the advanced research WRF Version 3. NCAR. 2008. Technical Report NCAR/TN-475+STR, 113 pp.

List of Symbols, Abbreviations, and Acronyms

3DVAR	three-dimensional variational
4DVAR	four-dimensional variational
ABL	atmospheric boundary layer
ACARS	Aircraft Communications Addressing and Reporting System
AGL	above ground level
ARL	US Army Research Laboratory
GFS	Global Forecast System
GRIB	Gridded Binary
MADIS	Meteorological Assimilation Data Ingest System
MAE	mean absolute error
MYJ	Mellor-Yamada-Janjić
NOHRSC	National Operational Hydrologic Remote Sensing Center
RRTM	Rapid Radiative Transfer Model
RTMA	Real-Time Mesoscale Analysis
SAO	surface airways observations
SNODAS	Snow Data Assimilation System
TAMDAR	Tropospheric Airborne Meteorological Data Reporting
TKE	turbulent kinetic energy
UTC	Coordinated Universal Time
WRF-ARW	Advanced Research version of the Weather Research and Forecasting model

1 (PDF)	DEFENSE TECHNICAL INFORMATION CTR DTIC OCA
2 (PDF)	DIRECTOR US ARMY RESEARCH LAB RDRL CIO LL IMAL HRA MAIL & RECORDS MGMT
1 (PDF)	GOVT PRINTG OFC A MALHOTRA
5 (PDF)	DIRECTOR US ARMY RESEARCH LAB RDRL CIE M R DUMAIS JR H CAI P HAINES J PASSNER B REEN

INTENTIONALLY LEFT BLANK.